NASA Technical Paper 1902

Amplified Crossflow Disturbances in the Laminar Boundary Layer on Swept Wings With Suction

J. Ray Dagenhart

NOVEMBER 1981

NASA

NASA Technical Paper 1902

Amplified Crossflow Disturbances in the Laminar Boundary Layer on Swept Wings With Suction

J. Ray Dagenhart
Langley Research Center
Hampton, Virginia

SUMMARY

Amplified disturbances in the laminar boundary layer on a swept wing with suction are investigated using small perturbation theory. A review of the derivation of the governing Orr-Sommerfeld stability equation for oscillations normal to the disturbance wave front in the three-dimensional boundary layer is given. Emphasis is placed on boundary-layer crossflow effects. Solution charts of the Orr-Sommerfeld equation for stationary crossflow disturbances are presented for 10 typical velocity profiles on a swept laminar-flow-control (LFC) wing. The critical Reynolds number, below which no disturbances are amplified, is determined for each velocity profile. This critical crossflow Reynolds number is shown to be a function of a boundary-layer shape factor. Amplification rates for crossflow disturbances are shown to be proportional to the maximum crossflow velocity. A computer stability program called MARIA, employing the amplification rate data for the 10 crossflow velocity profiles, is constructed. This code is shown to adequately approximate the more involved computer stability codes using less than 2 percent as much computer time while retaining the essential physical disturbance growth model. Applications of the MARIA algorithm to the problem of determining LFC suction requirements for several design cases are demonstrated.

INTRODUCTION

Recent political and economic events have served to emphasize the need for energy conservation. One method of such conservation is the application of laminar flow control (LFC) to reduce aircraft drag. Large drag reductions (approximately 30 percent) are possible by employing LFC on commercial aircraft. Although the airline industry uses only a small fraction of the national fuel supply, employing LFC can result in considerable energy and monetary savings. Conceptual design studies of large, transonic, transport aircraft employing LFC by suction are presently in progress.

To control the boundary layer in a laminar state with suction requires some knowledge of the effects of suction on the stability of the laminar boundary layer. Older transition prediction methods (e.g. refs. 1 and 2) rely on empirical relations to predict transition location with no information about the growth of disturbances. Recently, several computational methods (e.g. refs. 3, 4, and 5) have been developed to describe the disturbance growth in the laminar boundary layer using small perturbation theory. The pertinent equation to be solved is the Orr-Sommerfeld stability equation. This equation and its boundary conditions constitute an eigenvalue problem which is time-consuming to solve. One of the eigenvalues is the growth rate of a disturbance within the boundary layer. It seems that this disturbance growth rate could be adequately approximated from a range of known solutions of the Orr-Sommerfeld equation while bypassing the time-consuming and expensive eigenvalue problem.

This paper examines the stability of the three-dimensional boundary layer formed on a swept, infinite, transonic LFC wing. The assumptions required in the derivation of the Orr-Sommerfeld equation are reviewed. Solutions of this equation are compared to experimental amplification rate data for the Blasius boundary layer. Two types of boundary-layer disturbances are investigated - Tollmien-Schlichting waves and cross-

flow waves. Emphasis is placed on the crossflow instability which is dominant in the regions of large pressure gradient on a swept wing at high Reynolds numbers. Amplification-rate solution charts are generated for 10 typical crossflow velocity profiles on an LFC airfoil. Characteristics of these solutions are discussed. An approximate disturbance growth algorithm employing these stability charts, while eliminating the eigenvalue solution problem, is developed. Applications of this technique to predict disturbance amplification are demonstrated.

SYMBOLS

c	chord length
c_i	imaginary part of complex wave velocity
c_l	section lift coefficient
C_p	pressure coefficient, $\dfrac{P - P_\infty}{\frac{1}{2}\rho_\infty U_\infty^2}$
C_Q	suction coefficient, $\dfrac{\rho_w V_w}{\rho_\infty U_\infty}$
f	frequency
H_c	crossflow boundary-layer shape factor, y_{w_M}/δ_{10}
k	scale factor (see eq. (20))
M	Mach number
n	logarithmic amplification ratio
P	pressure in basic laminar flow
p	pressure, $P + p'$
p'	perturbation pressure
R	Reynolds number
s	arc length
t	time
U,V,W	steady-state velocity components in x-, y-, and z-directions, respectively (see eq. (1))
u,v,w	velocity components in x-, y-, and z-directions, respectively (see eq. (1))

u',v',w' perturbation velocity components in x-, y-, and z-directions, respectively (see eq. (1))

V_g group velocity

W_M maximum local crossflow velocity, $W_{n,max}$

x,y,z Cartesian coordinates

α wave number

δ boundary-layer thickness where $\frac{u}{U} = 0.99$

δ_1 boundary-layer displacement thickness

δ_{10} height in boundary layer at which crossflow velocity is 10 percent of maximum value where $\delta_{10} > y_{W_M}$

ε angle of potential flow velocity with respect to x-axis

Λ wing sweep angle

λ wavelength

μ dynamic viscosity

ν kinematic viscosity

ρ mass density

$\phi_1,\phi_2,\phi_3,\phi_4$ amplitude functions for perturbation quantities u', v', w', and p', respectively

ψ wave angle of perturbation vortices with respect to potential flow direction

ω circular frequency, $2\pi f$

Subscripts:

c   chord

cr   critical

e   edge

i   imaginary

n   normal to potential flow direction

o   point of initial instability or constant value

r   real

s   spatial

T	temporal
t	tangent to potential flow direction
w	wall (wing surface)
∞	free stream
1,2,3	x-, y-, and z-directions, respectively

Superscripts:

*	dimensional quantity in equations (18) to (20)
—	weighted average
'	perturbation quantity
^	tabulated stability data
~	in direction normal to disturbance waves

Abbreviations:

LFC	laminar flow control
TS	Tollmien-Schlichting

ANALYSIS

Orr-Sommerfeld Equation

The process of transition from a laminar to a turbulent boundary layer by amplification of small disturbances is a stability problem. The derivation of the disturbance equations governing this problem will be outlined here. A complete derivation is given in reference 6 by Stuart.

The problem can be analyzed by beginning with the incompressible, time-dependent Navier-Stokes equations. These equations are derived by Schlichting in reference 2. Figure 1 shows the right-handed coordinate system used in this analysis. The potential-flow velocity components in the free stream and at an arbitrary location on the wing are also shown.

Perturbation assumptions.- The boundary-layer flow is assumed to consist of a steady, parallel, laminar, mean flow plus perturbations in the velocity components and pressure as

$$u(x,y,z,t) = U(y) + u'(x,y,z,t) \tag{1a}$$

$$v(x,y,z,t) = V(y) + v'(x,y,z,t) \tag{1b}$$

$$w(x,y,z,t) = W(y) + w'(x,y,z,t) \tag{1c}$$

4

and

$$p(x,y,z,t) = P(x) + p'(x,y,z,t) \tag{1d}$$

where

$$V(y) = \text{Constant} = V_o$$

When equations (1) are substituted into the time-dependent Navier-Stokes equations, a set of nonlinear partial differential equations results. These equations are linearized by neglecting quadratic terms in the perturbation quantities. Further reduction of these equations to ordinary differential form is accomplished by assuming the following complex forms for the disturbance quantities:

$$u' = \phi_1(y) \, \exp[i(\alpha_1 x + \alpha_3 z - \omega t)] \tag{2a}$$

$$v' = \phi_2(y) \, \exp[i(\alpha_1 x + \alpha_3 z - \omega t)] \tag{2b}$$

$$w' = \phi_3(y) \, \exp[i(\alpha_1 x + \alpha_3 z - \omega t)] \tag{2c}$$

and

$$p' = \phi_4(y) \, \exp[i(\alpha_1 x + \alpha_3 z - \omega t)] \tag{2d}$$

Equations (2) represent traveling periodic disturbance waves (vortices) which move in the xz-wing plane. The shape of these vortices in the transverse dimension y depends on the amplitude functions $\phi_1(y)$ through $\phi_4(y)$. The strength of these perturbations varies with time or space if either ω or α_1 and α_3 are taken as complex. An arbitrary disturbance can be represented by a Fourier series of such wave components.

Squire transformation.- Betchov and Criminale (ref. 7) give a transformation due to Squire which can be used to reduce the three-dimensional disturbance equations to a single quasi-two-dimensional disturbance equation in the direction of propagation of the disturbance wave front. These transformations are

$$\alpha^2 = \alpha_1^2 + \alpha_3^2 \tag{3a}$$

$$\alpha \tilde{U} = \alpha_1 U + \alpha_3 W \tag{3b}$$

and

$$\alpha \tilde{x} = \alpha_1 x + \alpha_3 z \tag{3c}$$

where the direction of propagation of the disturbance wave with respect to the local potential flow direction is specified by the angle ψ as

$$\psi = \text{arc tan} \left(\frac{\alpha_3}{\alpha_1} \right) - \varepsilon \tag{4}$$

while

$$\varepsilon = \text{arc tan} \frac{W_e}{U_e} \tag{5}$$

The orientation of a disturbance wave is illustrated in figure 2.

With the use of equations (3), the disturbance equation in nondimensional variables becomes

$$\left(\tilde{U} - \frac{\omega}{\alpha} \right) \left(\phi_2'' - \alpha^2 \phi_2 \right) - \tilde{U}'' \phi_2 = i \frac{V_O}{\alpha} \left(\phi_2''' - \alpha^2 \phi_2' \right) - \frac{i}{\alpha R} \left(\phi_2'''' - 2\alpha^2 \phi_2'' + \alpha^4 \phi_2 \right) \tag{6}$$

with boundary conditions

$$\phi_2(0) = \phi_2'(0) = \phi_2(\infty) = \phi_2'(\infty) = 0 \tag{7}$$

where a prime denotes differentiation with respect to y. The boundary conditions specify that the perturbation velocity components u and v must vanish at the boundaries of the flow field.

If the normal component of the velocity in the mean flow V_O is neglected, equation (6) becomes

$$\left(\tilde{U} - \frac{\omega}{\alpha} \right) \left(\phi_2'' - \alpha^2 \phi_2 \right) - \tilde{U}'' \phi_2 = \frac{-i}{\alpha R} \left(\phi_2'''' - 2\alpha^2 \phi_2'' + \alpha^4 \phi_2 \right) \tag{8}$$

Equation (8), along with boundary conditions (7), defines the basic problem to be studied in this paper. This equation, which is referred to as the Orr-Sommerfeld equation, was obtained by Stuart in reference 6 for disturbances normal to the wave front. It can be applied to a three-dimensional stability problem by solving a

series of two-dimensional problems with various wave propagation angles. Solutions to this equation are obtained using the method of Srokowski and Orszag (ref. 5) by employing a version of their SALLY incompressible, three-dimensional, parallel flow stability code.

Temporal and spatial instabilities.- Betchov and Criminale (ref. 7) indicate that both temporal and spatial growth of small wavelike disturbances contribute to the breakdown of the laminar flow in a boundary layer. However, most theoretical analyses of the boundary-layer stability problem are restricted to either the temporal or spatial approximations.

Srokowski and Orszag consider a temporal stability problem with

$$\alpha = \alpha_r \tag{9a}$$

and

$$\omega = \omega_r + i\omega_i \tag{9b}$$

The disturbance wave number $\alpha = 2\pi/\lambda$ is real and the frequency ω is complex. Substitution of equations (9) into equations (2) shows that a disturbance will amplify with time as $e^{\omega_i t}$. If ω_i is allowed to be a function of time (or location), the amplification will go as e^n where

$$n(t) = \int_{t_o}^{t} \omega_i(t) \, dt \tag{10a}$$

or

$$n(s) = \int_{s_o}^{s} \frac{\omega_i(t)}{ds/dt} \, ds \tag{10b}$$

where s is the arc length along the disturbance growth path. The variable n is referred to as the logarithmic amplification ratio.

The boundary-layer disturbance can alternately be considered to amplify spatially where

$$\alpha = \alpha_r + i\alpha_i \tag{11a}$$

and

$$\omega = \omega_r \tag{11b}$$

7

Substitution of equations (11) into equations (2) and using equation (3c) shows that a spatially amplifying disturbance grows as $e^{-\alpha_i x}$ or e^n where

$$n(s) = -\int_{s_o}^{s} \alpha_i(s) \, ds \qquad (12)$$

when the amplification rate varies with location.

Gaster transformation.- Gaster (ref. 8) has shown that temporal and spatial amplification rates are related to one another to first-order accuracy as

$$(\alpha_r)_S = (\alpha)_T \qquad (13a)$$

$$(\alpha_i)_S = \frac{-(\omega_i)_T}{V_g} \qquad (13b)$$

and

$$(\omega)_S = (\omega_r)_T \qquad (13c)$$

where the disturbance-wave group velocity is

$$V_g = \frac{\partial(\omega_r)_T}{\partial(\alpha)_T}$$

Srokowski and Orszag (ref. 5) note that the disturbance-wave energy is transmitted at the group velocity. Comparison of equations (10b), (12), and (13b) shows that $ds/dt = V_g$. Thus, temporal amplification rates can be converted to spatial rates so that the amplification of disturbances along the growth path can be determined using either equation (10b) or (12). The Gaster transformation, equations (13), is used in the SALLY stability code to convert temporal amplification rates to spatial rates for application of equation (12).

Eigenvalue problem.- Equation (8) along with boundary conditions (7) constitute an eigenvalue problem. The boundary-layer profile U and its second derivative U'' are specified functions in this analysis, and ϕ_2 is the eigenfunction to be determined. The most straightforward analysis would consider the wave number α, the Reynolds number R, and the orientation angle ψ as specified parameters; while the complex frequency $\omega = \omega_r + i\omega_i$ is the complex eigenvalue. However, any two of the five variables α, R, ψ, ω_r, and ω_i may be considered as the eigenvalue while the other three must be specified. For a detailed discussion of the eigenvalue problem see, for example, Schlichting (ref. 2) and Brown (ref. 9).

Stability of Blasius Boundary Layer

Figure 3 shows the neutral curve for the Blasius boundary layer generated using the SALLY stability code. The abscissa variable is the boundary-layer Reynolds number R_{δ_1} based on the displacement thickness of the layer. The ordinate is the nondimensional disturbance frequency. The Blasius boundary-layer velocity data were generated using the method of Blottner (ref. 10). For frequency and Reynolds number combinations inside the neutral curve, amplification with time will result; outside the neutral curve, damping in time will occur.

Experimental data for neutral oscillations from Schubauer and Skramstad (ref. 11) are shown in figure 3 for comparison. Reasonable agreement between the experimental and theoretical values are observed along both the upper and lower branches of the neutral curve. However, in the hook region where the upper and lower branches merge, the experimental neutral disturbance frequency exceeds the theoretical value by about 20 percent. Saric and Nayfeh (ref. 3) showed that by using nonparallel flow assumptions instead of equations (1), this discrepancy was largely eliminated. (See fig. 3.)

Figures 4(a) and (b) show comparisons of experimental amplification data from reference 11 with computational results obtained from SALLY and from Kaplan (ref. 12) for $R_{\delta_1} = 630$ and 2200. Here the abscissa is the nondimensional wave number $\alpha_r \delta_1$ and the ordinate is the nondimensional variable c_i/U_e where $c_i = \omega_i/\alpha$ is the complex disturbance velocity. The temporal amplification rate is given by $\omega_i = \alpha c_i$. Note that the SALLY results are practically the same as the Kaplan data for both cases. However, for the lower Reynolds number, the wave number at maximum amplification is well predicted, but the maximum computed amplification rate is about 50 percent below the maximum experimental rate. This discrepancy in amplification rate is consistent with the neutral curve discrepancies of figure 3. For $R_{\delta_1} = 2200$, excellent agreement is obtained between the computed and experimental data over the entire range of the variables.

Swept-Wing Boundary Layers

Pfenninger has studied the design of large, transonic, transport aircraft employing LFC. In reference 13, he has presented several transonic airfoil designs intended specifically for LFC applications. Figure 5 shows the pressure coefficient distribution for Pfenninger's 970 airfoil at the design point of $M_{\infty,n} = 0.749$ and $c_l = 0.675$. These pressure data were computed by using the method of Bauer, Garabedian, and Korn (ref. 14). A typical suction distribution for a swept ($\Lambda = 25°$) LFC wing employing the 970 airfoil is shown in figure 6. Figures 7(a) to (j) show nondimensional tangential (streamwise) and crossflow velocity profiles at several stations on the upper surface of the 970 airfoil at the design condition. Nondimensional numerical data used for stability analyses of these velocity profiles are given in the appendix. These spanwise and chordwise velocity profiles were computed by the method of Kaups and Cebeci (ref. 15). These profiles and the stability charts generated for them will form the basis of an approximate disturbance growth algorithm to be developed herein. Figure 8 shows typical dimensional crossflow velocity profiles at several stations along the chord of the 970 airfoil. The characteristics of these profiles are discussed later at length.

Tollmien-Schlichting and crossflow disturbances.- Figure 9 shows the temporal amplification rate versus orientation angle for the two wavelengths $\lambda/c = 0.0012$ and 0.0030. These data are for the upper surface of the 970 airfoil at its design condition and at a fractional chord location of $x/c = 0.0644$. A single sharply defined amplification region with maximum at $\psi \approx 88°$ is observed for the smaller wavelength. The situation is much different for the larger wavelength - two amplification regions are observed. In addition to the sharp peak at $\psi \approx 88°$, there is another broad amplification region with maximum at $\psi \approx 0°$. Thus, the boundary-layer stability problem can be divided into two parts according to the wave orientation. Disturbance waves with orientation angle $\psi = 0°$ travel in the local potential flow direction (see fig. 2) while those with angle $\psi = 90°$ progress normal to the potential flow direction. The former, which are associated with the tangential boundary layer, are often referred to as Tollmien-Schlichting (TS) waves since they are very similar to the two-dimensional waves studied by Tollmien and Schlichting (ref. 2). The latter are generally called crossflow disturbances since they are associated with the crossflow boundary layer. These disturbances arise from the three-dimensional character of the boundary layer on a swept wing. They are not present in two-dimensional flows.

Pfenninger (ref. 13) notes that this separation of the stability problem into two independent parts is physically acceptable so long as strongly amplified crossflow and TS waves do not occur simultaneously. Relatively weak oblique TS waves can distort and stretch crossflow disturbance vortices to produce rapid, resonancelike amplification and transition. (See Pfenninger, ref. 13.) For this reason, the mutual interaction of amplified disturbances of the two types should be avoided.

Dynamic and viscous instabilities.- Rayleigh and Tollmien (in ref. 2) have shown that the stability problem can be further classified according to the type of mechanism involved. They have shown that velocity profiles with inflection points are dynamically highly unstable in the absence of viscosity. Such profiles have low critical Reynolds numbers and large amplification rates over a wide band of wavelengths. On the other hand, velocity profiles without inflection points exhibit a relatively mild, viscous, TS-type instability with substantially higher critical Reynolds numbers and lower amplification rates than inflected profiles. In the limit of infinite Reynolds number, i.e. in the absence of viscosity, convex boundary-layer profiles are stable for all disturbance wavelengths.

Figure 7 shows that the crossflow profiles all have inflection points, while the tangential profiles do not. However, the tangential profiles can also develop inflection points close to the wing surface with insufficient suction in a pressure rise area. Thus, the crossflow disturbance problem is an example of dynamic instability, while TS waves are primarily a viscous instability problem.

Suction effects on stability.- Removal of a portion of a laminar boundary layer by suction through the surface reduces the layer thickness and modifies the velocity profile $\tilde{U}$ and the second derivative $\tilde{U}''$, critically affecting the boundary-layer stability. (See eq. (8).) Suction reduces disturbance amplification rates within the boundary layer in two ways: primarily through an increase in critical Reynolds number and secondarily through a decrease in the boundary-layer Reynolds number which is proportional to the boundary-layer thickness. Several investigators, as pointed out by Pfenninger (ref. 13), have shown that suction draws the disturbance vortices nearer to the wing surface where dissipation decreases the disturbance growth rate. Schlichting (ref. 2) notes a rapid increase in the critical Reynolds number with

10

increasingly full profiles. As an example, the critical Reynolds number of the asymptotic suction profile, $\left(R_{\delta_1}\right)_{cr} \approx 70\ 000$, is over 100 times that of the Blasius boundary layer without suction, $\left(R_{\delta_1}\right)_{cr} \approx 600$.

According to Brown (ref. 9) and Mack (ref. 4), suction is more effective in controlling TS disturbance amplification than crossflow disturbance amplification, presumably due to the different nature of the boundary-layer instabilities involved. The crossflow instability is inflectional in character, whereas the TS instability is not necessarily of that type. Suction cannot eliminate the inflection point in the crossflow boundary layer because the boundary conditions on this layer require that $\tilde{U}$ be zero at the wing surface and that it approach zero asymptotically as y becomes large. Thus, the crossflow boundary layer retains an essentially similar shape in the presence of suction, although the maximum crossflow velocity and the layer thickness decrease as suction is increased. The shape of the tangential velocity profile is rather sensitive to suction, especially in the region near the surface. An inflection point in the tangential boundary layer can be removed by increased suction.

Compressibility effects on stability.- The potential flow and boundary-layer computation techniques of references 14 and 15 include the effects of compressibility. In order to study these effects on stability, perturbations of density, temperature, and viscosity as well as velocity and pressure perturbations must be included in the analysis. However, since the inclusion of these effects adds tremendously to the difficulty and expense of the calculations, they are not included in the SALLY stability code.[1] Mack (ref. 4) conducted a limited evaluation of the effect of compressibility on disturbance amplification for a swept, transonic, LFC wing. He found that the disturbance amplification rates and the wave angle of the most highly amplified TS disturbances are strongly influenced by compressibility. In contrast, in the front crossflow region, Mack found that the incompressible theory overpredicted the compressible logarithmic amplification ratios by only about 10 percent with negligible influence on the wave angle of the most amplified disturbance. The analysis for crossflow in the pressure-recovery crossflow region are incomplete, but the initial estimates indicate that the overprediction may exceed 10 percent. Further work is needed to adequately establish the importance of compressibility effects, especially on the TS instability. However, it seems that for crossflow disturbances the incompressible theory is physically a reasonably adequate, though somewhat conservative, approximation of the compressible disturbance growth rates.

Since crossflow disturbances are usually the dominant mechanism of instability in the leading-edge region and in the rear pressure rise region of a swept wing at high Reynolds number, the present discussion concentrates on the analysis of the crossflow problem using the incompressible SALLY stability code while deemphasizing the TS instability which is critically affected by compressibility.

---

[1]A compressible version of SALLY is under development.

Crossflow profiles and pressure gradient.- Figure 5 shows the 970 airfoil pressure distribution at the design condition. On the upper surface, the pressure drops rapidly in the leading-edge region and rises strongly in the last 25 percent of the chord. Between these two regions, the static pressure is nearly constant.

Figures 7(a) to (c) show velocity profiles for the upper surface of the 970 airfoil in the leading-edge region where the strong negative pressure gradient produces large crossflow velocity ratios $W_M/U_{e,t}$. Here the crossflow velocities are negative; i.e., the crossflow is directed toward the wing root. Figures 7(d) to (j) show corresponding crossflow profiles in the rear pressure recovery region where the crossflow velocities are positive; i.e., the crossflow is directed toward the wing tip. In general, the maximum crossflow velocity varies as the pressure gradient and it does not exceed 8 percent of the local potential flow velocity for this case.

The crossflow profile assumes a crossover shape with both small positive and negative velocities in an adjustment region between the two principal crossflow regions. Figure 8 shows several dimensional crossflow velocity profiles which illustrate the development of the boundary layer along the wing chord. The pressure gradient has the largest influence on the low momentum portion of the boundary layer close to the wing surface. When the pressure gradient is reversed, the crossflow changes sign beginning at the surface.

Figure 10 illustrates the definitions of a crossflow shape factor H_c and Reynolds number $R_{\delta_{10}}$ used by Pfenninger (ref. 13). The height y_{W_M} is the height at which the crossflow profile has its maximum velocity and δ_{10} is the height at which the crossflow velocity is 10 percent of the maximum value. The crossflow shape factor is defined by the ratio of these two heights as

$$H_c = y_{W_M} \Big/ \delta_{10} \tag{14}$$

The crossflow Reynolds number is based on the height δ_{10} and the maximum crossflow velocity W_M as

$$R_{\delta_{10}} = \frac{\rho_e |W_M| \delta_{10}}{\mu_e} \tag{15}$$

The three velocity profiles in the leading-edge region, figures 7(a) to (c), have comparatively large shape factors, indicating that the maximum crossflow velocity occurs relatively far from the wing surface. In contrast, the profiles in the pressure recovery region, figures 7(d) to (j), have much smaller shape factors, indicating that the maximum crossflow develops relatively close to the wing surface. Also, the shape factor decreases as the pressure gradient increases. The stability of the crossflow boundary layer is strongly related to the shape of the boundary-layer crossflow profile as shown later.

The reason that the shape factors are large in the leading-edge region but much smaller in the pressure recovery region is seen by examining the growth rate of the boundary layer. Schlichting (ref. 2) has shown that, in the absence of suction, the boundary-layer thickness grows as

$$\delta \propto x(R_x)^{-0.5} \tag{16}$$

It was mentioned previously that the crossflow boundary layer develops because the portions of the layer with depleted momentum respond more rapidly to pressure gradients than does the potential flow. If the condition of no-slip at the surface did not apply in the crossflow direction, then the crossflow boundary-layer shape would be determined completely by the streamwise pressure gradient and the momentum distribution in the tangential boundary layer. For such a pressure-dominated crossflow profile, the maximum velocity would occur at the surface where the tangential momentum is a minimum. However, the condition of no-slip does apply in this direction also. Pfenninger (ref. 13) points out that this causes a retardation of the crossflow in a viscous sublayer near the surface. Reference 13 indicates that the viscous sublayer grows in thickness as

$$y_{cr} \propto (\nu t)^{0.5} \propto x(R_x)^{-0.5} \tag{17}$$

where y_{cr} is the dividing point between the pressure and viscosity dominated portions of the layer and t is the time since the beginning of the pressure gradient. Thus, in the leading-edge region, the boundary layer and the viscous sublayer grow from a common origin at approximately the same rate to produce crossflow boundary-layer profiles having relatively large shape factors. (See figs. 7(a) to (c).)

The crossflow direction changes in the pressure recovery region. The boundary layer continues to grow in thickness according to equation (16). However, a new viscous sublayer develops according to equation (17) only from the start of the crossflow crossover at $x/c \approx 0.30$. Thus, due to the difference in origins of the boundary layer and the viscous sublayer, the maximum crossflow velocity is relatively close to the wing surface in the pressure rise area. (See figs. 7(d) to (j).)

Stationary crossflow disturbances.- Gregory, Stuart, and Walker (ref. 6) and Pfenninger (ref. 13) have made flow visualization studies of the stationary ($f = 0$) disturbance vortex pattern on swept wings. The vortex pattern is made visible owing to the differential evaporation of a liquid or the sublimation of a solid according to variations of the surface shear stress. A pattern of nearly equally spaced striations or disturbance vortices, aligned approximately in the potential flow direction, was observed. Srokowski and Orszag (ref. 5) have computed the crossflow disturbance amplification ratios for a range of frequencies of a transonic LFC airfoil. Their limited calculations indicate that the stationary waves are usually the most strongly amplified. For these reasons, the constraints of zero frequency and fixed wavelength are applied in the crossflow stability calculations which follow.

It should be noted that other investigators do not always apply these restrictions to their calculations. For example, Mack (ref. 4) and Srokowski and Orszag (ref. 5) allow for other than stationary crossflow disturbances. Furthermore, to

minimize computation time, Srokowski and Orszag employ an envelope method which seeks the maximum amplification rate at each boundary-layer station. This method does not correspond to fixed wavelength.

Selected rotation of crossflow vortices.- Brown (ref. 9) computed the flow field in a crossflow boundary layer in the presence of amplified crossflow vortices. He found that the combination of the mean flow and perturbation velocities produces a layer of vortices with similar selected rotation. It was noted earlier that the crossflow reverses direction when the pressure gradient changes sign. This reversal of the mean flow changes the selected rotational direction of the vortices within the layer. Figure 9 shows that the wave angles of amplified crossflow disturbances are confined to a narrow band near $\psi = 90°$. This indicates that the vortices in regions of opposite crossflow are approximately parallel but of opposite rotation. The vortex axes are not exactly parallel because of the curvature of the boundary-layer streamlines. The reversal of the vortex rotation in regions of opposite crossflow implies that amplified oscillations in one region will be negated by the opposing flow in the second. Amplification of the perturbations will begin anew in the second region. Although the amplified disturbances of one region do not continue to amplify in the following region, they can affect the amplification rates there. Pfenninger (ref. 13) points out that the amplified oscillations produce periodic distortions of the mean flow velocity profile. This is a higher order effect and is not included here.

In a previous section, experimental and theoretical amplification rate data were compared for the Tollmien-Schlichting instability of the Blasius boundary layer. A similar comparison for the crossflow instability on a swept wing is impossible due to the lack of experimental data.

Solution charts for crossflow instability.- Figures 11(a) to (j) show curves of constant spatial amplification rate $\alpha_i \delta_{10}$ for stationary crossflow disturbances for the three-dimensional velocity profiles of figures 7(a) to (j), respectively. These computed stability characteristics were obtained from a version of the SALLY stability code which solves the Orr-Sommerfeld equation (8) with boundary conditions (7). The specified parameters in this eigenvalue problem are zero frequency $\omega_r = 2\pi f = 0$, nondimensional wave number $\alpha_r \delta_{10}$, and boundary-layer Reynolds number $R_{\delta_{10}}$. Further

computational data to support this restriction to zero frequency is presented later. The complex eigenvalue is then represented by the temporal amplification rate $\omega_i \delta_{10}/W_M$ and the wave orientation angle ψ. The temporal amplification rate is converted to a spatial rate by applying the Gaster transformation of equation (13b). Tables I(a) to (j) show the spatial amplification rate at the computational points of wave number and Reynolds number for the profiles of figures 7(a) to (j), respectively. The wave orientation angles are not presented, as these data do not serve any useful purpose in the following discussion.

Characteristics of solution.- Examination of figures 11(a) to (j) reveals several important characteristics of the solution which can be utilized in the development of an approximate disturbance growth algorithm. First, the curves of constant amplification rate have similar shapes for all 10 velocity profiles. Second, each velocity profile has a critical Reynolds number below which no amplification occurs for disturbances of any wavelength. And third, the amplification rate increases linearly with $W_M/U_{e,t}$.

The constant amplification rate curves for all 10 velocity profiles open to the right in two branches from some minimum Reynolds number. The lower branch is for disturbances of relatively small wave number and, thus, large wavelength. The upper branch is for disturbances of relatively large wave number or small wavelength. For a given amplification rate, the upper and lower branches separate as the Reynolds number increases at least up to $R_{\delta_{10}} = 2000$. As noted previously, Rayleigh and Tollmien (in ref. 2) showed that the instability persists to the limiting case of infinite Reynolds number for inflectional velocity profiles. Tollmien (in ref. 2) also showed that for inflectional profiles the upper and lower branches are far apart. Although the amplification curves are similar in shape, dissimilarities are also evident. The bandwidth of amplified disturbances and the wave number of maximum amplification rate differ from profile to profile. However, these small dissimilarities have little impact on the approximate disturbance growth model to be developed.

The critical Reynolds number can be related to the shape of the crossflow velocity profile. Figure 12 and table II show the variation of the critical Reynolds number $\left(R_{\delta_{10}}\right)_{cr}$ with shape factor H_c. These data were computed using the modified SALLY stability code for crossflow profiles on the 970 airfoil at the design condition. The critical Reynolds numbers from figures 22 to 31 are included. The boundary-layer history causes some slight scatter of the data, but the faired curve is a good representation of the variation of the critical Reynolds number with shape factor. Similar computational data obtained from Brown (ref. 9) for crossflow velocity profiles on a low-speed swept wing and a rotating disk are shown for comparison; excellent agreement is obtained.

Large values of the shape factor ($H_c > 0.3$) indicate that the maximum crossflow velocity is relatively far from the wing surface. Figure 12 shows that, in such cases, the critical crossflow Reynolds number is quite low. For smaller values of the shape factor, the maximum crossflow velocity occurs relatively closer to the wing surface. The critical crossflow Reynolds number decreases as the shape factor is increased. This decrease is rapid at first, but it becomes more gradual for shape factors above $H_c = 0.23$. The critical Reynolds number for $H_c = 0.15$ is more than five times that for $H_c = 0.50$. Figures 13 and 14 give the variation of crossflow shape factor and crossflow Reynolds number for the 970 airfoil at the design condition. Examination of figures 12 and 13 shows that the crossflow is highly unstable in the front crossflow region where the shape factors are relatively large; however, figure 14 indicates that in this region the crossflow Reynolds numbers are not large. In contrast, the crossflow is relatively more stable in the pressure recovery region where the shape factors are much smaller (see fig. 13); but, due to boundary-layer growth, the crossflow Reynolds numbers are substantially larger in this region. (See fig. 14.)

The crossflow velocity ratio $W_M/U_{e,t}$ indicates the relative strength of the crossflow. The influence of this ratio on the amplification rate was emphasized by Pfenninger in reference 13 and is examined by considering equation (8). Recall that this equation is written in nondimensional form. For the crossflow instability problem, the reference length is taken as δ_{10}^* and the reference velocity as W_M^* where, for purposes of clarity, the star is used to denote a dimensional quantity. Then the nondimensional variables in equation (8) become

$$\tilde{U} = \frac{\tilde{U}*}{W_M^*} \tag{18a}$$

$$\alpha = \alpha^* \delta_{10}^* \tag{18b}$$

and

$$\omega = \frac{\omega^* \delta_{10}^*}{W_M^*} \tag{18c}$$

Taking the real and imaginary parts of equation (18c) yields

$$\omega_r = \frac{\omega_r^* \delta_{10}^*}{W_M^*} \tag{19a}$$

and

$$\omega_i = \frac{\omega_i^* \delta_{10}^*}{W_M^*} \tag{19b}$$

Equation (19b) indicates that the dimensional temporal amplification rate scales as the maximum crossflow velocity when all other parameters are kept fixed. Mack's numerical results (ref. 4) substantiate this even though he does not give a physical interpretation.

To examine this phenomenon in greater detail, consider two three-dimensional velocity profiles. The first three-dimensional profile is a reference case with known solutions to the Orr-Sommerfeld equation (8) for the crossflow instability. The second profile has tangential velocity components exactly equal to those for the reference case, but with crossflow velocity components scaled by some constant factor k. The modified profile has the same shape factor as the reference profile. While all crossflow velocities are larger by the factor k, the heights above the surface of the maximum velocity and 10 percent of the maximum velocity have not changed. Thus, in the pure crossflow direction ($\psi = 90°$), the nondimensional variables $\tilde{U}$ and $\tilde{U}''$ are identical for the reference and the modified cases. The nondimensional solutions of equation (8) for the same values of wave number and Reynolds number are identical for the two cases.

The nondimensional solution consists of the complex eigenvalue $\omega = \omega_r + i\omega_i$ and the eigenfunction $\phi_2(y)$. The temporal amplification rate for the modified profile can be put in dimensional terms by use of equation (19b) as

$$\omega_i^* = \frac{\omega_i k W_M^*}{\delta_{10}^*} \tag{20}$$

where kW_M^* is the maximum crossflow velocity in the modified case. Equation (20) clearly shows that the temporal amplification rate varies directly as k. The magnitudes of both amplification and damping rates increase directly as k while neutral oscillations are unaffected. Thus, the neutral curve is unchanged as k varies. In particular, this means that the critical crossflow Reynolds number for a particular velocity profile is independent of k.

The argument presented above is strictly applicable only for the pure crossflow direction ($\psi = 90°$) because $\tilde{U}$ and $\tilde{U}''$ are dependent on the wave orientation angle. (See eqs. (3b) and (4).) However, the wave angle for stationary crossflow disturbances differs little from 90° so that equation (20) is an adequate approximation to the actual situation.

In order to illustrate this phenomena numerically, the crossflow velocities of figure 10 were scaled by $k = 1.05$. Dimensional temporal and spatial amplification rates for both the reference and the scaled cases are given in table III. These data are for the two nondimensional wave numbers $\alpha_r \delta_{10} = 0.0008$ and 0.0018 for range crossflow Reynolds numbers from $R_{\delta_{10}} = 30$ to 2000. As expected, comparison of the amplification rates confirms equation (20).

The restriction, in the above discussion, that the tangential velocity profile not be scaled is quite important. If the tangential velocities were scaled as k, then the dimensional group velocity would increase as k. Equation (13b) indicates that, in this case, the dimensional spatial amplification rate would be unchanged. Thus, the strength of the dimensional spatial amplification rate is determined by the crossflow velocity ratio $W_M/U_{e,t}$.

Crossflow Disturbance Growth Prediction Method

An approximate crossflow disturbance growth algorithm can now be developed using the stability characteristics generated in the previous sections. This model is an extension of a hand computation method used by Pfenninger (ref. 13) for crossflow stability analysis. Tables I(a) to (j) give the local spatial amplification rate for the velocity profiles of figures 7(a) to (j), respectively. For other crossflow velocity profiles, these data can be used to approximate the local spatial amplification rate. To do so requires an interpolation scheme.

Interpolation method.- To begin, a three-dimensional boundary-layer solution is necessary. This solution gives the variations of the boundary-layer thickness δ_{10}, the shape factor H_c, the velocity ratio $W_M/U_{e,t}$, and the Reynolds number $R_{\delta_{10}}$ for the crossflow boundary layer along the wing chord.

At each boundary-layer computational station, the critical crossflow Reynolds number $\left(R_{\delta_{10}}\right)_{cr}$ is estimated using the shape factor H_c and the data of figure 12. Next, the stability chart (from table I) with critical Reynolds number $\left(\hat{R}_{\delta_{10}}\right)_{cr}$ nearest to $\left(R_{\delta_{10}}\right)_{cr}$ is selected. In general, $\left(R_{\delta_{10}}\right)_{cr}$ and $\left(\hat{R}_{\delta_{10}}\right)_{cr}$ differ. Direct use of the selected stability chart will incorrectly predict the onset of instability due to this discrepancy. To eliminate this problem, the actual crossflow Reynolds number is adjusted using

$$\hat{R}_{\delta_{10}} - \left(\hat{R}_{\delta_{10}}\right)_{cr} = R_{\delta_{10}} - \left(R_{\delta_{10}}\right)_{cr} \tag{21}$$

where $\hat{R}_{\delta_{10}}$ is the adjusted boundary-layer Reynolds number. Equation (21) requires that the excess of the adjusted Reynolds number over the critical Reynolds number for the stability chart be the same as for the actual boundary layer. Solving for the adjusted Reynolds number yields

$$\hat{R}_{\delta_{10}} = R_{\delta_{10}} + \left(\hat{R}_{\delta_{10}}\right)_{cr} - \left(R_{\delta_{10}}\right)_{cr} \tag{22}$$

Thus, the actual boundary-layer Reynolds number is adjusted by the difference in critical Reynolds numbers of the stability chart and the actual boundary layer. Equation (22) correctly predicts the onset of instability as the Reynolds number is increased.

It was mentioned previously that both experimental and theoretical evidence indicate that crossflow disturbance amplification produces stationary vortices having fixed wave spacing. This wavelength is not known a priori; therefore, computations must be made for a range of wavelengths. The most likely wave spacing then corresponds to the disturbance wavelength having the maximum integrated amplification over the crossflow region. The nondimensional wave number $\hat{\alpha}_r \hat{\delta}_{10}$ corresponding to a disturbance wavelength λ/c can be obtained as

$$\hat{\alpha}_r \hat{\delta}_{10} = \frac{2\pi}{\lambda/c} \frac{\delta_{10}}{c} \tag{23}$$

where $\hat{\alpha}_r \hat{\delta}_{10}$ refers to values found in the stability chart.

Now, $\hat{R}_{\delta_{10}}$ and $\hat{\alpha}_r \hat{\delta}_{10}$ can be used to obtain amplification rate information from the selected stability chart. The amplfication rate $\hat{\alpha}_i \hat{\delta}_{10}$ is obtained from the stability chart by use of a second-order interpolation in $\hat{R}_{\delta_{10}}$ and $\hat{\alpha}_r \hat{\delta}_{10}$. This rate must be scaled to account for the crossflow velocity effects described by equation (20). The nondimensional amplification rate can now be written as

$$\alpha_i \delta_{10} = \frac{\hat{\alpha}_i \hat{\delta}_{10} \left(W_M/U_{e,t}\right)}{\left(\hat{W}_M/\hat{U}_{e,t}\right)} \tag{24}$$

18

where $W_M/U_{e,t}$ and $\hat{W}_M/\hat{U}_{e,t}$ represent, respectively, the crossflow velocity ratios at the local boundary-layer station and for the stability chart.

Division of flow field into crossflow regions.- It was shown earlier that the crossflow disturbance vortices in consecutive regions of opposite pressure gradient are approximately parallel but have opposite directions of rotation. This characteristic serves to divide the wing into crossflow regions according to the sign of the crossflow velocity. However, the demarcation of the various regions is not well defined because of the crossover shape of the boundary layer in the adjustment region. In this adjustment region where $dp/dx \approx 0$, the crossflow Reynolds numbers are usually quite small so that little or no disturbance amplification occurs. The SALLY stability code does not divide the wing into crossflow regions; it divides the wing into regions of amplified and damped crossflow disturbances. The reversal of the rotation of the crossflow vortices is indicated when there is a small, abrupt shift ($\approx 5°$) in the disturbance wave angle following a pressure gradient sign change.

Since this wave angle shift cannot be adequately predicted by an approximate disturbance growth model, another method to divide the flow into regions is necessary. The demarcation between the various regions is made precise by considering the sign of a weighted average crossflow velocity $\overline{W}_n$ defined by

$$\overline{W}_n = \frac{\int_0^\delta [1 - \rho(y) \, U_t(y)] W_n(y) \, dy}{\int_0^\delta [1 - \rho(y) \, U_t(y)] \, dy} \tag{25}$$

The weighting function of this average is the tangential momentum defect within the boundary layer. This weighting function takes into account the sensitivity of the low momentum portions of the boundary layer to pressure gradient reversals. Comparisons of the locations of the sign reversal of $\overline{W}_n$ to the wave angle shift from SALLY stability analyses confirm that $\overline{W}_n$ is a good indicator of the division between crossflow regions.

Integrated amplification.- The procedure outlined above is used to predict local spatial amplification rates for a range of disturbance wavelengths in the boundary layer on a swept wing. However, disturbance intensity rather than amplification rates is of primary importance. The logarithmic disturbance amplification ratios for the selected range of wavelengths are obtained from equation (12). This integral gives the logarithm of the amplification ratio from the point of instability as a function of position along the growth path. Hefner and Bushnell (ref. 16) indicate that no universally accepted definition of the disturbance growth path exists. Some investigators use the group velocity trajectory while others use the potential flow streamline as the growth path. But, the difference between these two paths is not large. Comparisons over a range of wavelengths for the 970 airfoil indicate that the angle between the group velocity vector and the potential flow velocity vector is less than 3°. Furthermore, the arc lengths along the potential flow streamline and the group velocity trajectory differ by less than 1.8 percent over the wavelength range. Thus, for simplicity, the potential flow streamline is taken as the growth path for equation (12).

19

Computer code.- A computer code called MARIA which incorporates the above steps to form an approximate crossflow disturbance amplification algorithm has been written. MARIA accepts three-dimensional laminar boundary-layer data generated by a modified version of the Kaups and Cebeci (ref. 15) swept and tapered wing boundary-layer code. These computational data include potential flow velocity components, boundary-layer thickness, shape factor, Reynolds number, and the maximum crossflow velocity ratio at each boundary-layer computational station. Equation (25) is used to divide the flow into crossflow regions. Equations (22) to (24) and the stability characteristics of table I are used to estimate local amplification rates for a range of up to 20 disturbance wavelengths. Logarithmic amplification ratios are determined using equation (12) for each wavelength and are plotted against wavelength for each crossflow region.

The MARIA code has several distinct advantages over the more involved computer stability codes. First, the MARIA code retains the essential disturbance growth characteristics of the crossflow boundary layer to produce approximate amplification data of reasonable accuracy. Second, the code operates quickly and inexpensively; it takes less than 2 percent as much computer time as the SALLY stability code. MARIA can compute amplification data for up to 20 disturbance wavelengths, simultaneously, and plot the results obtained. This is in contrast to the SALLY code which can compute for only one wavelength at a time. The MARIA program requires 102 K octal storage and 5.1 CPU (Central Processor Unit) seconds execution time on a Control Data CYBER 175 computer system to analyze for crossflow instability at 20 wavelengths at 76 boundary-layer stations. Third, the MARIA code is extremely easy to apply. It is only necessary to select the wavelengths for analysis and the plotting option; otherwise program operation is automatic. And finally, the code can compute through damping regions embedded between two amplification regions. Such embedded regions sometimes exist because of variations in the pressure gradient and the suction distribution. Eigenvalue solution methods often have considerable difficulty tracking the proper disturbance wave through a region of damping.

For LFC applications, suction requirements must be determined for a range of flight variables including lift coefficient, Mach number, and Reynolds number. At each flight condition, the boundary layer must be iteratively analyzed for stability with assumed suction distributions until an acceptable disturbance amplification is obtained. The MARIA code can be employed for such iterations as a design tool which rapidly and inexpensively predicts the disturbance amplification ratios.

Correlation Between Amplification and Transition

Solutions of the Orr-Sommerfeld stability equation (8) give the local disturbance amplification rate subject to the specified constraints of wavelength and frequency. The disturbance amplification ratio is given by e^n where n is the integral of the local amplification rate according to equation (12). This linear theory does not describe an initial value disturbance growth problem. It gives only local disturbance amplification rates and overall amplification ratios. Application of this theory to LFC suction design problems requires a correlation between computed disturbance amplification ratios and experimental transition data.

Hefner and Bushnell (ref. 16) indicate that very little detailed knowledge concerning the disturbance environment exists. Possible LFC boundary-layer disturbance sources include free-stream vorticity; external or internal acoustic excitations; wing surface roughness, waviness, or vibrations; and suction system induced fluctuations.

20

Hefner and Bushnell (ref. 16) used the SALLY stability code to generate amplification ratio data for comparison with experimental data taken in low disturbance wind tunnels and in powered flight. They found that crossflow disturbances of fixed wavelength with amplification ratios up to an average value of $e^{7.2}$ were possible before transition on both suction and nonsuction wings. Pfenninger (ref. 13) made a similar study for swept, suction wings using his hand-computation method. He found that full chord laminar flow could be maintained in the presence of fixed wavelength crossflow disturbances having amplification ratios of up to e^7. However, Pfenninger indicates that amplification ratios of up to e^7 are possible only if the nonlinear interaction of crossflow and Tollmien-Schlichting waves is avoided. Such interaction can be minimized by preventing simultaneous relatively large amplification of both TS and crossflow waves by appropriate use of geometry and suction distribution in the airfoil design. For a further discussion, see reference 17.

Much more work is needed to firmly establish the role of linear stability theory in the transition prediction process. But for the present, a limit on the crossflow disturbance amplification ratio of e^7 is selected as a suction design goal for applications in low-disturbance wind tunnels or powered flight. However, this selection is only as good as the knowledge of the disturbance environment. For an amplification ratio of e^7 to be acceptable, the experiment must, in fact, have a low disturbance environment and no interaction of TS and crossflow vortices.

RESULTS AND DISCUSSION

Comparison of MARIA and SALLY Stability Codes 970 Airfoil

Figures 15(a), (b), and (c) show the computed local amplification rates versus fractional chord location for three disturbance wavelengths ($\lambda/c = 0.0004$, 0.0016, and 0.0020) on the upper surface of the 970 airfoil at the design condition. Characteristics from both MARIA and SALLY stability codes are shown for comparison. The smallest and largest wavelengths shown were selected because they have maximum amplification ratios in the front and rear crossflow regions, respectively. The intermediate wavelength is strongly amplified in both regions. The MARIA results are seen to reasonably approximate the SALLY stability calculations over the complete wing chord. The MARIA calculations are obtained from a piecewise approximation technique and, as such, do not exhibit as smooth a solution as is given by the SALLY method. However, all of the major fluctuations predicted by SALLY are duplicated by MARIA. In the front crossflow region, disturbances of very small wavelength are strongly amplified over short surface distances. This is where the largest discrepancy between MARIA and SALLY is observed. For $\lambda/c = 0.0004$, the MARIA code overpredicts the SALLY amplification rate by about 50 percent at the peak amplification point. However, the amplification rates agree very well over the remainder of the region, and the integrated amplification ratio is not much affected by the overprediction of the peak amplification rate.

The maximum values of the integrated logarithmic amplification ratios are shown in figure 16 as functions of wavelength for the front and rear crossflow regions. The front crossflow region extends from $x/c = 0$ to 0.38 while the rear region is from $x/c = 0.38$ to 1.0. Figure 6 shows that the minimum pressure is attained at about $x/c = 0.02$, but the strong crossflow generated in the first 2 percent of chord persists until $x/c = 0.38$. Excellent agreement between MARIA and SALLY is obtained. Note that the SALLY stability characteristics for nonstationary disturbances are included for comparison. The peak amplification ratio in the front crossflow region was found for a frequency of $f = 4000$ Hz but this exceeds the maximum amplification

for stationary disturbances by only 3.8 percent. In the rear crossflow region, the stationary disturbances were found to be maximum amplified. Thus, these results are in accord with the conclusion of Srokowski and Orszag (ref. 5) that only stationary crossflow disturbances need be considered in preliminary analysis.

Figures 17(a) and (b) show maximum logarithmic amplification ratios versus wavelength for the 970 airfoil upper surface for chord Reynolds numbers of 25, 40, 60, and 100×10^6 for the front and rear crossflow regions. SALLY predictions for stationary disturbances are again shown for comparison. Schlichting (ref. 2) indicates that the nondimensional boundary-layer thickness varies inversely as the square root of the chord Reynolds number. For the larger Reynolds numbers, the suction coefficient from figure 7 for $R_c = 25 \times 10^6$ was scaled according to this inverse square-root relationship so that the same fraction of the boundary layer was removed by suction as for $R_c = 25 \times 10^6$. This results in larger crossflow Reynolds numbers as the chord Reynolds number increases. The data of table I indicate that the disturbance amplification should increase as crossflow Reynolds numbers increase. Indeed, figure 17 shows this expected increase in amplification. In the front crossflow region, the MARIA results fall below the SALLY results as Reynolds number is increased, but the discrepancy does not exceed 10 percent. The wavelengths at maximum amplification are in good agreement. In the rear region, excellent agreement between the predictions is obtained. Note that the wavelength corresponding to maximum amplification decreases as chord Reynolds number increases. In fact, the wavelength at maximum amplification varies inversely as the square root of the chord Reynolds number just as the boundary-layer thickness does.

In the above calculations, the same fraction of the boundary layer was removed by suction for all Reynolds numbers. For Reynolds numbers greater than $R_c = 25 \times 10^6$, the logarithmic amplification ratios exceed $n = 7$. Appropriate increases in suction for these higher Reynolds number cases would reduce the maximum amplification ratios to $n = 7$ in each case.

Predictions for Other Airfoils

Thus far, the MARIA stability code has been applied only to the 970 airfoil. To demonstrate other applications, two candidate airfoils for the NASA Langley LFC wind-tunnel experiment are analyzed. Again, SALLY stability characteristics are given for reference.

The first airfoil considered is designated the LFC-73-06-135 by Allison and Dagenhart (ref. 18). Figure 18 shows the pressure distribution for this airfoil for the design condition of $M_{\infty,n} = 0.73$ and $c_l = 0.60$. A possible suction distribution for the upper surface of this airfoil at $R_c = 15 \times 10^6$ with $\Lambda = 35°$ is shown in figure 19. This suction distribution was determined before the SALLY and MARIA stability codes were available by successively applying Pfenninger's hand-computation method (ref. 13) using the crossflow stability characteristics of Brown (ref. 9). The suction spike near the leading edge and the large suction values beyond $x/c = 0.60$ are necessary to control the crossflow instability. The low suction rates between $x/c = 0.10$ and 0.60 control the Tollmien-Schlichting instability in the region of small adverse pressure gradient.

Figure 20 shows the logarithmic amplification ratio versus wavelength for stationary crossflow disturbances in the two crossflow regions. Amplification ratios obtained by Mack (ref. 4) for this airfoil in the front crossflow region are included

in figure 20(a). Good agreement for all three methods is observed; the wavelengths at maximum amplification are identical while the maximum logarithmic amplification ratios agree to within 10 percent in both regions.

The second airfoil analyzed is designated the 989C airfoil by Pfenninger (ref. 17). This is a later-generation airfoil designed for improved LFC performance. Figure 21 shows the pressure distribution for the 989C airfoil for $M_{\infty,n} = 0.755$ and $c_l = 0.55$. The upper-surface suction distribution for this airfoil at $R_c = 20 \times 10^6$ and $\Lambda = 23°$ is shown in figure 22. This suction distribution was established using the MARIA stability code. An initial suction estimate was modified iteratively to obtain maximum crossflow disturbance amplification ratios of $n \approx 7$ in accordance with the transition correlation data.

Figure 23 shows the logarithmic amplification ratio for stationary crossflow disturbances versus wavelength for the front and rear crossflow regions. The front region extends from $x/c = 0$ to 0.32 and the rear region from $x/c = 0.62$ to 1.0. No amplification was detected in two intermediate regions of weak crossflow. Excellent agreement between MARIA and SALLY is observed in the front region. Note that the maximum logarithmic amplification ratio is only $n = 4$. This is not indicative of excessive suction (compare figs. 19 and 22); the specified suction for $x/c < 0.1$ in figure 22 is necessary to control the TS instability. The amplification in this region is well below the limit of $n \approx 7$ due to design improvements of the 989C airfoil. In particular, the very steep pressure gradient near the leading edge minimizes the crossflow disturbance amplification. The maximum amplification ratios agree to within 10 percent in the rear region.

Figure 24 gives the lower-surface suction distribution for the 989C airfoil for specified test conditions. Figure 21 shows that there are three tight turns on the lower surface which produce strong compressions followed by strong flow accelerations. These sharp turns are intended to minimize the extent of concave curvature regions where the Gortler type centrifugal instability is amplified. (See refs. 2 and 6.) At each of these turns, the suction must be increased considerably to maintain attached laminar flow. The reversals of the pressure gradient for this case produce nine separate crossflow regions on the lower surface. Neither SALLY nor MARIA includes the centrifugal effects which produce the Gortler instability in the concave regions. Furthermore, the large pressure gradients and suction requirements in these regions make the parallel flow assumption questionable. Thus, the predictions obtained by both SALLY and MARIA may be appreciably in error for such a surface.

Figure 25 shows the logarithmic amplification ratio versus wavelength for crossflow regions 5 and 6 on the lower surface of the 989C airfoil. Only these two regions have large disturbance amplification. The accelerated flow region from $x/c = 0.16$ to 0.51 has a maximum logarithmic amplification ratio of $n \approx 7$. Here the MARIA algorithm predicts a maximum value 12 percent above the SALLY results. In the strong compression region from $x/c = 0.51$ to 0.87, the maximum logarithmic amplification predicted by the MARIA code exceeds the SALLY value by about 15 percent. This is not a particularly significant discrepancy because the amplification in this region is kept low ($n \approx 4$) to minimize the possible interaction of crossflow disturbances with amplified Görtler vortices.

Figure 26 shows the suction distribution for the upper surface of the 989C airfoil at $R_c = 40 \times 10^6$ and $\Lambda = 23°$. The pressure distribution for this case is given in figure 21 for $M_{\infty,n} = 0.755$ and $c_l = 0.55$. The logarithmic amplification ratio versus wavelength for the two crossflow regions is shown in figure 27. The

23

maximum amplification ratios agree to within 5 percent in the front region and 8 percent in the rear region. Note that the maximum amplification in the front region (n $\approx$ 8) is only marginally acceptable according to the transition correlation data of reference 16. However, this amplification is determined according to the incompressible stability theory which is somewhat conservative. For the peak amplified wavelength ($\lambda/c = 0.0003$), nearly all of this amplification occurs ahead of $x/c = 0.03$ where suction starts so that increases in suction beginning at $x/c = 0.03$ will have little effect. This indicates the need for a suction spike similar to, but smaller than, the one in figure 19 for the LFC-73-06-135 airfoil. The addition of such a spike amounts to a wing design modification in order to reach $R_c = 40 \times 10^6$ since suction beginning at $x/c = 0.03$ is acceptable for the 989C airfoil at the design Reynolds number of $R_c = 20 \times 10^6$. (See fig. 22.)

The applications cases demonstrated here constitute only a tiny fraction of the cases of interest for LFC applications. The MARIA program provides a very adequate alternative to the eigenvalue solutions of other much more involved and expensive stability codes while retaining the essential character of the physical problem. Its use is therefore recommended for parameter studies and design studies where a large range of variables must be considered. The more involved and expensive methods can be used to verify final MARIA results.

CONCLUSIONS

Amplified disturbances in the laminar boundary layer on a swept wing with suction are investigated using small perturbation theory. Solution charts of the Orr-Sommerfeld equation for stationary crossflow disturbances are presented for 10 typical velocity profiles on a swept laminar-flow-control (LFC) wing. A computer stability program called MARIA, employing the amplification characteristics for the 10 crossflow velocity profiles, is constructed. Applications of the MARIA algorithm to the problem of determining LFC suction requirements for several design cases are demonstrated.

The following conclusions are drawn:

1. The critical crossflow Reynolds number varies as a function of the crossflow boundary-layer shape factor.

2. Crossflow disturbance amplification rates are proportional to the maximum crossflow velocity when all other factors are held constant.

3. Amplification rates for stationary crossflow disturbances can be adequately approximated using solution charts of the Orr-Sommerfeld equation obtained from the SALLY stability code. The MARIA algorithm can perform these computations using less than 2 percent as much computer time as more involved stability codes.

4. The MARIA algorithm can be employed as an effective design tool for the iterative calculations required for crossflow boundary-layer stability analyses on swept suction wings. Only final check computations using a more involved and expensive computer stability code are necessary.

Langley Research Center
National Aeronautics and Space Administration
Hampton, VA 23665
August 11, 1981

24

APPENDIX

NONDIMENSIONAL VELOCITY PROFILES ON 970 AIRFOIL

The nondimensional numerical data used for the stability analyses are tabulated for spanwise and chordwise velocity profiles. These data correspond to the nondimensional tangential and crossflow velocity profiles of figure 7.

VELOCITY PROFILES AT x/c = 0

y/δ_1	U/U_e	$(U/U_e)''$	W/U_e	$(W/U_e)''$
0.	0.	-.3989746464522E+00	0.	-.2753405460680E-03
.7320188164837E-01	.5657026611692E-01	-.3980331502328E+00	.8650975979229E-01	-.1237328053540E-02
.1500610507768E+00	.1136715054643E+00	-.3961649864870E+00	.1773345553367E+00	-.4253474878292E-02
.2307570055432E+00	.1711047878543E+00	-.3931445967492E+00	.2726662567436E+00	-.9812300529903E-02
.3154775148105E+00	.2286476469700E+00	-.3888716023073E+00	.3726836865679E+00	-.1816336314977E-01
.4044189272714E+00	.2860541737007E+00	-.3832463781012E+00	.4775438619133E+00	-.2954921480093E-01
.4977864867220E+00	.3430557609504E+00	-.3761730492524E+00	.5873708878925E+00	-.4419117512422E-01
.5957946554230E+00	.3993626513484E+00	-.3675633004470E+00	.7022421678505E+00	-.6227004139450E-01
.6986674490413E+00	.4546664462537E+00	-.3573410631788E+00	.8221716604533E+00	-.8390098705018E-01
.8066387888860E+00	.5086437322011E+00	-.3454481031057E+00	.9470900493963E+00	-.1091022217883E+00
.9199528801753E+00	.5609609652914E+00	-.3318504650390E+00	.1076821925620E+01	-.1377576013127E+00
.1038864629007E+01	.6112807201049E+00	-.3165456418558E+00	.1211060444046E+01	-.1695743800094E+00
.1163640115532E+01	.6592693523956E+00	-.2995702124985E+00	.1349340433179E+01	-.2040387731724E+00
.1294557146378E+01	.7046060393405E+00	-.2810075415178E+00	.1491011620033E+01	-.2403739551556E+00
.1431905915059E+01	.7469930442117E+00	-.2609949506665E+00	.1635214472032E+01	-.2775074631211E+00
.1575989804095E+01	.7861669037172E+00	-.2397295707067E+00	.1780862093933E+01	-.3140574029385E+00
.1727126365299E+01	.8219100606218E+00	-.2174718785821E+00	.1926632528793E+01	-.3483487915683E+00
.1885648513322E+01	.8540622734451E+00	-.1945457566386E+00	.2070976492511E+01	-.3784719373284E+00
.2051905959875E+01	.8825309500023E+00	-.1713338323504E+00	.2212145731908E+01	-.4023928256536E+00
.2226266900156E+01	.9072994033678E+00	-.1482669463478E+00	.2348246485806E+01	-.4181198915951E+00
.2409119938094E+01	.9284319575932E+00	-.1258069452801E+00	.2477320601632E+01	-.4239215979174E+00
.2600876204219E+01	.9460748810196E+00	-.1044226882780E+00	.2597453491964E+01	-.4185752514987E+00
.2801971583389E+01	.9604523382924E+00	-.8456022637812E-01	.2706903360635E+01	-.4016115914690E+00
.3012868936314E+01	.9718569527133E+00	-.6660949204736E-01	.2804240484841E+01	-.3735060949679E+00
.3234060177922E+01	.9806351508825E+00	-.5087129158950E-01	.2888479853467E+01	-.3357625552658E+00
.3466068075945E+01	.9871681681921E+00	-.3752952826293E-01	.2959186673500E+01	-.2908431827420E+00
.3709447659920E+01	.9918503203969E+00	-.2663390087530E-01	.3016533912046E+01	-.2419253972335E+00
.3964787183193E+01	.9950667422764E+00	-.1809739270217E-01	.3061295540168E+01	-.1925060376435E+00
.4232708650270E+01	.9971730919123E+00	-.1171055528609E-01	.3094768827840E+01	-.1459190863173E+00
.4513867995619E+01	.9984795822406E+00	-.7171247869774E-02	.3118632579453E+01	-.1048677331811E+00
.4808955063224E+01	.9992410820993E+00	-.4124962064317E-02	.3134762459081E+01	-.7107991276470E-01
.5118693576826E+01	.9996540107782E+00	-.2208266186616E-02	.3145035231220E+01	-.4516975892487E-01
.5443841302060E+01	.9998595540863E+00	-.1087499300435E-02	.3151156826816E+01	-.2673054217728E-01
.5785190581258E+01	.9999516317220E+00	-.4848952582875E-03	.3154542741300E+01	-.1461654088364E-01
.6143569371547E+01	.9999875049676E+00	-.1906693541722E-03	.3156264896883E+01	-.7318268443818E-02
.6519184843796E+01	.9999988160676E+00	-.7017369081255E-04	.3157061548627E+01	-.3318999777001E-02
.6914915517422E+01	.1000000000000E+01	-.7400368439842E-05	.3157392289999E+01	-.1345711728537E-02
.7329733832975E+01	.1000000000000E+01	0.	.3157513510697E+01	-.4799165586366E-03
.7765289019817E+01	.1000000000000E+01	0.	.3157551914400E+01	-.1474204643688E-03
.8222620112143E+01	.1000000000000E+01	0.	.3157562138944E+01	-.3792753928925E-04
.8702817000408E+01	.1000000000000E+01	0.	.3157564337248E+01	-.7854248452431E-05
.9207023460790E+01	.1000000000000E+01	0.	.3157564696266E+01	-.1231575379420E-05
.9736440160439E+01	.1000000000000E+01	0.	.3157564736266E+01	-.1313350510542E-06
.1029232767367E+02	.1000000000000E+01	0.	.3157564738647E+01	-.7465163194249E-08
.1087600955823E+02	.1000000000000E+01	0.	.3157564738666E+01	-.5212523774571E-10
.1148887553636E+02	.1000000000000E+01	0.	.3157564738666E+01	0.

VELOCITY PROFILES AT   x/c = 0.015

y/δ_1	U/U_e	$(U/U_e)''$	W/U_e	$(W/U_e)''$
0.	0.	-.1126101582522E+00	0.	-.2983006197610E-07
.2534436810074E-01	.1633484469782E-01	-.1111602007558E+00	.3393975520078E-02	.3283626347020E-03
.5195374732482E-01	.3340817190581E-01	-.1101960792300E+00	.6957581202989E-02	.6741607956760E-03
.7988869637415E-01	.5124806955160E-01	-.1098161215313E+00	.1069922467052E-01	.1044753084382E-02
.1092121788542E+00	.6988252487118E-01	-.1102262841777E+00	.1462772719355E-01	.1443551378447E-02
.1399895743152E+00	.8933896580738E-01	-.1116305432533E+00	.1875234730601E-01	.1872183395469E-02
.1722886740841E+00	.1096436641220E+00	-.1142142977252E+00	.2308280511401E-01	.2329247887604E-02
.2061796597551E+00	.1308209896106E+00	-.1181268010773E+00	.2762930539552E-01	.2809021473036E-02
.2417350623462E+00	.1528925136720E+00	-.1234643958522E+00	.3240255642261E-01	.3300262503819E-02
.2790297004433E+00	.1758759718282E+00	-.1302566067679E+00	.3741378006264E-01	.3785286027233E-02
.3181405961650E+00	.1997841076046E+00	-.1384571788098E+00	.4267470723361E-01	.4239493105581E-02
.3591468685305E+00	.2246234328013E+00	-.1479418481585E+00	.4819755137774E-01	.4631518474517E-02
.4021296048072E+00	.2503929494398E+00	-.1585139681479E+00	.5399495150565E-01	.4924106073760E-02
.4471717116699E+00	.2770828841797E+00	-.1699181106996E+00	.6007987581158E-01	.5075730099335E-02
.4943577494979E+00	.3046734846910E+00	-.1818605346148E+00	.6646547709519E-01	.5042855603385E-02
.5437737548842E+00	.3331339182671E+00	-.1940341503448E+00	.7316489236860E-01	.4782591752920E-02
.5955070584039E+00	.3624212964102E+00	-.2061445634587E+00	.8019098099366E-01	.4255358554456E-02
.6496461069285E+00	.3924798278801E+00	-.2179332082796E+00	.8755599811423E-01	.3427098948331E-02
.7062803023028E+00	.4232400815623E+00	-.2291936947628E+00	.9527120233556E-01	.2270563327815E-02
.7654998710941E+00	.4546183257989E+00	-.2397783735087E+00	.1033463976326E+00	.7653094383162E-03
.8273957834206E+00	.4865159091442E+00	-.2495936935335E+00	.1117894083988E+00	-.1103683478024E-02
.8920597425812E+00	.5188186639628E+00	-.2585849249107E+00	.1206054828170E+00	-.3348508741100E-02
.9595842711985E+00	.5513963506436E+00	-.2667128453707E+00	.1297966136586E+00	-.5981224206665E-02
.1030062923572E+01	.5841022135667E+00	-.2739266034877E+00	.1393607588262E+00	-.9016068852160E-02
.1103590657387E+01	.6167727824165E+00	-.2801378031779E+00	.1492909394967E+00	-.1246979132402E-01
.1180264400120E+01	.6492281122014E+00	-.2852007236971E+00	.1595741955713E+00	-.1635908942657E-01
.1260183845588E+01	.6812726989599E+00	-.2889025632565E+00	.1701903900174E+00	-.2069474643750E-01
.1343452513156E+01	.7126973234213E+00	-.2909659663792E+00	.1811108775252E+00	-.2547287783002E-01
.1430179095430E+01	.7432820533919E+00	-.2910642841860E+00	.1922970876321E+00	-.3066449310728E-01
.1520479109006E+01	.7728005740225E+00	-.2888484148801E+00	.2036991141000E+00	-.3620502862348E-01
.1614476846766E+01	.8010259148984E+00	-.2839829093915E+00	.2152544455980E+00	-.4198547078939E-01
.1712307609112E+01	.8277375091047E+00	-.2761883245218E+00	.2268870135758E+00	-.4784631120205E-01
.1814120166114E+01	.8527293586326E+00	-.2652817277926E+00	.2385067701257E+00	-.5357526001810E-01
.1920079373827E+01	.8758189507003E+00	-.2512223817288E+00	.2500100408607E+00	-.5890982546131E-01
.2030368839530E+01	.8968563294466E+00	-.2341492901521E+00	.2612809200481E+00	-.6354652520476E-01
.2145193507832E+01	.9157325620380E+00	-.2143922388978E+00	.2721939718559E+00	-.6715900730861E-01
.2264782023736E+01	.9323868898614E+00	-.1924742411713E+00	.2826184461076E+00	-.6942691717630E-01
.2389388724846E+01	.9468117304558E+00	-.1690929270852E+00	.2924240795561E+00	-.7007503793191E-01
.2519295129529E+01	.9590547306330E+00	-.1450702177855E+00	.3014883194335E+00	-.6891815404241E-01
.2654810818808E+01	.9692173715550E+00	-.1212831385087E+00	.3097044943797E+00	-.6590294490567E-01
.2796274353288E+01	.9774499348144E+00	-.9858438038896E-01	.3169901284400E+00	-.6113615333631E-01
.2944049319957E+01	.9839430121872E+00	-.7772296084817E-01	.3232943333231E+00	-.5488976502118E-01
.3098530262280E+01	.9889161562921E+00	-.5927725054144E-01	.3286031088092E+00	-.4757871764394E-01
.3260134104987E+01	.9926046488535E+00	-.4360998636778E-01	.3329414917936E+00	-.3971299489238E-01
.3429301737248E+01	.9952456630905E+00	-.3085523779715E-01	.3363718439507E+00	-.3183183484079E-01
.3606495261838E+01	.9970651375479E+00	-.2092652537428E-01	.3389881369020E+00	-.2443199413447E-01
.3792196041573E+01	.9982668434819E+00	-.1355460155801E-01	.3409068078900E+00	-.1790406622886E-01
.3986903067519E+01	.9990248489848E+00	-.8353108752994E-02	.3422554720870E+00	-.1249003141665E-01
.4191131855179E+01	.9994796419136E+00	-.4880045567272E-02	.3431612825183E+00	-.8270756539628E-02
.4405414031809E+01	.9997380026518E+00	-.2691781574606E-02	.3437408240655E+00	-.5184454839397E-02
.4630297689398E+01	.9998762238162E+00	-.1394977634937E-02	.3440930265398E+00	-.3068463296512E-02
.4866348484493E+01	.9999542191499E+00	-.6745433944613E-03	.3442957880184E+00	-.1710700071762E-02
.5114151392744E+01	.9999776204721E+00	-.3014199081978E-03	.3444060874831E+00	-.8964637689217E-03
.5374312971199E+01	.9999915110215E+00	-.1240000563958E-03	.3444626527933E+00	-.4407168589718E-03
.5647463953357E+01	.9999970632564E+00	-.4726021917029E-04	.3444899416275E+00	-.2029061197045E-03
.5934261989833E+01	.9999990980766E+00	-.1656916328925E-04	.3445023012768E+00	-.8734740764998E-04
.6235394365109E+01	.9999978678556E+00	-.5255890877892E-05	.3445075467010E+00	-.3510093036894E-04
.6551580589209E+01	.9999999581749E+00	-.1468541736643E-05	.3445096287143E+00	-.1314852373336E-04
.6883574834486E+01	.1000000000000E+01	-.3702138577621E-06	.3445104000901E+00	-.4583611075284E-05
.7232168232449E+01	.1000000000000E+01	0.	.3445106663062E+00	-.1484564852046E-05
.7598191075231E+01	.1000000000000E+01	0.	.3445107516772E+00	-.4457160004695E-06
.7982514976700E+01	.1000000000000E+01	0.	.3445107770498E+00	-.1235548596783E-06
.8386055044741E+01	.1000000000000E+01	0.	.3445107840499E+00	-.3168830899148E-07
.8809772106636E+01	.1000000000000E+01	0.	.3445107858461E+00	-.7583699348645E-08
.9254675019014E+01	.1000000000000E+01	0.	.3445107862669E+00	-.1651855959742E-08
.9721823077010E+01	.1000000000000E+01	0.	.3445107863568E+00	-.3199111342369E-09
.1021232853791E+02	.1000000000000E+01	0.	.3445107863760E+00	-.7996704991388E-10

APPENDIX

VELOCITY PROFILES AT   x/c = 0.020

y/δ_1	U/U_e	$(U/U_e)''$	W/U_e	$(W/U_e)''$
0.	0.	-.8409510140700E-01	0.	-.1726685216363E-01
.2015941189193E-01	.1205097685616E-01	-.8322468390243E-01	.3004425526598E-02	-.1694107319206E-01
.4132580513009E-01	.2466751212352E-01	-.8236256119804E-01	.6151515565605E-02	-.1658813911888E-01
.6354831614926E-01	.3787385427209E-01	-.8150179257689E-01	.9447635495404E-02	-.1619840267206E-01
.8687824870497E-01	.5169500489347E-01	-.8044749813657E-01	.1289940472116E-01	-.1577815937463E-01
.1113691290331E+00	.6615681678413E-01	-.7902099574156E-01	.1651370194643E-01	-.1533261437431E-01
.1370767552464E+00	.8128612680687E-01	-.7708597304549E-01	.2029766995589E-01	-.1486444323660E-01
.1640592393995E+00	.9711091222274E-01	-.7457507630691E-01	.2425872094099E-01	-.1437243670293E-01
.1923770403662E+00	.1136604474678E+00	-.7151368796908E-01	.2840454404653E-01	-.1385048813671E-01
.2220929853459E+00	.1309654246438E+00	-.6803725650745E-01	.3274311745241E-01	-.1328721555831E-01
.2532722774609E+00	.1490579867710E+00	-.6439861003742E-01	.3728272775632E-01	-.1266650237563E-01
.2859824865535E+00	.1679716103070E+00	-.6096236521563E-01	.4203199945092E-01	-.1196917735614E-01
.3202935199786E+00	.1877407653334E+00	-.5818488634338E-01	.4699993660195E-01	-.1117592586200E-01
.3562775699867E+00	.2084002810751E+00	-.5658017918644E-01	.5219597714000E-01	-.1027133258005E-01
.3940090342882E+00	.2299843535566E+00	-.5667438471226E-01	.5763005725591E-01	-.9248718187116E-02
.4335644066828E+00	.2525251525277E+00	-.5895378544756E-01	.6331267918308E-01	-.8115183647825E-02
.4750221353556E+00	.2760510157438E+00	-.6381296583485E-01	.6925497037879E-01	-.6896069107555E-02
.5184624476842E+00	.3005842573122E+00	-.7151049557253E-01	.7546871635710E-01	-.5637934023547E-02
.5639671422809E+00	.3261386578803E+00	-.8213888067165E-01	.8196634412148E-01	-.4409234727016E-02
.6116193515747E+00	.3527167411355E+00	-.9561346828692E-01	.8876082950763E-01	-.3298158614815E-02
.6615032815398E+00	.3803069665773E+00	-.1116817687568E+00	.9586550098515E-01	-.2407568478250E-02
.7137039392005E+00	.4088809778286E+00	-.1299508912012E+00	.1032937153855E+00	-.1847645174934E-02
.7683068632128E+00	.4383910377313E+00	-.1499273313703E+00	.1110583875491E+00	-.1727439894797E-02
.8253978780549E+00	.4687677598743E+00	-.1710610705360E+00	.1191713647420E+00	-.2146943839593E-02
.8850628980077E+00	.4999182195180E+00	-.1927854707842E+00	.1276426454951E+00	-.3191236415487E-02
.9473878129556E+00	.5317245063284E+00	-.2145459590827E+00	.1364794484722E+00	-.4927665482374E-02
.1012458493740E+01	.5640427776243E+00	-.2358136165361E+00	.1456851382392E+00	-.7405931819293E-02
.1080360959820E+01	.5967028903292E+00	-.2560837229394E+00	.1552580119521E+00	-.1065973088049E-01
.1151181755617E+01	.6295087315708E+00	-.2748630439507E+00	.1651899478834E+00	-.1470775130457E-01
.1225008583131E+01	.6622394226179E+00	-.2916522941567E+00	.1754649197512E+00	-.1955179171921E-01
.1301931236286E+01	.6946516225134E+00	-.3059312278220E+00	.1860573965394E+00	-.2517066592033E-01
.1382042875746E+01	.7264831871798E+00	-.3171530804464E+00	.1969306792262E+00	-.3151008806248E-01
.1465441670748E+01	.7574584298699E+00	-.3247599860237E+00	.2080352716391E+00	-.3847019473431E-01
.1552232816265E+01	.7872951177673E+00	-.3282054690609E+00	.2193074360299E+00	-.4589311260188E-01
.1642530908558E+01	.8157132714467E+00	-.3269951416902E+00	.2306681375156E+00	-.5355296440263E-01
.1736462629192E+01	.8424456527728E+00	-.3207598680232E+00	.2420226301454E+00	-.6115505051597E-01
.1834169650560E+01	.8672494349597E+00	-.3093210447085E+00	.2532609773756E+00	-.6831467882662E-01
.1935811638100E+01	.8899183757398E+00	-.2927503575009E+00	.2642598240139E+00	-.7461423939805E-01
.2041569188193E+01	.9102945964584E+00	-.2714246195142E+00	.2748857255822E+00	-.7958353749147E-01
.2151646515127E+01	.9282787805659E+00	-.2460485526437E+00	.2850002593376E+00	-.8276586059816E-01
.2266273693528E+01	.9438375428586E+00	-.2176342078938E+00	.2944669515516E+00	-.8377211096410E-01
.2385708278487E+01	.9570068421536E+00	-.1874337207339E+00	.3031597445112E+00	-.8235076831637E-01
.2510236165882E+01	.9678906173008E+00	-.1568296418797E+00	.3109723291099E+00	-.7844820138653E-01
.2640171617731E+01	.9766543225627E+00	-.1271982881970E+00	.3178272733175E+00	-.7224800612283E-01
.2775856455519E+01	.9835136501617E+00	-.9976257782905E-01	.3236836028022E+00	-.6417110454748E-01
.2917658506724E+01	.9887194841612E+00	-.7547528029112E-01	.3285414499171E+00	-.5483200229708E-01
.3065969470124E+01	.9925405380076E+00	-.5494124906360E-01	.3324426523438E+00	-.4495631322845E-01
.3221202437148E+01	.9952455124507E+00	-.3837799734216E-01	.3354667612931E+00	-.3527524562802E-01
.3383789043205E+01	.9970870713509E+00	-.2565233467243E-01	.3377227380317E+00	-.2641973915511E-01
.3554178646287E+01	.9982893048447E+00	-.1636186976999E-01	.3393375073163E+00	-.1883819646406E-01
.3732833462240E+01	.9990397080784E+00	-.9931323568747E-02	.3404432483814E+00	-.1275601839271E-01
.3920230446439E+01	.9994862014941E+00	-.5721033122366E-02	.3411655846782E+00	-.8183284571121E-02
.4116859482619E+01	.9997386917526E+00	-.3119321809294E-02	.3416145440046E+00	-.4962730446608E-02
.4323224248259E+01	.9998739764024E+00	-.1604217523059E-02	.3418793731700E+00	-.2839325098174E-02
.4539843567898E+01	.9999424799349E+00	-.7761462754239E-03	.3420272833215E+00	-.1529697404393E-02
.4767253403782E+01	.9999752095471E+00	-.3528279328150E-03	.3421053295416E+00	-.7747283258133E-03
.5006009284032E+01	.9999899372812E+00	-.1505592746919E-03	.3421441561263E+00	-.3682558100562E-03
.5256688947178E+01	.9999961643634E+00	-.6020776524860E-04	.3421623308260E+00	-.1640338926398E-03
.5519895006710E+01	.9999986308253E+00	-.2250365525604E-04	.3421703202760E+00	-.6836438202708E-04
.5796257502527E+01	.9999995427408E+00	-.7824036186349E-05	.3421736119519E+00	-.2661571312623E-04
.6086436275467E+01	.9999998571170E+00	-.2524961666889E-05	.3421748804014E+00	-.9662972993330E-05
.6391123162525E+01	.9999999583893E+00	-.7604302165337E-06	.3421753365736E+00	-.3265314178922E-05
.6711044051831E+01	.9999999887486E+00	-.2128372620964E-06	.3421754893080E+00	-.1024711866581E-05
.7046960854288E+01	.9999999971815E+00	-.5509079951055E-07	.3421755368035E+00	-.2979728496472E-06
.7399673450423E+01	.9999999993456E+00	-.1313092456883E-07	.3421755504868E+00	-.8013155999480E-07
.7770021661304E+01	.9999999998597E+00	-.2896240163768E-08	.3421755541253E+00	-.1985809903279E-07
.8158887278059E+01	.9999999999721E+00	-.5850868198870E-09	.3421755550143E+00	-.4522865670239E-08
.8567196174450E+01	.9999999999948E+00	-.1080912612398E-09	.3421755552116E+00	-.9378092871769E-09
.8995920515660E+01	.9999999999993E+00	-.2004446922921E-10	.3421755552506E+00	-.1577690328830E-09
.9446081073931E+01	.1000000000000E+01	-.3576477474279E-11	.3421755552603E+00	-.4781785446616E-10

APPENDIX

VELOCITY PROFILES AT   x/c = 0.711

y/δ_1	U/U_e	$(U/U_e)''$	W/U_e	$(W/U_e)''$
0.	0.	-.1887760665209E+01	0.	-.8808355300207E+00
.4722884351474E-02	.5071249068631E-02	-.1862194460472E+01	.2187863031303E-02	-.8726303320039E+00
.9681873101277E-02	.1035131371499E-01	-.1834653561820E+01	.4464152273465E-02	-.8642960039979E+00
.1488872348879E-01	.1584673216485E-01	-.1804415937637E+01	.6831341216094E-02	-.8557185126940E+00
.2035577027018E-01	.2156411924231E-01	-.1774843669608E+01	.9291855576385E-02	-.8467162683344E+00
.2609595289283E-01	.2751006004590E-01	-.1748947135177E+01	.1184806293487E-01	-.8371367277485E+00
.3212284376061E-01	.3369096954302E-01	-.1728955116776E+01	.1450226227684E-01	-.8268842731716E+00
.3845067760528E-01	.4011292900208E-01	-.1715938012823E+01	.1725667239282E-01	-.8159417103562E+00
.4509438198012E-01	.4678151855285E-01	-.1709554577808E+01	.2011341761371E-01	-.8043796302696E+00
.5206960889541E-01	.5370167273581E-01	-.1707988462340E+01	.2307450907252E-01	-.7923487093328E+00
.5939276762330E-01	.6087759046550E-01	-.1708121814008E+01	.2614181979642E-01	-.7800523381695E+00
.6708105871027E-01	.6831272990938E-01	-.1705958398626E+01	.2931705263805E-01	-.7677007895806E+00
.7515250924902E-01	.7600991020475E-01	-.1697260933875E+01	.3260170147349E-01	-.7554530629056E+00
.8362600947523E-01	.8397152469133E-01	-.1678314042271E+01	.3599700817756E-01	-.7433576441078E+00
.9252135076438E-01	.9219984549538E-01	-.1646677288246E+01	.3950392032207E-01	-.7313072763651E+00
.1018592651057E+00	.1006973707317E+00	-.1601766647569E+01	.4312305670300E-01	-.7190237600164E+00
.1116614661199E+00	.1094671400616E+00	-.1545110992377E+01	.4685468879011E-01	-.7060852940697E+00
.1219506916622E+00	.1185129306184E+00	-.1480180551291E+01	.5069874502521E-01	-.6920002752259E+00
.1327500740138E+00	.1278392519890E+00	-.1411721327903E+01	.5465548085765E-01	-.6763186151980E+00
.1440865556202E+00	.1374510912944E+00	-.1345062660257E+01	.5872233051714E-01	-.6587572937575E+00
.1559841962929E+00	.1473534158788E+00	-.1284498584545E+01	.6290036798114E-01	-.6393055974396E+00
.1684709617733E+00	.1575505114188E+00	-.1232853906219E+01	.6718795694203E-01	-.6182726648168E+00
.1815754035679E+00	.1680452973547E+00	-.1190657349065E+01	.7158396633695E-01	-.5962498127406E+00
.1953273840196E+00	.1788387971152E+00	-.1156199288805E+01	.7608709254953E-01	-.5739832999266E+00
.2097581286640E+00	.1899299258603E+00	-.1126122043315E+01	.8069576323524E-01	-.5521846909399E+00
.2249002800207E+00	.2013156877780E+00	-.1096428602069E+01	.8540799872675E-01	-.5313349602363E+00
.2407879530428E+00	.2129917609599E+00	-.1063608399396E+01	.9022126859795E-01	-.5115511599272E+00
.2574567924700E+00	.2249533251425E+00	-.1025528302023E+01	.9513239360823E-01	-.4925703651996E+00
.2749440322613E+00	.2371959019280E+00	-.9818222418103E+00	.1001375381309E+00	-.4738646648987E+00
.2932885571348E+00	.2497159681670E+00	-.9336914774989E+00	.1052323126084E+00	-.4548471884773E+00
.3125309660275E+00	.2625111844067E+00	-.8832453489601E+00	.1104119668422E+00	-.4350883307591E+00
.3327136370812E+00	.2755802261472E+00	-.8326823545335E+00	.1156716193582E+00	-.4144538264074E+00
.3538807706382E+00	.2889223533713E+00	-.7835471535886E+00	.1210064540887E+00	-.3931139100938E+00
.3760785707472E+00	.3025369802823E+00	-.7364907167221E+00	.1264118330965E+00	-.3714319823065E+00
.3993550818788E+00	.3164234488856E+00	-.6914505803777E+00	.1318833163359E+00	-.3498118000457E+00
.4237604859023E+00	.3305810812616E+00	-.6479295930191E+00	.1374166249384E+00	-.3285430485904E+00
.4493470545599E+00	.3450095191889E+00	-.6054855852533E+00	.1430076092801E+00	-.3077685557651E+00
.4761692405254E+00	.3597091592156E+00	-.5640429666030E+00	.1486522736118E+00	-.2875096674953E+00
.5042837547890E+00	.3746841551275E+00	-.5238615022866E+00	.1543468715090E+00	-.2677491512337E+00
.5337495895952E+00	.3899289966047E+00	-.4853758912441E+00	.1600880444845E+00	-.2485032709656E+00
.5646281747401E+00	.4054553694860E+00	-.4490016759564E+00	.1658729539243E+00	-.2298500941830E+00
.5969833510484E+00	.4212648869330E+00	-.4150133802039E+00	.1716993637728E+00	-.2119123844037E+00
.6308814753204E+00	.4373622943525E+00	-.3835394529380E+00	.1775656593795E+00	-.1948188004082E+00
.6663914676030E+00	.4537524879569E+00	-.3546162168804E+00	.1834708162893E+00	-.1786722904477E+00
.7035848639399E+00	.4704402266264E+00	-.3282654400878E+00	.1894143433347E+00	-.1635412641443E+00
.7425358657678E+00	.4874297572096E+00	-.3045045053901E+00	.1953962132259E+00	-.1494690201654E+00
.7833213859756E+00	.5047243236202E+00	-.2833181089951E+00	.2014167740879E+00	-.1364861449112E+00
.8260210915380E+00	.5223255898681E+00	-.2646601602902E+00	.2074766251832E+00	-.1246149451671E+00
.8707174433187E+00	.5402329756207E+00	-.2484318440768E+00	.2135764453083E+00	-.1138660509525E+00
.9174957346783E+00	.5584429574488E+00	-.2344933064466E+00	.2197167748548E+00	-.1042338228460E+00
.9664441312595E+00	.5769483449243E+00	-.2226836325449E+00	.2258977596642E+00	-.9569585507929E-01
.1017653715232E+01	.5957375173257E+00	-.2128222685042E+00	.2321188627723E+00	-.8821497689810E-01
.1071218538349E+01	.6147936412933E+00	-.2047161555465E+00	.2383785467785E+00	-.8174138317627E-01
.1127235689209E+01	.6340938789285E+00	-.1981641108777E+00	.2446739308142E+00	-.7621382369341E-01
.1185805381593E+01	.6536086022522E+00	-.1929595548496E+00	.2510004209812E+00	-.7156061964545E-01
.1247031072585E+01	.6733006364053E+00	-.1888934144609E+00	.2573513884386E+00	-.6770092023935E-01
.1311019620962E+01	.6931245558441E+00	-.1857549028743E+00	.2637177196067E+00	-.6454603242573E-01
.1377881498257E+01	.7130260685690E+00	-.1833311672024E+00	.2700875696740E+00	-.6200064654261E-01
.1447731066759E+01	.7329415346655E+00	-.1814070321941E+00	.2764460240763E+00	-.5996407909825E-01
.1520686940344E+01	.7527976744020E+00	-.1797645467229E+00	.2827748798207E+00	-.5833166626695E-01
.1596872445477E+01	.7725115320531E+00	-.1781833939663E+00	.2890525089760E+00	-.5699630062185E-01
.1676416200197E+01	.7919907699231E+00	-.1764424810167E+00	.2952538403687E+00	-.5585035450093E-01
.1759452828505E+01	.8111343694720E+00	-.1743232938069E+00	.3013504871548E+00	-.5478744923152E-01
.1846123825667E+01	.8298338140359E+00	-.1716151450176E+00	.3073106466959E+00	-.5370521007615E-01
.1936578586321E+01	.8479748156945E+00	-.1681221983814E+00	.3131015952741E+00	-.5250798149749E-01
.2030975601530E+01	.8654396291103E+00	-.1636719119673E+00	.3186863932190E+00	-.5111007077661E-01
.2129483823007E+01	.8821099668024E+00	-.1581244003217E+00	.3240288059144E+00	-.4943917290321E-01
.2232284182556E+01	.8978704937569E+00	-.1513821808925E+00	.3290924330270E+00	-.4743981562262E-01
.2339571242798E+01	.9126128341213E+00	-.1433997761217E+00	.3338424224137E+00	-.4507660171672E-01
.2451554941817E+01	.9262399678554E+00	-.1341925726733E+00	.3382469247667E+00	-.4233700430755E-01
.2568462380568E+01	.9386708296580E+00	-.1238440877859E+00	.3422786403862E+00	-.3923343571525E-01
.2690539588860E+01	.9498448476730E+00	-.1125103751208E+00	.3459163311341E+00	-.3580424926642E-01
.2818053194997E+01	.9597260819020E+00	-.1004198832109E+00	.3491462601403E+00	-.3211326389401E-01

VELOCITY PROFILES AT   x/c = 0.711 - Concluded

y/δ_1	U/U_e	$(U/U_e)''$	W/U_e	$(W/U_e)''$
.2951291917673E+01	.9683065553938E+00	-.8786693125463E-01	.3519633623287E+00	-.2824737450078E-01
.3090567798385E+01	.9756083353124E+00	-.7519735670709E-01	.3543720493015E+00	-.2431189312436E-01
.3236217100337E+01	.9816839395659E+00	-.6278594730015E-01	.3563864990064E+00	-.2042350790537E-01
.3388600817045E+01	.9866147389017E+00	-.5100690085593E-01	.3580303205324E+00	-.1670115323342E-01
.3548104761164E+01	.9905072049093E+00	-.4020042211933E-01	.3593355319386E+00	-.1325559384193E-01
.3715139240698E+01	.9934871135390E+00	-.3064015695138E-01	.3603408641821E+00	-.1017901293532E-01
.3890138373336E+01	.9956921199579E+00	-.2250693232563E-01	.3610894979808E+00	-.7536199604701E-02
.4073559135981E+01	.9972634183100E+00	-.1587380330047E-01	.3616264378112E+00	-.5358907797750E-02
.4265880289432E+01	.9983374177772E+00	-.1070559709597E-01	.3619958066539E+00	-.3644533396139E-02
.4467601350314E+01	.9990384343176E+00	-.6873292347741E-02	.3622383829955E+00	-.2359469851805E-02
.4679241796113E+01	.9994732708833E+00	-.4180374219435E-02	.3623896797839E+00	-.1446528561353E-02
.4901340678207E+01	.9997282413210E+00	-.2395679329573E-02	.3624787788306E+00	-.8349152987557E-03
.5134456779643E+01	.9998687472919E+00	-.1286023212702E-02	.3625279978906E+00	-.4507194049000E-03
.5379169391944E+01	.9999410550174E+00	-.6425116188652E-03	.3625533139138E+00	-.2258860570219E-03
.5636079707889E+01	.9999755660102E+00	-.2966758988771E-03	.3625653366087E+00	-.1042112845609E-03
.5905812749849E+01	.9999907276234E+00	-.1256474034227E-03	.3625705576031E+00	-.4382880293246E-04
.6189019692825E+01	.9999968086324E+00	-.4840880848089E-04	.3625726076830E+00	-.1661577543386E-04
.6486380411719E+01	.9999990149503E+00	-.1681501592012E-04	.3625733259621E+00	-.5602939814210E-05
.6798606089943E+01	.9999997313727E+00	-.5212623985215E-05	.3625735469482E+00	-.1653791455881E-05
.7126441766794E+01	.9999999367179E+00	-.1423999643106E-05	.3625736054709E+00	-.4188590337662E-06
.7470668760190E+01	.9999999876146E+00	-.3365391211712E-06	.3625736184699E+00	-.8870848981542E-07
.7832106960822E+01	.9999999981382E+00	-.6659839018906E-07	.3625736208060E+00	-.1515691225418E-07
.8211617037362E+01	.9999999998243E+00	-.1028772285628E-07	.3625736211280E+00	-.1976800893776E-08
.8610102612159E+01	.1000000000000E+01	-.1106551291248E-08	.3625736211596E+00	-.1989456525088E-09

VELOCITY PROFILES AT x/c = 0.761

y/δ_1	U/U_e	$(U/U_e)''$	W/U_e	$(W/U_e)''$
0.	0.	-.2855202796549E+01	0.	-.1352444053169E+01
.5844321942936E-02	.7792323838424E-02	-.2817545195213E+01	.3376188347912E-02	-.1332280931692E+01
.1198074663227E-01	.1587054125512E-01	-.2780018746685E+01	.6872146684751E-02	-.1311639086575E+01
.1842374325472E-01	.2423968224845E-01	-.2742269221390E+01	.1048960728093E-01	-.1290200858015E+01
.2518847595979E-01	.3290423641915E-01	-.2702074671790E+01	.1423007097297E-01	-.1268069863130E+01
.3229083437464E-01	.4186817341386E-01	-.2657460280452E+01	.1809477454808E-01	-.1245331278957E+01
.3974746520154E-01	.5113499185242E-01	-.2606697952346E+01	.2208465601426E-01	-.1222033723234E+01
.4757580492783E-01	.6070778583440E-01	-.2549947978374E+01	.2620031905410E-01	-.1198175683335E+01
.5579411367625E-01	.7058931002236E-01	-.2486616769778E+01	.3044199849993E-01	-.1173700303491E+01
.6442151021860E-01	.8078201719762E-01	-.2418189125348E+01	.3480952900439E-01	-.1148501701961E+01
.7347800816903E-01	.9128803830530E-01	-.2346698786818E+01	.3930231901098E-01	-.1122444355099E+01
.8298455336599E-01	.1021090767980E+00	-.2274732597064E+01	.4391933146074E-01	-.1095394464275E+01
.9296306244560E-01	.1132461986092E+00	-.2204999306422E+01	.4865907129889E-01	-.1067258914881E+01
.1034364626088E+00	.1246995171457E+00	-.2139838823726E+01	.5351957784482E-01	-.1038024102261E+01
.1144287325920E+00	.1364677979257E+00	-.2080741483618E+01	.5849841780496E-01	-.1007784507215E+01
.1259649448713E+00	.1485480357358E+00	-.2027990135847E+01	.6359267280003E-01	-.9767505782172E+00
.1380713091622E+00	.1609350814352E+00	-.1980521872155E+01	.6879891465279E-01	-.9452281648210E+00
.1507752173256E+00	.1736214070401E+00	-.1936071424574E+01	.7411316329207E-01	-.9135677886704E+00
.1641052898384E+00	.1865970882373E+00	-.1891597417386E+01	.7953082659617E-01	-.8820907310734E+00
.1780914240404E+00	.1998500485349E+00	-.1843918517656E+01	.8504662865193E-01	-.8510082653524E+00
.1927648446013E+00	.2133665515006E+00	-.1790418927389E+01	.9065454136442E-01	-.8203572399862E+00
.2081581550629E+00	.2271318587394E+00	-.1729644854620E+01	.9634774142672E-01	-.7899761095839E+00
.2243053948948E+00	.2411309113977E+00	-.1661624564483E+01	.1021186168291E+00	-.7595378507863E+00
.2412420952580E+00	.2553488654356E+00	-.1587810344475E+01	.1079588412054E+00	-.7286400012108E+00
.2590053406224E+00	.2697713340244E+00	-.1510648174513E+01	.1138595193717E+00	-.6969311565595E+00
.2776338321418E+00	.2843842681251E+00	-.1432898263673E+01	.1198113861777E+00	-.6642351955242E+00
.2971679542794E+00	.2991735215227E+00	-.1356915059657E+01	.1258050203123E+00	-.6306282045211E+00
.3176498446047E+00	.3141242625174E+00	-.1284112641459E+01	.1318310245548E+00	-.5964358017131E+00
.3391234669496E+00	.3292204653918E+00	-.1214776987869E+01	.1378801321047E+00	-.5621446756746E+00
.3616346882006E+00	.3444447049379E+00	-.1148259545746E+01	.1439432262022E+00	-.5282630497529E+00
.3852313590992E+00	.3597783802484E+00	-.1083444415612E+01	.1500112983474E+00	-.4951826251060E+00
.4099633993992E+00	.3752023424620E+00	-.1019279696229E+01	.1560754019130E+00	-.4631000485701E+00
.4358828879182E+00	.3906977617152E+00	-.9552222139406E+00	.1621266653638E+00	-.4320255085288E+00
.4630441573836E+00	.4062469620974E+00	-.8913349854572E+00	.1681564053741E+00	-.4018643013928E+00
.4915038942866E+00	.4218340316815E+00	-.8281173663128E+00	.1741563348026E+00	-.3725235456269E+00
.5213212429968E+00	.4374451529909E+00	-.7662978984721E+00	.1801188170710E+00	-.3439910374376E+00
.5525579133676E+00	.4530686593196E+00	-.7065212422728E+00	.1860370998394E+00	-.3163549984614E+00
.5852782910280E+00	.4686949968509E+00	-.6491726915726E+00	.1919054766447E+00	-.2897685951845E+00
.6195495496836E+00	.4843167779864E+00	-.5944249076476E+00	.1977193647936E+00	-.2643915940816E+00
.6554417650072E+00	.4999289588847E+00	-.5423492930554E+00	.2034753256687E+00	-.2403448875821E+00
.6930280298885E+00	.5155290821611E+00	-.4930273277968E+00	.2091710677466E+00	-.2176969189823E+00
.7323845706005E+00	.5311174624523E+00	-.4466024265694E+00	.2148054584377E+00	-.1964776638798E+00
.7735908629050E+00	.5466972022461E+00	-.4032580407399E+00	.2203785416352E+00	-.1767019410342E+00
.8167297466655E+00	.5622739993845E+00	-.3631691893137E+00	.2258915346258E+00	-.1583843102951E+00
.8618875375636E+00	.5778557641672E+00	-.3264504852529E+00	.2313467751153E+00	-.1415389919969E+00
.9091541524718E+00	.5934521122925E+00	-.2931504843248E+00	.2367476051522E+00	-.1261707062585E+00
.9586231258217E+00	.6090737514367E+00	-.2632698705050E+00	.2420981981871E+00	-.1122658303920E+00
.1010391885285E+01	.6247317339714E+00	-.2367577048066E+00	.2474033428732E+00	-.9979611312481E-01
.1064561675486E+01	.6404365953758E+00	-.2135238868551E+00	.2526681912958E+00	-.8871212523132E-01
.1121237743898E+01	.6561973635614E+00	-.1934342277763E+00	.2578979704770E+00	-.7895675336969E-01
.1180529424969E+01	.6720204749815E+00	-.1763050549803E+00	.2630976545768E+00	-.7046130732424E-01
.1242550244615E+01	.6879086583431E+00	-.1619117231325E+00	.2682716036359E+00	-.6314652600127E-01
.1307418047260E+01	.7038598208171E+00	-.1499944645267E+00	.2734231765888E+00	-.5692322332513E-01
.1375255130004E+01	.7198659885343E+00	-.1402667745518E+00	.2785543390173E+00	-.5169373069811E-01
.1446188416391E+01	.7359123521953E+00	-.1324249354935E+00	.2836652746890E+00	-.4735364901679E-01
.1520349666426E+01	.7519764662565E+00	-.1261573373617E+00	.2887542046219E+00	-.4379374352635E-01
.1597875742048E+01	.7680276494508E+00	-.1211542857666E+00	.2938161534827E+00	-.4090210868588E-01
.1678908934525E+01	.7840266252552E+00	-.1171171735275E+00	.2988445185109E+00	-.3856661752420E-01
.1763597379103E+01	.7999254315666E+00	-.1137660003016E+00	.3038290678528E+00	-.3667745644847E-01
.1852095560864E+01	.8156676220773E+00	-.1108452360266E+00	.3087567765516E+00	-.3512953539127E-01
.1944564932640E+01	.8311887742222E+00	-.1081217539110E+00	.3136116788898E+00	-.3382462331731E-01
.2041174655830E+01	.8464173155495E+00	-.1054156142429E+00	.3183750261836E+00	-.3267309858891E-01
.2142102476312E+01	.8612756790127E+00	-.1025425874607E+00	.3230255751467E+00	-.3159526345267E-01
.2247535742388E+01	.8756817977810E+00	-.9937160056835E-01	.3275400117097E+00	-.3052227304428E-01
.2357672569823E+01	.8895509480462E+00	-.9579529699376E-01	.3318935120888E+00	-.2939677944998E-01
.2472723151563E+01	.9027979408992E+00	-.9173572727441E-01	.3360604388422E+00	-.2817341699452E-01
.2592911203707E+01	.9153396488776E+00	-.8714491895502E-01	.3400151638833E+00	-.2681921433159E-01
.2718475530639E+01	.9270978276404E+00	-.8200603183907E-01	.3437330023708E+00	-.2531395749123E-01
.2849671682691E+01	.9380021584866E+00	-.7633472227271E-01	.3471912309432E+00	-.2365045410096E-01
.2986773669487E+01	.9479933949604E+00	-.7018012173020E-01	.3503701511178E+00	-.2193458161019E-01
.3130075681906E+01	.9570264502204E+00	-.6362472268822E-01	.3532541448308E+00	-.1988495641968E-01
.3279893766608E+01	.9650732166555E+00	-.5678246350037E-01	.3558326555013E+00	-.1783204566872E-01
.3436567390573E+01	.9721248725080E+00	-.4979441728830E-01	.3581010164797E+00	-.1571656439711E-01

APPENDIX

VELOCITY PROFILES AT   x/c = 0.761 - Concluded

y/δ_1	U/U_e	$(U/U_e)''$	W/U_e	$(W/U_e)''$
.3600460830525E+01	.9781934115250E+00	-.4282172551584E-01	.3600610427868E+00	-.1358706049095E-01
.3771964325078E+01	.9833121404462E+00	-.3603578181300E-01	.3617213031584E+00	-.1149668844963E-01
.3951494937024E+01	.9875349362479E+00	-.2960615357156E-01	.3630970024965E+00	-.9499306160836E-02
.4139497090366E+01	.9909341463546E+00	-.2368727242825E-01	.3642094306448E+00	-.7645182505003E-02
.4336442771469E+01	.9935971504569E+00	-.1840542129308E-01	.3650849733499E+00	-.5976750748259E-02
.4542831415137E+01	.9956217707381E+00	-.1384784745921E-01	.3657537325400E+00	-.4524944069912E-02
.4759189532281E+01	.9971108944674E+00	-.1005579577393E-01	.3662478594111E+00	-.3306662801822E-02
.4986070172399E+01	.9981668244169E+00	-.7022802013794E-02	.3665997552224E+00	-.2323817381346E-02
.5224052346267E+01	.9988859592443E+00	-.4698744468095E-02	.3668403288354E+00	-.1564163828306E-02
.5473740556085E+01	.9993543947950E+00	-.2999080108966E-02	.3669975053234E+00	-.1003834751267E-02
.5735764586028E+01	.9996449136706E+00	-.1817651638712E-02	.3670951495645E+00	-.6111390098153E-03
.6010779691520E+01	.9998156083814E+00	-.1040736291919E-02	.3671525042346E+00	-.3509467254806E-03
.6299467289598E+01	.9999101076730E+00	-.5598443634147E-03	.3671841548378E+00	-.1888737201725E-03
.6602536199150E+01	.9999591124739E+00	-.2812359041194E-03	.3672004455633E+00	-.9457094275385E-04
.6920724416872E+01	.9999827651026E+00	-.1310756155656E-03	.3672082017542E+00	-.4368892693376E-04
.7254801354575E+01	.9999933176942E+00	-.5628414033702E-04	.3672115851943E+00	-.1844284619488E-04
.7605570418571E+01	.9999976371786E+00	-.2210138639243E-04	.3672129224917E+00	-.7034715499315E-05
.7973871792183E+01	.9999992459553E+00	-.7872634138880E-05	.3672133951125E+00	-.2392472405124E-05
.8360585291445E+01	.9999997858539E+00	-.2520737043829E-05	.3672135420901E+00	-.7139044496165E-06
.8766633197793E+01	.9999999470342E+00	-.7171925081101E-06	.3672135815135E+00	-.1832003369722E-06
.9192983018858E+01	.9999999890102E+00	-.1781982680373E-06	.3672135903998E+00	-.3939282688443E-07
.9640650175698E+01	.9999999982233E+00	-.3747462679121E-07	.3672135920238E+00	-.6848196193131E-08
.1011070064976E+02	.9999999998142E+00	-.6243387350974E-08	.3672135922519E+00	-.9132840601644E-09
.1060425363971E+02	.1000000000000E+01	-.7628004315351E-09	.3672135922743E+00	-.9187528810476E-10

APPENDIX

VELOCITY PROFILES AT   x/c = 0.791

y/δ_1	U/U_e	$(U/U_e)''$	W/U_e	$(W/U_e)''$
0.	0.	-.3287941150295E+01	0.	-.1616045985487E+01
.6564099793244E-02	.9489342068975E-02	-.3234063955348E+01	.4293884946491E-02	-.1587728906186E+01
.1345622137663E-01	.1930291976011E-01	-.3180095817705E+01	.8728719792259E-02	-.1558931982466E+01
.2069254743559E-01	.2944404109539E-01	-.3125465335634E+01	.1330534687672E-01	-.1529254180129E+01
.2829002575933E-01	.3991516870041E-01	-.3068433946103E+01	.1802421224702E-01	-.1498787946189E+01
.3626640134852E-01	.5071792173508E-01	-.3007467565267E+01	.2288532238015E-01	-.1467611202190E+01
.4464024955422E-01	.6185310660787E-01	-.2941457066513E+01	.2788819914197E-01	-.1435772740901E+01
.5343101028181E-01	.7332076572498E-01	-.2869906560540E+01	.3303183451133E-01	-.1403281484361E+01
.6265902329396E-01	.8512022559240E-01	-.2793054334084E+01	.3831464716040E-01	-.1370102678721E+01
.7234556464614E-01	.9725011877674E-01	-.2711891130606E+01	.4373444332794E-01	-.1336163527851E+01
.8251288428605E-01	.1097083507707E+00	-.2628055701969E+01	.4928838434410E-01	-.1301369381330E+01
.9318424484878E-01	.1224919851143E+00	-.2543603336418E+01	.5497296247428E-01	-.1265629419248E+01
.1043839616832E+00	.1355970301530E+00	-.2460670156899E+01	.6078398535229E-01	-.1228880083337E+01
.1161374441575E+00	.1490181292138E+00	-.2381082931306E+01	.6671656726536E-01	-.1191155849567E+01
.1284712383139E+00	.1627481811809E+00	-.2305987154312E+01	.7276512331071E-01	-.1152531122656E+01
.1414130709810E+00	.1767779460723E+00	-.2235577042733E+01	.7892336064889E-01	-.1113204964994E+01
.1549105189545977E+00	.1910957131284E+00	-.2169003137110E+01	.8518426065205E-01	-.1073442779559E+01
.1692379392638E+00	.2056871184349E+00	-.2104503168463E+01	.9154004761258E-01	-.1033542154228E+01
.1841827533877E+00	.2205351873285E+00	-.2039752427175E+01	.9798214438846E-01	-.9937731732774E+00
.1998592647508E+00	.2356206399744E+00	-.1972371024922E+01	.1045011226224E+00	-.9543149011393E+00
.2163018308366E+00	.2509224400836E+00	-.1900473344344E+01	.1110866634557E+00	-.9152068658925E+00
.2335462976702E+00	.2664184993438E+00	-.1823118116318E+01	.1177275511712E+00	-.8763344272164E+00
.2516306011952E+00	.2820863941058E+00	-.1740530403107E+01	.1244117234291E+00	-.8374600218596E+00
.2705921323713E+00	.2979039290429E+00	-.1654022810547E+01	.1311263947733E+00	-.7982987541561E+00
.2904732062410E+00	.3138494116147E+00	-.1565630531395E+01	.1378582542720E+00	-.7586200611479E+00
.3113157351939E+00	.3299015826289E+00	-.1477566705892E+01	.1445937167898E+00	-.7183435017854E+00
.3331640066672E+00	.3460392624385E+00	-.1391667455704E+01	.1513191878733E+00	-.6775924211116E+00
.3560642255495E+00	.3622408811489E+00	-.1309002202843E+01	.1580212940511E+00	-.6366870325686E+00
.3800646016026E+00	.3784841199820E+00	-.1229766390758E+01	.1646870407596E+00	-.5960597139354E+00
.4052154422482E+00	.3947458677385E+00	-.1153468939758E+01	.1713038890145E+00	-.5561491721125E+00
.4315692510800E+00	.4110025902476E+00	-.1079315913013E+01	.1778597792527E+00	-.5172907084409E+00
.4591808324242E+00	.4272310596517E+00	-.1006618846264E+01	.1843431589323E+00	-.4796628294142E+00
.4881074021631E+00	.4434092623757E+00	-.9351137991234E+00	.1907430730463E+00	-.4433030480175E+00
.5184087048725E+00	.4595172171146E+00	-.8649991414393E+00	.1970493486471E+00	-.4091778182298E+00
.5501471370387E+00	.4755375288951E+00	-.7967715417195E+00	.2032528581107E+00	-.3742658866998E+00
.5833878756862E+00	.4914556502872E+00	-.7310524709325E+00	.2093458055445E+00	-.3416136831074E+00
.6181990115242E+00	.5072598757260E+00	-.6683512315268E+00	.2153219679100E+00	-.3103416427571E+00
.6546516858167E+00	.5229412513278E+00	-.6089475549678E+00	.2211768435292E+00	-.2806090718485E+00
.6928202303051E+00	.5384935705673E+00	-.5529459020022E+00	.2269077019835E+00	-.2525657063261E+00
.7327823097715E+00	.5539134702349E+00	-.5003682953910E+00	.2325135645573E+00	-.2263179361418E+00
.7746190670362E+00	.5692005595462E+00	-.4512358940192E+00	.2379951536885E+00	-.2019215262213E+00
.8184596909894E+00	.5843574702068E+00	-.4056001539045E+00	.2433544327243E+00	-.1793945001865E+00
.8642594597787E+00	.5993897393183E+00	-.3635208413930E+00	.2485965296418E+00	-.1587346595559E+00
.9122440989105E+00	.6143055122018E+00	-.3250316098749E+00	.2537256206713E+00	-.1399290194744E+00
.9624657181662E+00	.6291150980848E+00	-.2901087468102E+00	.2587487527385E+00	-.1229522512078E+00
.1015025061751E+01	.6438304449254E+00	-.2586759655666E+00	.2636736022225E+00	-.1077601637039E+00
.1070027230858E+01	.6584645451357E+00	-.2306245420471E+00	.2685085854283E+00	-.9428607573911E-01
.1127581826751E+01	.6730307432333E+00	-.2058136266486E+00	.2732625404232E+00	-.8244287090119E-01
.1187803094713E+01	.6875419576320E+00	-.1840815659037E+00	.2779443923583E+00	-.7212833742383E-01
.1250810070582E+01	.7020098033423E+00	-.1652437926615E+00	.2825628059919E+00	-.6323009876037E-01
.1316726732733E+01	.7164436409976E+00	-.1490902543716E+00	.2871258282214E+00	-.5562867059195E-01
.1385682162593E+01	.7308499990559E+00	-.1353920128644E+00	.2916440286559E+00	-.4919978015212E-01
.1457810727138E+01	.7452295911125E+00	-.1239044795211E+00	.2961126496868E+00	-.4391700196946E-01
.1533252267280E+01	.7595803694185E+00	-.1143716944340E+00	.3005462766696E+00	-.3935448975215E-01
.1612152340369E+01	.7738926587429E+00	-.1065311477958E+00	.3049435373978E+00	-.3568929151080E-01
.1694662488088E+01	.7881504172795E+00	-.1001185570911E+00	.3093043402342E+00	-.3270311922779E-01
.1780940565324E+01	.8023302748437E+00	-.9487338718865E-01	.3136261613703E+00	-.3028370904292E-01
.1871151136022E+01	.8164011939010E+00	-.9054456177318E-01	.3179038924258E+00	-.2832587874541E-01
.1965465949930E+01	.8303243923820E+00	-.8689548573577E-01	.3221297598375E+00	-.2673231604090E-01
.2064064517021E+01	.8440535599736E+00	-.8370930109829E-01	.3262933275335E+00	-.2541416625235E-01
.2167134790939E+01	.8575353883721E+00	-.8079229502777E-01	.3303815938536E+00	-.2429150536094E-01
.2274873975098E+01	.8707104259764E+00	-.7797692614734E-01	.3343791921022E+00	-.2329374279634E-01
.2387489460636E+01	.8835142565287E+00	-.7512354242838E-01	.3382687014405E+00	-.2235960043151E-01
.2505199902224E+01	.8958789940105E+00	-.7212057317950E-01	.3420310711621E+00	-.2143917512918E-01
.2628236432060E+01	.9077350735441E+00	-.6888527820307E-01	.3456461568683E+00	-.2049050538154E-01
.2756844013699E+01	.9190133132556E+00	-.6536218467653E-01	.3490933617592E+00	-.1948322477763E-01
.2891282905388E+01	.9296472061186E+00	-.6152262786787E-01	.3523523702133E+00	-.1839669235466E-01
.3031830245330E+01	.9395753858785E+00	-.5736662259433E-01	.3554039539328E+00	-.1722015267245E-01
.3178781700122E+01	.9487441879585E+00	-.5290696567165E-01	.3582308230420E+00	-.1595238818336E-01
.3332453159676E+01	.9571101982048E+00	-.4819745332849E-01	.3608184857045E+00	-.1460118447150E-01
.3493182428854E+01	.9646426512743E+00	-.4330129731552E-01	.3631560705730E+00	-.1318254605615E-01
.3661330866645E+01	.9713255111772E+00	-.3830298006687E-01	.3652370577899E+00	-.1171958934766E-01
.3837284918531E+01	.9771590454702E+00	-.3330109244332E-01	.3670598579978E+00	-.1024105056507E-01

VELOCITY PROFILES AT x/c = 0.791 - Concluded

y/δ_1	U/U_e	$(U/U_e)''$	W/U_e	$(W/U_e)''$
.4021457486911E+01	.9821606994135E+00	-.2840274376634E-01	.3686281770079E+00	-.8779384398035E-02
.4214289088408E+01	.9863650946101E+00	-.2371670103535E-01	.3699511086584E+00	-.7368491800458E-02
.4416248756569E+01	.9898230242184E+00	-.1934566590236E-01	.3710429119282E+00	-.6041194158038E-02
.4627834664554E+01	.9925993962598E+00	-.1537838382199E-01	.3719224515924E+00	-.4826652494735E-02
.4849574464797E+01	.9947701846006E+00	-.1188249698675E-01	.3726123140908E+00	-.3747996505637E-02
.5082025370426E+01	.9964185730877E+00	-.8899133937505E-02	.3731376490961E+00	-.2820459169584E-02
.5325774034243E+01	.9976306031977E+00	-.6440118948504E-02	.3735248272475E+00	-.2050291026046E-02
.5581436312026E+01	.9984907343296E+00	-.4488363507734E-02	.3738000382317E+00	-.1434644829354E-02
.5849657023408E+01	.9990777720755E+00	-.3001504959788E-02	.3739879724364E+00	-.9624817447537E-03
.6131109840525E+01	.9994615929376E+00	-.1918278240044E-02	.3741107265705E+00	-.6163777624394E-03
.6426497437442E+01	.9997009876830E+00	-.1166583994422E-02	.3741870455170E+00	-.3749420894534E-03
.6736552018674E+01	.9998427735357E+00	-.6718956934230E-03	.3742319618678E+00	-.2154426003407E-03
.7062036312768E+01	.9999221218176E+00	-.3646335808401E-03	.3742568304543E+00	-.1162038774099E-03
.7403745070110E+01	.9999638597623E+00	-.1854439204976E-03	.3742696922571E+00	-.5841553075459E-04
.7762507050330E+01	.9999843794304E+00	-.8787438913022E-04	.3742758559599E+00	-.2714575285530E-04
.8139187433735E+01	.9999937521788E+00	-.3856386083083E-04	.3742785674601E+00	-.1155150188434E-04
.8534690553626E+01	.9999977045634E+00	-.1557521320662E-04	.3742796505340E+00	-.4451913544478E-05
.8949962830040E+01	.9999992324781E+00	-.5750824863316E-05	.3742800382822E+00	-.1533724783646E-05
.9385995793244E+01	.9999997694329E+00	-.1926569666974E-05	.3742801607579E+00	-.4649124216660E-06
.9843829113751E+01	.9999999390175E+00	-.5797871335778E-06	.3742801942262E+00	-.1215829296138E-06
.1032455359587E+02	.9999999862847E+00	-.1542738760554E-06	.3742802019395E+00	-.2674195114608E-07
.1082931413236E+02	.9999999975447E+00	-.3525513902854E-07	.3742802033874E+00	-.4777938414029E-08
.1135931264862E+02	.9999999997004E+00	-.6537178554763E-08	.3742802035974E+00	-.6599495575688E-09
.1191581108077E+02	.9999999999876E+00	-.8674952781727E-09	.3742802036185E+00	-.6454834486856E-10
.1250013443321E+02	.1000000000000E+01	-.3540797479678E-10	.3742802036191E+00	-.1679396935455E-11
.1311367395323E+02	.1000000000000E+01	0.	.3742802036191E+00	.3573217280259E-14
.1375789044926E+02	.1000000000000E+01	0.	.3742802036191E+00	0.

VELOCITY PROFILES AT   x/c = 0.820

y/δ_1	U/U_e	$(U/U_e)''$	W/U_e	$(W/U_e)''$
0.	0.	-.3392299061845E+01	0.	-.1898555109372E+01
.7125649858444E-02	.1058283330440E-01	-.3328106014544E+01	.5210201271570E-02	-.1860953764964E+01
.1460734232653E-01	.2151259152522E-01	-.3263872155742E+01	.1057904758114E-01	-.1822794824359E+01
.2246259458328E-01	.3279146251465E-01	-.3198929592185E+01	.1610615846350E-01	-.1783564499558E+01
.3070974356039E-01	.4442062660358E-01	-.3131841926427E+01	.2179058792742E-01	-.1743354700772E+01
.3936797938619E-01	.5640025212816E-01	-.3061352676226E+01	.2763077497234E-01	-.1702246363893E+01
.4845737984771E-01	.6872951992113E-01	-.2986571886310E+01	.3362449361735E-01	-.1660296922880E+01
.5799894591082E-01	.8140666593538E-01	-.2907133169352E+01	.3976880428845E-01	-.1617531337458E+01
.6801463834193E-01	.9442902336561E-01	-.2823291243334E+01	.4606000898513E-01	-.1573939346570E+01
.7852741547577E-01	.1077930390783E+00	-.2735932293172E+01	.5249361297940E-01	-.1529481056810E+01
.8956127217610E-01	.1214942360811E+00	-.2646479293239E+01	.5906429567908E-01	-.1484101699058E+01
.1011412800402E+00	.1355270965261E+00	-.2556691168880E+01	.6576589252476E-01	-.1437754435090E+01
.1132936289078E+00	.1498848502015E+00	-.2468376406030E+01	.7259138830463E-01	-.1390427733049E+01
.1260456697545E+00	.1645591720805E+00	-.2383064850206E+01	.7953292018472E-01	-.1342171562182E+01
.1394259590798E+00	.1795398174957E+00	-.2301700228472E+01	.8658178647191E-01	-.1293115205859E+01
.1534643049470E+00	.1948142502833E+00	-.2224423937039E+01	.9372845536884E-01	-.1243469634198E+01
.1681918148876E+00	.2103673405962E+00	-.2150512303443E+01	.1009625676770E+00	-.1193509714252E+01
.1836409459494E+00	.2261812164458E+00	-.2078502466306E+01	.1082729294575E+00	-.1143536161111E+01
.1998455572284E+00	.2422353389670E+00	-.2006499087448E+01	.1156474955389E+00	-.1093823365042E+01
.2168409652762E+00	.2585068328728E+00	-.1932604364360E+01	.1230733520322E+00	-.1044565478176E+01
.2346601021881E+00	.2749710450437E+00	-.1855371384016E+01	.1305367140064E+00	-.9958371319746E+00
.2533530810881E+00	.2916022390612E+00	-.1774161373542E+01	.1380229602777E+00	-.9475845287332E+00
.2729482565143E+00	.3083742823108E+00	-.1689300400616E+01	.1455167274070E+00	-.8996559871166E+00
.2934913015592E+00	.3252611670876E+00	-.1601982189613E+01	.1530020768097E+00	-.8518688691809E+00
.3150257806127E+00	.3422372427371E+00	-.1513939174675E+01	.1604627322158E+00	-.8040956849690E+00
.3375917123740E+00	.3592771209602E+00	-.1426979882193E+01	.1678823634303E+00	-.7563410443829E+00
.3612527491347E+00	.3763553289064E+00	-.1342538602317E+01	.1752448741996E+00	-.7087800384785E+00
.3860420835198E+00	.3934458854292E+00	-.1261381136641E+01	.1825346463369E+00	-.6617396274147E+00
.4120167328417E+00	.4105220219424E+00	-.1183554160117E+01	.1897367055074E+00	-.6156264165770E+00
.4392305518185E+00	.4275562333173E+00	-.1108574248388E+01	.1968368047782E+00	-.5708275705970E+00
.4677397633178E+00	.4445207313152E+00	-.1035761934714E+01	.2038214588157E+00	-.5276249503494E+00
.4976030819197E+00	.4613882255740E+00	-.9645727305076E+00	.2106779866692E+00	-.4861573090621E+00
.5288818361008E+00	.4781328434894E+00	-.8948362575248E+00	.2173946191615E+00	-.4464423143529E+00
.5616401108413E+00	.4947309327666E+00	-.8267563004154E+00	.2239606954631E+00	-.4084408524409E+00
.5959448887577E+00	.5111615994534E+00	-.7607532148844E+00	.2303669271585E+00	-.3721268602139E+00
.6318662021501E+00	.5274066825000E+00	-.6973179289852E+00	.2366056552005E+00	-.3375289516545E+00
.6694772907732E+00	.5434522993002E+00	-.6368297423050E+00	.2426711530452E+00	-.3047297433928E+00
.7088547651784E+00	.5592858663076E+00	-.5794810063463E+00	.2485595846874E+00	-.2738333039364E+00
.7500787749320E+00	.5748991942521E+00	-.5253388376412E+00	.2542692084667E+00	-.2449262856501E+00
.7932331811953E+00	.5902871891588E+00	-.4744252946859E+00	.2598002716751E+00	-.2180549902822E+00
.8384057332718E+00	.6054454367655E+00	-.4267773262950E+00	.2651549841962E+00	-.1932250744303E+00
.8856882484592E+00	.6203848360636E+00	-.3824612799223E+00	.2703374673008E+00	-.1704157233961E+00
.9351767940335E+00	.6351023928627E+00	-.3415468878221E+00	.2753536807584E+00	-.1495945115022E+00
.9869718698770E+00	.6496100198071E+00	-.3040768631696E+00	.2802113007941E+00	-.1307236158451E+00
.1041178590494E+01	.6639195260475E+00	-.2700424250497E+00	.2849195282258E+00	-.1137568845432E+00
.1097906865765E+01	.6780449064534E+00	-.2393873271823E+00	.2894888254399E+00	-.9863377027683E-01
.1157271580618E+01	.6920019722091E+00	-.2120220688213E+00	.2939305967243E+00	-.8527626302368E-01
.1219392774760E+01	.7058069960746E+00	-.1878211155687E+00	.2982568290148E+00	-.7359020642595E-01
.1284395823950E+01	.7194764202811E+00	-.1666302024039E+00	.3024797039117E+00	-.6346865110568E-01
.1352411624750E+01	.7330256092374E+00	-.1482651187580E+00	.3066111873665E+00	-.5479466771151E-01
.1423576786000E+01	.7464679004218E+00	-.1325121930084E+00	.3106626060199E+00	-.4744311141987E-01
.1498033831611E+01	.7598136028911E+00	-.1191367987477E+00	.3146442282939E+00	-.4128255646609E-01
.1575931420593E+01	.7730690280923E+00	-.1078893453884E+00	.3185648628767E+00	-.3617810969981E-01
.1657424591862E+01	.7862355934215E+00	-.9851205954411E-01	.3224315019645E+00	-.3199468385562E-01
.1742675042681E+01	.7993090362712E+00	-.9074570092489E-01	.3262490124788E+00	-.2860015676041E-01
.1831851450752E+01	.8122787740132E+00	-.8433545789709E-01	.3300198928459E+00	-.2586816103413E-01
.1925129851295E+01	.8251274454153E+00	-.7903640323689E-01	.3337441022227E+00	-.2368041750257E-01
.2022694081390E+01	.8378306643912E+00	-.7461809250695E-01	.3374189687731E+00	-.2192851553634E-01
.2124736304457E+01	.8503570130688E+00	-.7086812909842E-01	.3410391808291E+00	-.2051506168239E-01
.2231457627812E+01	.8626682978181E+00	-.6759499644383E-01	.3445968631987E+00	-.1935422735544E-01
.2343068825541E+01	.8747200851985E+00	-.6463001051847E-01	.3480817400187E+00	-.1837180466661E-01
.2459791177544E+01	.8864625279111E+00	-.6182879788227E-01	.3514813849707E+00	-.1750491950701E-01
.2581857433244E+01	.8978414815860E+00	-.5907183666563E-01	.3547815590210E+00	-.1670149820189E-01
.2709512904955E+01	.9087999029155E+00	-.5626481014612E-01	.3579666346324E+00	-.1591968046989E-01
.2843016691487E+01	.9192795079814E+00	-.5333814382081E-01	.3610201031798E+00	-.1512719276849E-01
.2982643026908E+01	.9292226569209E+00	-.5024628328428E-01	.3639251587814E+00	-.1430076386139E-01
.3128682743623E+01	.9385744171286E+00	-.4696654103232E-01	.3666653468878E+00	-.1342556750005E-01
.3281444829835E+01	.9472847415330E+00	-.4349764278309E-01	.3692252599281E+00	-.1249466417504E-01
.3441258058185E+01	.9553106807774E+00	-.3985798047530E-01	.3715912554266E+00	-.1150839522610E-01
.3608472650129E+01	.9626185286236E+00	-.3608353040482E-01	.3737521647639E+00	-.1047367660873E-01
.3783461938175E+01	.9691857799758E+00	-.3222533839672E-01	.3756999538530E+00	-.9403142056570E-02
.3966623981054E+01	.9750027635642E+00	-.2834644525305E-01	.3774302913100E+00	-.8314094814256E-02
.4158383084635E+01	.9800738010367E+00	-.2451814877593E-01	.3789429764407E+00	-.7227244821856E-02

VELOCITY PROFILES AT   x/c = 0.820 - Concluded

y/δ_1	U/U_e	$(U/U_e)''$	W/U_e	$(W/U_e)''$
.4359191181621E+01	.9844177465508E+00	-.2081558377216E-01	.3802421799616E+00	-.6165236308342E-02
.4569529027442E+01	.9880677814860E+00	-.1731274115087E-01	.3813364563407E+00	-.5151009338126E-02
.4789907178850E+01	.9910703817467E+00	-.1407721619272E-01	.3822384991894E+00	-.4206084180068E-02
.5020866736223E+01	.9934834413250E+00	-.1116513658642E-01	.3829646307164E+00	-.3348901245854E-02
.5262979850161E+01	.9953736218092E+00	-.8616830049393E-02	.3835340420539E+00	-.2593380889537E-02
.5516850016969E+01	.9968130941493E+00	-.6453810092332E-02	.3839678308584E+00	-.1947875233859E-02
.5783112214049E+01	.9978759314942E+00	-.4677560736809E-02	.3842879118012E+00	-.1414659954484E-02
.6062432952469E+01	.9986344816590E+00	-.3270383759404E-02	.3845158988932E+00	-.9900549955451E-03
.6355510346035E+01	.9991560759081E+00	-.2198262790664E-02	.3846720701337E+00	-.6651753825168E-03
.6663074310242E+01	.9995004033866E+00	-.1415355816214E-02	.3847745199891E+00	-.4272116337031E-03
.6985887006382E+01	.9997177943798E+00	-.8694310603347E-03	.3848385817976E+00	-.2610460566071E-03
.7324743633505E+01	.9998485217806E+00	-.5073916282401E-03	.3848765628024E+00	-.1509508086982E-03
.7680473643501E+01	.9999230742498E+00	-.2800472197002E-03	.3848977862095E+00	-.8210512636763E-04
.8053942415139E+01	.9999632112915E+00	-.1454939053935E-03	.3849088879722E+00	-.4171894032540E-04
.8446053377442E+01	.9999835137588E+00	-.7080457954469E-04	.3849142820438E+00	-.1964734352294E-04
.8857750529303E+01	.9999931148263E+00	-.3211573925977E-04	.3849166946490E+00	-.8498346285473E-05
.9290021269508E+01	.9999973374102E+00	-.1350872489563E-04	.3849176776240E+00	-.3340568950712E-05
.9743899435877E+01	.9999990544344E+00	-.5241206969662E-05	.3849180379393E+00	-.1178458509048E-05
.1022046845694E+02	.9999996952643E+00	-.1863988117059E-05	.3849181549906E+00	-.3674905526119E-06
.1072086454199E+02	.9999999125102E+00	-.6023169200849E-06	.3849181880666E+00	-.9942169160394E-07
.1124627986886E+02	.9999999783008E+00	-.1742870388619E-06	.3849181960034E+00	-.2278080274001E-07
.1179796576357E+02	.9999999955983E+00	-.4400021895894E-07	.3849181975686E+00	-.4279671628522E-08
.1237723589431E+02	.9999999993478E+00	-.9235619145930E-08	.3849181978102E+00	-.6291111607719E-09
.1298546951798E+02	.9999999999493E+00	-.1459185230644E-08	.3849181978367E+00	-.6644863071003E-10
.1362411482067E+02	.1000000000000E+01	-.1212013464521E-09	.3849181978380E+00	-.3193511010656E-11
.1429469238836E+02	.1000000000000E+01	0.	.3849181978380E+00	.5473561275861E-14
.1499879883445E+02	.1000000000000E+01	0.	.3849181978380E+00	0.

APPENDIX

VELOCITY PROFILES AT   x/c = 0.860

y/δ_1	U/U_e	$(U/U_e)''$	W/U_e	$(W/U_e)''$
0.	0.	-.3150530408035E+01	0.	-.2660528908760E+01
.6833030972767E-02	.9715753608475E-02	-.3082583935085E+01	.6401819727851E-02	-.2606727570917E+01
.1400752764956E-01	.1976213549044E-01	-.3013424100266E+01	.1299257222660E-01	-.2552265985314E+01
.2154034274402E-01	.3014334256453E-01	-.2942074125780E+01	.1977110946865E-01	-.2496440774598E+01
.2944912840284E-01	.4086303699495E-01	-.2870181215221E+01	.2673553243585E-01	-.2439182308526E+01
.3775237024108E-01	.5192420266330E-01	-.2799205139659E+01	.3388313876314E-01	-.2380446454403E+01
.4646942244528E-01	.6332897137007E-01	-.2730218477531E+01	.4121037221086E-01	-.2320230122391E+01
.5562054395814E-01	.7507843112926E-01	-.2663740069550E+01	.4871277349765E-01	-.2258582270291E+01
.6522693576923E-01	.8717243672802E-01	-.2599635093764E+01	.5638493163705E-01	-.2195607212191E+01
.7531077935170E-01	.9960944915094E-01	-.2537111104981E+01	.6422043481763E-01	-.2131457846813E+01
.8589527630590E-01	.1123864332995E+00	-.2474827902090E+01	.7221182026987E-01	-.2066318048157E+01
.9700468929603E-01	.1254988403752E+00	-.2411120301733E+01	.8035052365632E-01	-.2000375859622E+01
.1086643843928E+00	.1389406906399E+00	-.2344308924076E+01	.8862683036047E-01	-.1933791945343E+01
.1209008749611E+00	.1527047537646E+00	-.2273049345957E+01	.9702983345861E-01	-.1866670329572E+01
.1337418672510E+00	.1667827996709E+00	-.2196650769682E+01	.1055574056480E+00	-.1799039920435E+01
.1472163078615E+00	.1811658674450E+00	-.2115288722492E+01	.1141661941647E+00	-.1730854768399E+01
.1613544332458E+00	.1958444808071E+00	-.2030047935057E+01	.1228714677510E+00	-.1662017830553E+01
.1761878214143E+00	.2108087340403E+00	-.1942763329615E+01	.1316480821074E+00	-.1592427240124E+01
.1917494459763E+00	.2260481889848E+00	-.1855674894928E+01	.1404787846230E+00	-.1522036713529E+01
.2080737326509E+00	.2415515636977E+00	-.1770965351568E+01	.1493461511468E+00	-.1450914797534E+01
.2251966183818E+00	.2573062510493E+00	-.1690292047706E+01	.1582318391246E+00	-.1379283885043E+01
.2431556132313E+00	.2732977666644E+00	-.1614439876760E+01	.1671169157473E+00	-.1307521897560E+01
.2619898652956E+00	.2895092697354E+00	-.1543199139776E+01	.1759819803716E+00	-.1236118486516E+01
.2817402289894E+00	.3059213067117E+00	-.1475118525591E+01	.1848072497980E+00	-.1165592256929E+01
.3024493371566E+00	.3225118847083E+00	-.1409847425157E+01	.1935726124511E+00	-.1096391486496E+01
.3241616775601E+00	.3392568934949E+00	-.1344661353783E+01	.2022576783496E+00	-.1028811451017E+01
.3469236743557E+00	.3561307869864E+00	-.1278989001093E+01	.2108418674445E+00	-.9629603259171E+00
.3707837751351E+00	.3731073467129E+00	-.1212401155543E+01	.2193045800727E+00	-.8987900806417E+00
.3957925440475E+00	.3901603203357E+00	-.1145298067727E+01	.2276254746265E+00	-.8361829776622E+00
.4220027613787E+00	.4072637784737E+00	-.1078518761183E+01	.2357848425733E+00	-.7750591741023E+00
.4494695298330E+00	.4243921500438E+00	-.1013011715408E+01	.2437640331967E+00	-.7154597696608E+00
.4782503876673E+00	.4415200327772E+00	-.9495150609140E+00	.2515458585111E+00	-.6575703757657E+00
.5084054288274E+00	.4586219648831E+00	-.8883551533904E+00	.2591149164433E+00	-.6016791806387E+00
.5399974303114E+00	.4756723824114E+00	-.8294943155125E+00	.2664578066137E+00	-.5480959181974E+00
.5730919871563E+00	.4926458597521E+00	-.7727210118813E+00	.2735632594178E+00	-.4970749407281E+00
.6077576557037E+00	.5095175831950E+00	-.7177969748217E+00	.2804222293826E+00	-.4487766057777E+00
.6440661057615E+00	.5262639785444E+00	-.6646186442258E+00	.2870280012764E+00	-.4032761272123E+00
.6820922819112E+00	.5428633075553E+00	-.6132614344360E+00	.2933763248148E+00	-.3606011501297E+00
.7219145737854E+00	.5592960964972E+00	-.5638945540716E+00	.2994655523416E+00	-.3207700587859E+00
.7636149946914E+00	.5755454124215E+00	-.5166959140054E+00	.3052967306706E+00	-.2838078338080E+00
.8072793676755E+00	.5915790512236E+00	-.4717994673190E+00	.3108736055489E+00	-.2497386146017E+00
.8529975182527E+00	.6074397060721E+00	-.4292887690392E+00	.3162025253823E+00	-.2185671920241E+00
.9008634734180E+00	.6230651390854E+00	-.3892228352216E+00	.3212922588310E+00	-.1902644938131E+00
.9509756667770E+00	.6384683148238E+00	-.3516569199324E+00	.3261537518469E+00	-.1647644525403E+00
.1003437149470E+01	.6536474382431E+00	-.3166536877914E+00	.3307998420094E+00	-.1419700321550E+00
.1058355809255E+01	.6686038357815E+00	-.2842693028327E+00	.3352449333301E+00	-.1217612582099E+00
.1115844575930E+01	.6833416733503E+00	-.2545344228927E+00	.3395046277801E+00	-.1040000240511E+00
.1176021675263E+01	.6978675393995E+00	-.2274551685629E+00	.3435953158108E+00	-.8853185931413E-01
.1239010826397E+01	.7121898791200E+00	-.2030057079662E+00	.3475337388866E+00	-.7518760903088E-01
.1304941488611E+01	.7263183026194E+00	-.1811300397567E+00	.3513365425339E+00	-.6378698961849E-01
.1373949095052E+01	.7402627709004E+00	-.1617634755670E+00	.3550198309788E+00	-.5414362940392E-01
.1446175301493E+01	.7540326690707E+00	-.1447318888843E+00	.3585987690104E+00	-.4606994294690E-01
.1521768235415E+01	.7676358096373E+00	-.1299499116742E+00	.3620871345583E+00	-.3938106629113E-01
.1600882774562E+01	.7810774038662E+00	-.1172279870502E+00	.3654970061625E+00	-.3389808863723E-01
.1683680835926E+01	.7943590480097E+00	-.1063745457208E+00	.3688384194764E+00	-.2945076380559E-01
.1770331067745E+01	.8074777770168E+00	-.9718181573123E-01	.3721191058437E+00	-.2587961505499E-01
.1861012356715E+01	.8204252395499E+00	-.8943172551683E-01	.3753442852076E+00	-.2303736954510E-01
.1955907936126E+01	.8331870493666E+00	-.8290225706782E-01	.3785165256268E+00	-.2078981639740E-01
.2055212148230E+01	.8457423647308E+00	-.7737401069891E-01	.3816356767967E+00	-.1901624995967E-01
.2159127830818E+01	.8580637395976E+00	-.7263642918638E-01	.3846988844720E+00	-.1760961829865E-01
.2267867655906E+01	.8701172808056E+00	-.6849706914316E-01	.3877006914480E+00	-.1647645534406E-01
.2381654390196E+01	.8818631324339E+00	-.6476834536730E-01	.3906332287211E+00	-.1553664476687E-01
.2500722617300E+01	.8932562945535E+00	-.6130719173042E-01	.3934864976770E+00	-.1472303017515E-01
.2625318762167E+01	.9042477688223E+00	-.5798149835776E-01	.3962487408873E+00	-.1398087071768E-01
.2755702588730E+01	.9147860087790E+00	-.5468938999080E-01	.3989068956524E+00	-.1326714828411E-01
.2892148270070E+01	.9248186382399E+00	-.5135589447724E-01	.4014471209635E+00	-.1254979438611E-01
.3034945658717E+01	.9342943867265E+00	-.4793198593463E-01	.4038553849919E+00	-.1180655772484E-01
.3184401654934E+01	.9431651759599E+00	-.4439372106163E-01	.4061180963472E+00	-.1102449394253E-01
.3340841655018E+01	.9513882759626E+00	-.4073967508170E-01	.4082227579668E+00	-.1019852559199E-01
.3504611055469E+01	.9589284334994E+00	-.3698668572500E-01	.4101586175920E+00	-.9330648648115E-02
.3676076783114E+01	.9657598604922E+00	-.3317678777915E-01	.4119172836826E+00	-.8428821193756E-02
.3855628816579E+01	.9718679575389E+00	-.2935373236426E-01	.4134932710391E+00	-.7505819327565E-02
.4043681661449E+01	.9772506405483E+00	-.2557904414754E-01	.4148844373888E+00	-.6577989389057E-02

VELOCITY PROFILES AT   x/c = 0.860 - Concluded

y/δ_1	U/U_e	$(U/U_e)''$	W/U_e	$(W/U_e)''$
.4240675740723E+01	.9819191403460E+00	-.2191765776951E-01	.4160922719719E+00	-.5663889315249E-02
.4447078664395E+01	.9858981598171E+00	-.1843524251483E-01	.4171220009465E+00	-.4782841563892E-02
.4663386347732E+01	.9892253041839E+00	-.1519341893960E-01	.4179824831576E+00	-.3953454741271E-02
.4890123957460E+01	.9919497491530E+00	-.1224517418211E-01	.4186858839011E+00	-.3192204112938E-02
.5127846678653E+01	.9941301777438E+00	-.9630866394923E-02	.4192471333450E+00	-.2512185350370E-02
.5377140312200E+01	.9958320943717E+00	-.7375241970845E-02	.4196831987283E+00	-.1922164215171E-02
.5638621732377E+01	.9971247045097E+00	-.5485846887532E-02	.4200122226515E+00	-.1426031868705E-02
.5912939254448E+01	.9980776165259E+00	-.3953083404130E-02	.4202525999365E+00	-.1022738908976E-02
.6200772981134E+01	.9987576640506E+00	-.2751957797673E-02	.4204220784274E+00	-.7067238153866E-03
.6502835211260E+01	.9992261492123E+00	-.1845314265084E-02	.4205369708662E+00	-.4687817445344E-03
.6819871000999E+01	.9995367620397E+00	-.1188109031812E-02	.4206115532939E+00	-.2972509544599E-03
.7152658965537E+01	.9997343416371E+00	-.7320944908460E-03	.4206577006255E+00	-.1793423150390E-03
.7502012395235E+01	.9998545241733E+00	-.4302512747513E-03	.4206847756781E+00	-.1024164628725E-03
.7868780736334E+01	.9999241947665E+00	-.2403306879048E-03	.4206997505118E+00	-.5503111549879E-04
.8253851454507E+01	.9999625528296E+00	-.1271474017912E-03	.4207075065534E+00	-.2763595362730E-04
.8658152265105E+01	.9999825373241E+00	-.6348866352590E-04	.4207112400067E+00	-.1287154402716E-04
.9082653682859E+01	.9999923517940E+00	-.2981440515662E-04	.4207128957164E+00	-.5511112629352E-05
.9528371822011E+01	.9999968746982E+00	-.1311621162515E-04	.4207135653741E+00	-.2147060156539E-05
.9996371369720E+01	.9999988193284E+00	-.5379644616620E-05	.4207138094456E+00	-.7519707886852E-06
.1048776866234E+02	.9999995930774E+00	-.2043074339941E-05	.4207138884630E+00	-.2333571789426E-06
.1100373481330E+02	.9999998745526E+00	-.7108013199890E-06	.4207139107856E+00	-.6303260557976E-07
.1154549886755E+02	.9999999664425E+00	-.2226681619565E-06	.4207139161643E+00	-.1448624608596E-07
.1211435098359E+02	.9999999925886E+00	-.6108321741549E-07	.4207139172358E+00	-.2747337235471E-08
.1271164566456E+02	.9999999987688E+00	-.1401197279603E-07	.4207139174041E+00	-.4108306334158E-09
.1333880507042E+02	.9999999998778E+00	-.2465334960451E-08	.4207139174231E+00	-.4432707881135E-10
.1399732244525E+02	.9999999999987E+00	-.2692708865508E-09	.4207139174243E+00	-.2618264609074E-11
.1468876568877E+02	.1000000000000E+01	-.2660297217905E-11	.4207139174243E+00	0.

VELOCITY PROFILES AT x/c = 0.897

y/δ_1	U/U_e	$(U/U_e)''$	W/U_e	$(W/U_e)''$
0.	0.	-.3667944301182E+01	0.	-.3302335549015E+01
.6481983616943E-02	.9715027546404E-02	-.3599020918114E+01	.7364312276788E-02	-.3237273704326E+01
.1328790821705E-01	.1975282793739E-01	-.3530050693048 7E+01	.1495027658186E-01	-.3171423812503E+01
.2043378293284E-01	.3011603840450E-01	-.3460338821422E+01	.2275706131475E-01	-.3103937549993E+01
.2793638033633E-01	.4080643287275E-01	-.3388147108027E+01	.3078299758665E-01	-.3034951648527E+01
.3581326963442E-01	.5182492870973E-01	-.3311986869546E+01	.3902550340752E-01	-.2964583601533E+01
.4408285110201E-01	.6317162167627E-01	-.3230808257756E+01	.4748100638497E-01	-.2892913515091F+01
.5276439181417E-01	.7484583806206E-01	-.3144188554877E+01	.5614486724985E-01	-.2819971870415E+01
.6187806274263E-01	.8684618556288E-01	-.3052438835976E+01	.6501130720313E-01	-.2745737039859E+01
.7144497728311E-01	.9917057851099E-01	-.2956603325165E+01	.7407334243610E-01	-.2670145342578E+01
.8148723127954E-01	.1118162108012E+00	-.2858332856181E+01	.8332272896534E-01	-.2593114311074E+01
.9202794460784E-01	.1247794534851E+00	-.2759635185637E+01	.9274991994915E-01	-.2514576811428E+01
.1030913043798E+00	.1380556651071E+00	-.2662531679370F+01	.1023440358676E+00	-.2434520198067E+01
.1147026098283E+00	.1516389215006E+00	-.2568676987751E+01	.1120928455690E+00	-.2353021638440E+01
.1268883189448E+00	.1655216957144E+00	-.2479018561302E+01	.1219827537728E+00	-.2270269199280E+01
.1396760969611E+00	.1796945430615E+00	-.2393578468885E+01	.1319987890626E+00	-.2186559331816E+01
.1530948668062E+00	.1941458637365E+00	-.2311424942785E+01	.1421245867776E+00	-.2102265688727E+01
.1671748617267E+00	.2088618179905E+00	-.2230863934010E+01	.1523423644292E+00	-.2017781550313E+01
.1819476803218E+00	.2238264502905E+00	-.2149827076904E+01	.1626328935868E+00	-.1933447115796E+01
.1974463443201E+00	.2390220380012E+00	-.2066374617773E+01	.1729754807149E+00	-.1849480897786E+01
.2137053594734E+00	.2544296233976E+00	-.1979188031145E+01	.1833479778678E+00	-.1765938108265E+01
.2307607799701E+00	.2700296299625E+00	-.1887915200149E+01	.1937268489764E+00	-.1682715304061E+01
.2486502767482E+00	.2858024251692E+00	-.1793261965127F+01	.2040873149795E+00	-.1599608612111E+01
.2674132100206E+00	.3017286915756E+00	-.1696794599911E+01	.2144035891038E+00	-.1516414744143E+01
.2870907062313E+00	.3177895156793E+00	-.1600509066967E+01	.2246491933785E+00	-.1433045530371E+01
.3077257395624E+00	.3339661920499E+00	-.1506303188791E+01	.2347973247159E+00	-.1349615965080E+01
.3293632180583E+00	.3502398420366E+00	-.1415524368828E+01	.2448212229365E+00	-.1266469923429E+01
.3520500744400E+00	.3665910227282E+00	-.1328738799942E+01	.2546944934743E+00	-.1184128700058F+01
.3758353617771E+00	.3829995166629E+00	-.1245783755806E+01	.2643913584960E+00	-.1103178900552E+01
.4007703543262E+00	.3994444312021E+00	-.1166054595780E+01	.2738868463347E+00	-.1024144063688E+01
.4269086539958E+00	.4159046172561E+00	-.1088888748625E+01	.2831569649389E+00	-.9473934017506E+00
.4543063029713E+00	.4323592011441E+00	-.1013676987299E+01	.2921789210351E+00	-.8731238280271E+00
.4830219029740E+00	.4487886642975E+00	-.9410326222833E+00	.3009314306955E+00	-.8014150845274E+00
.5131167414370E+00	.4651743950351E+00	-.8706994415438E+00	.3093951234572E+00	-.7323212827560E+00
.5446549245737E+00	.4814997533942E+00	-.8033302248269E+00	.3175529931781E+00	-.6659475189836E+00
.5777035169606E+00	.4977496018073E+00	-.7393390305014E+00	.3253908219290E+00	-.6024762935506E+00
.6123326871917E+00	.5139102468074E+00	-.6789555839100E+00	.3328975125169E+00	-.5421408351119E+00
.6486158594328E+00	.5299693260643E+00	-.6222051466989E+00	.3400653033254E+00	-.4851711755296E+00
.6866298710422E+00	.5459158242704E+00	-.5690111476403E+00	.3468898811168E+00	-.4317481574432E+00
.7264551367328E+00	.5617401667585E+00	-.5192796703222E+00	.3533704265045E+00	-.3819860059670E+00
.7681758198654E+00	.5774343082073E+00	-.4729406805450E+00	.3595096153382E+00	-.3359408015627F+00
.8118800112042E+00	.5929917450706E+00	-.4299426006316E+00	.3653135720404E+00	-.2936280711242E+00
.8576599150643E+00	.6084074302900E+00	-.3902213950590E+00	.3707917508150E+00	-.2550338407261E+00
.9056120426179E+00	.6236776243864E+00	-.3536821921146E+00	.3759567212864E+00	-.2201142862220E+00
.9558374124023E+00	.6387997212018E+00	-.3201926404685E+00	.3808238530030E+00	-.1887892130754E+00
.1008441758492E+01	.6537720842706E+00	-.2895988060759E+00	.3854109136226E+00	-.1609376867048F+00
.1063535747142E+01	.6685938830819E+00	-.2617434463335E+00	.3897376048948E+00	-.1364001078746E+00
.1121235202936E+01	.6832648953157E+00	-.2364638953064E+00	.3938250569250E+00	-.1149894880098E+00
.1181661345202E+01	.6977852865577E+00	-.2135997765377F+00	.3976952944427E+00	-.9647640356751F-01
.1244941035284E+01	.7121553481802E+00	-.1929930628804F+00	.4013706871486E+00	-.8964100011968E-01
.1311207035689E+01	.7263751931598E+00	-.1744859932383E+00	.4048733995534E+00	-.6723349076443E-01
.1380598202948E+01	.7404444097709E+00	-.1570384906852E+00	.4082248586633E+00	-.5600302125013E-01
.1453260172567E+01	.7543616522637E+00	-.1432014159888E+00	.4114452559152E+00	-.4669944266622E-01
.1529344867995E+01	.7681241365563E+00	-.1301411517147E+00	.4145530962679E+00	-.3907891815915E-01
.1609011620032E+01	.7817271544795E+00	-.1186243896094E+00	.4175648035516E+00	-.3290842478972E-01
.1692427116295E+01	.7951634081327E+00	-.1085179531725E+00	.4204943913700E+00	-.2796920673711E-01
.1779765855457E+01	.8084224139042E+00	-.9968643722590E-01	.4233532063352E+00	-.2405930415813E-01
.1871210555091E+01	.8214898740841E+00	-.9199061319996E-01	.4261497492866E+00	-.2099522925791E-01
.1966952599464E+01	.8343471140216E+00	-.8528697684773E-01	.4288895782623E+00	-.1861286797929E-01
.2067192535348E+01	.8469706369665E+00	-.7942881391329E-01	.4315752954540E+00	-.1676772475238E-01
.2172140624884E+01	.8593318584950E+00	-.7426862564946E-01	.4342066188131E+00	-.1533462350956F-01
.2282017465324E+01	.8713970798733E+00	-.6966670318052F-01	.4367805374524E+00	-.1420696422960E-01
.2397054685548E+01	.8831277502758E+00	-.6547038603898E-01	.4392915486462E+00	-.1329563904422E-01
.2517495728606E+01	.8944810528460E+00	-.6156850196962E-01	.4417319730310E+00	-.1252771803260E-01
.2643596727997E+01	.9054108301273E+00	-.5784548433254E-01	.4440923433524E+00	-.1184501233684E-01
.2775627482740E+01	.9158688421620E+00	-.5420975349553E-01	.4463618605010E+00	-.1120260824652F-01
.2913872532670E+01	.9258063272062E+00	-.5059107609412E-01	.4485289083126E+00	-.1056743932229E-01
.3058632330801E+01	.9351758120166E+00	-.4694175599337E-01	.4505816154997E+00	-.9916930071344E-02
.3210224504270E+01	.9439330971932E+00	-.4323663767554E-01	.4525084491403E+00	-.9237713166846E-02
.3368985189718E+01	.9520393239133E+00	-.3947199740995E-01	.4542988196321E+00	-.8524400003370E-02
.3535270423239E+01	.9594630122367E+00	-.3566345405669E-01	.4559436723518E+00	-.7778373818451E-02
.3709457559974E+01	.9661819487697E+00	-.3184305349126E-01	.4574360370004E+00	-.7006574131105E-02
.3891946694355E+01	.9721847941105E+00	-.2805569270021F-01	.4587715024359E+00	-.6220248164156E-02

VELOCITY PROFILES AT $x/c = 0.897$ - Concluded

y/δ_1	U/U_e	$(U/U_e)''$	W/U_e	$(W/U_e)''$
.4083162049663E+01	.9774722800430E+00	-.2435496933622E-01	.4599485834708E+00	-.5433657602836E-02
.4283553305364E+01	.9820578754075E+00	-.2079883514382E-01	.4609689475040E+00	-.4662746998801E-02
.4493596833179E+01	.9859678205945E+00	-.1744490011935E-01	.4618374737725E+00	-.3923802620813E-02
.4713796818294E+01	.9892404657535E+00	-.1434601460951E-01	.4625621270370E+00	-.3232154955758E-02
.4944686250708E+01	.9919248976035E+00	-.1154613493112E-01	.4631536407191E+00	-.2600999694214E-02
.5186827783352E+01	.9940789020911E+00	-.9077014117895E-02	.4636250212332E+00	-.2040425053868E-02
.5440814467727E+01	.9957663797159E+00	-.6955891480552E-02	.4639909039393E+00	-.1556732493130E-02
.5707270393558E+01	.9970543983081E+00	-.5184524557946E-02	.4642668093657E+00	-.1152120157431E-02
.5986851274919E+01	.9980101229664E+00	-.3749670076175E-02	.4644683630385E+00	-.8247640220938E-03
.6280245039577E+01	.9986978926034E+00	-.2624978080906E-02	.4646105502270E+00	-.5692847202981E-03
.6588172488924E+01	.9991767070926E+00	-.1774063231446E-02	.4647070755427E+00	-.3775361550866E-03
.6911388100611E+01	.9994983437718E+00	-.1154339096820E-02	.4647698854049E+00	-.2396053533510E-03
.7250681043246E+01	.9997062404879E+00	-.7210838916367E-03	.4648088897617E+00	-.1448822460374E-03
.7606876461505E+01	.9998351769727E+00	-.4311830994133E-03	.4648318913666E+00	-.8305152731967E-04
.7980837071277E+01	.9999116769599E+00	-.2460788731962E-03	.4648447015801E+00	-.4487993727532E-04
.8373465080086E+01	.9999549627583E+00	-.1336329215242E-03	.4648513971799E+00	-.2271793676908E-04
.8785704421734E+01	.9999782410671E+00	-.6883655301777E-04	.4648546583346E+00	-.1069459216488E-04
.9218543270104E+01	.9999900929787E+00	-.3352002308891E-04	.4648561265001E+00	-.4643663825714E-05
.9673016780085E+01	.9999957786449E+00	-.1536718145759E-04	.4648567317475E+00	-.1942216965836E-05
.1015020999661E+02	.9999983325352E+00	-.6596974171775E-05	.4648569577408E+00	-.6604041602059E-06
.1065126087723E+02	.9999993973556E+00	-.2631540045730E-05	.4648570331843E+00	-.2111510255996E-06
.1117736338761E+02	.9999998043888E+00	-.9643475827583E-06	.4648570553481E+00	-.5926720735144E-07
.1172977064960E+02	.9999999445056E+00	-.3191619998012E-06	.4648570609651E+00	-.1431713881875E-07
.1230979814170E+02	.9999999868084E+00	-.9298235473485E-07	.4648570621608E+00	-.2899655293346E-08
.1291882696897E+02	.9999999975589E+00	-.2291233308468E-07	.4648570623664E+00	-.4740246886782E-09
.1355830722858E+02	.9999999997003E+00	-.4459598211301E-08	.4648570623931E+00	-.5854588312688E-10
.1422976149988E+02	.9999999999860E+00	-.5895190756806E-09	.4648570623953E+00	-.4716108988252E-11
.1493478848472E+02	.1000000000000E+01	-.2811791307070E-10	.4648570623953E+00	-.9649004231176E-13

VELOCITY PROFILES AT x/c = 0.965

y/δ_1	U/U_e	$(U/U_e)''$	W/U_e	$(W/U_e)''$
0.	0.	-.3512582155672E+01	0.	-.2400598236374E+01
.8028906256254E-02	.1282891225654E-01	-.3442271776351E+01	.8534931975047E-02	-.2354515279332E+01
.1645899976420E-01	.2606004861972E-01	-.3370599272714E+01	.1733299065795E-01	-.2307993590197E+01
.2531003459456E-01	.3969408114144E-01	-.3296529348078E+01	.2639385374980E-01	-.2260460440471E+01
.3460269408918E-01	.5373048457555E-01	-.3221206992866E+01	.3571625053937E-01	-.2211862266993E+01
.4435862971541E-01	.6816734918399E-01	-.3145635079697E+01	.4529788320547E-01	-.2162168631245E+01
.5460050116720E-01	.8300116659829E-01	-.3070534051751E+01	.5513534754656E-01	-.2111385146854E+01
.6535201776085E-01	.9822660241088E-01	-.2996230022661E+01	.6522405217891E-01	-.2059560241646E+01
.7663798119350E-01	.1138362765212E+00	-.2922595084076E+01	.7555813486915E-01	-.2006791356165E+01
.8848432976060E-01	.1298205778158E+00	-.2849059256701E+01	.8613037472967E-01	-.1953204008866E+01
.1009181841642E+00	.1461675413637E+00	-.2774703661743E+01	.9693209975637E-01	-.1898945260040E+01
.1139678950859E+00	.1628628119153E+00	-.2698429656002E+01	.1079530907970E+00	-.1844152524331E+01
.1276630927442E+00	.1798897058996E+00	-.2619180095973E+01	.1191814854702E+00	-.1788927490788E+01
.1420347387020E+00	.1972293657513E+00	-.2536179336856E+01	.1306036884658E+00	-.1733313646413E+01
.1571151802286E+00	.2148609780850E+00	-.2449122451716E+01	.1422042973319E+00	-.1677285909952E+01
.1729382075532E+00	.2327620062477E+00	-.2358294362953E+01	.1539660542735E+00	-.1620758166190E+01
.1895391143579E+00	.2509083752946E+00	-.2264550312276E+01	.1658698335675E+00	-.1563610639490E+01
.2069547455583E+00	.2692745505583E+00	-.2169166825428E+01	.1778946701858E+00	-.1505733355362E+01
.2252236468461E+00	.2878334741534E+00	-.2073582984299E+01	.1900178282566E+00	-.1447075785652E+01
.2443859739302E+00	.3065563656939E+00	-.1979093777396E+01	.2022148994925E+00	-.1387688260868E+01
.2644837324902E+00	.3254124453464E+00	-.1886578013988E+01	.2144599144892E+00	-.1327740135054E+01
.2855607785605E+00	.3443686832064E+00	-.1796341351504E+01	.2267254474411E+00	-.1267504535023E+01
.3076629222108E+00	.3633897000170E+00	-.1708125501045E+01	.2389827004175E+00	-.1207309578938E+01
.3308380209659E+00	.3824379257760E+00	-.1621283657403E+01	.2512015676414E+00	-.1147468578878E+01
.3551360799623E+00	.4014740623374E+00	-.1535065776590E+01	.2633507000785E+00	-.1088212190445E+01
.3806093596262E+00	.4204578086278E+00	-.1448917051893E+01	.2753976087760E+00	-.1029648394528E+01
.4073124016791E+00	.4393487230653E+00	-.1362687143855E+01	.2873088524136E+00	-.9717682483447E+00
.4353026042069E+00	.4581070529315E+00	-.1276682146117E+01	.2990503432459E+00	-.9144977770621E+00
.4646394563612E+00	.4766943793824E+00	-.1191554018156E+01	.3105877761270E+00	-.8577759777114E+00
.4953855830361E+00	.4950740078871E+00	-.1108086910230E+01	.3218871477190E+00	-.8016257918614E+00
.5276064496359E+00	.5132111447758E+00	-.1026977474467E+01	.3329153047082E+00	-.7461872789091E+00
.5613706168881E+00	.5310729893145E+00	-.9487019931987E+00	.3436404570195E+00	-.6917006114390E+00
.5967499156332E+00	.5486288873197E+00	-.8734798446878E+00	.3540326187650E+00	-.6384517040673E+00
.6338196315816E+00	.5658506664482E+00	-.8013731144500E+00	.3640639828222E+00	-.5867112808708E+00
.6726587001740E+00	.5827131333885E+00	-.7324210059103E+00	.3737092691026E+00	-.5366976042496E+00
.7133499118384E+00	.5991946070115E+00	-.6666917257792E+00	.3829460902542E+00	-.4885744319583E+00
.7559801277914E+00	.6152774024272E+00	-.6043190667270E+00	.3917553506370E+00	-.4424740572373E+00
.8006450506902E+00	.6309481545309E+00	-.5454768800842E+00	.4001216537499E+00	-.3985236394990E+00
.8474267372713E+00	.6461979456171E+00	-.4903095044058E+00	.4080336662462E+00	-.3568564501068E+00
.8964392886772E+00	.6610223115793E+00	-.4388997813977E+00	.4154843897457E+00	-.3176044770588E+00
.9477836565740E+00	.6754211869824E+00	-.3912665215521E+00	.4224713179257E+00	-.2808819515432E+00
.1001570625510E+01	.6893988121951E+00	-.3473817998153E+00	.4289964836007E+00	-.2467718280841E+00
.1057916534756E+01	.7029635841588E+00	-.3071898085064E+00	.4350664112231E+00	-.2153209707334E+00
.1116943551797E+01	.7161278090810E+00	-.2706125025289E+00	.4406919834632E+00	-.1865421570202E+00
.1178779952649E+01	.7289073374321E+00	-.2375509622131E+00	.4458882186009E+00	-.1604179021418E+00
.1243560408661E+01	.7413210722534E+00	-.2078811160307E+00	.4506739508231E+00	-.1369027673875E+00
.1311426279650E+01	.7533903689109E+00	-.1814515691100E+00	.4550714114914E+00	-.1159241773217E+00
.1382525913499E+01	.7651383526665E+00	-.1580914864710E+00	.4591057197684E+00	-.9738368739205E-01
.1457014953129E+01	.7765891449057E+00	-.1376114111546E+00	.4628042970324E+00	-.8115975566919E-01
.1535056652413E+01	.7877670215906E+00	-.1198067507235E+00	.4661962201696E+00	-.6711155676452E-01
.1616822202846E+01	.7986955226661E+00	-.1044607757891E+00	.4693115286748E+00	-.5508294986966E-01
.1702491073425E+01	.8093965396453E+00	-.9134678529853E-01	.4721805029853E+00	-.4490613738984E-01
.1792251367079E+01	.8198894264941E+00	-.8022967438109E-01	.4748329365252E+00	-.3640518816952E-01
.1886300197828E+01	.8301901724368E+00	-.7087513777664E-01	.4772974282930E+00	-.2939965995998E-01
.1984844093661E+01	.8403106788010E+00	-.6304920981691E-01	.4796007247910E+00	-.2370828482001E-01
.2088099431053E+01	.8502581791227E+00	-.5652576805504E-01	.4817671402854E+00	-.1915262183253E-01
.2196292907468E+01	.8600348332710E+00	-.5109086619768E-01	.4838180826791E+00	-.1556061486784E-01
.2309662058755E+01	.8696375157858E+00	-.4654707440933E-01	.4857717078323E+00	-.1276995412980E-01
.2428455828513E+01	.8790578058574E+00	-.4271691553914E-01	.4876427177750E+00	-.1063107035291E-01
.2552935196322E+01	.8882821739742E+00	-.3944505860061E-01	.4894423086517E+00	-.9009556924861E-02
.2683373871429E+01	.8972923509499E+00	-.3659918974303E-01	.4911782637200E+00	-.7787837688844E-02
.2820059576662E+01	.9060658591757E+00	-.3406960905591E-01	.4928551767773E+00	-.6865961071946E-02
.2963292294481E+01	.9145766847220E+00	-.3176780035890E-01	.4944747835317E+00	-.6161494011261E-02
.3113390377917E+01	.9227960711062E+00	-.2962433876287E-01	.4960363738136E+00	-.5608598493890E-02
.3270686363856E+01	.9306934195271E+00	-.2758645015896E-01	.4975372565604E+00	-.5156462154195E-02
.3435530654669E+01	.9382372837251E+00	-.2561565242589E-01	.4989732517589E+00	-.4767323338640E-02
.3608292168500E+01	.9453964481821E+00	-.2368559331596E-01	.5003391878662E+00	-.4414327756581E-02
.3789359588588E+01	.9521410747233E+00	-.2178024143720E-01	.5016293883973E+00	-.4079431897173E-02
.3979142687739E+01	.9584438944802E+00	-.1989238927094E-01	.5028381351251E+00	-.3751500568960E-02
.4178073720416E+01	.9642814106270E+00	-.1802237522251E-01	.5039600992055E+00	-.3424676172345E-02
.4386608872071E+01	.9696350642673E+00	-.1617689909761E-01	.5049907310636E+00	-.3097034265854E-02
.4605229752338E+01	.9744923037631E+00	-.1436781752775E-01	.5059266004407E+00	-.2769496533574E-02
.4834444915992E+01	.9788474891396E+00	-.1261084568591E-01	.5067656761521E+00	-.2444951034568E-02

VELOCITY PROFILES AT   x/c = 0.965 - Concluded

y/δ_1	U/U_e	$(U/U_e)''$	W/U_e	$(W/U_e)''$
.5074791393494E+01	.9827025600298E+00	-.1092414285988E-01	.5075075341557E+00	-.2127527242205E-02
.5326836211970E+01	.9860673994952E+00	-.9326808522802E-02	.5081534824425E+00	-.1821983371820E-02
.5591177888143E+01	.9889598378103E+00	-.7837354214590E-02	.5087065928813E+00	-.1533179151079E-02
.5868447877323E+01	.9914052601312E+00	-.6472241796466E-02	.5091716338198E+00	-.1265623214696E-02
.6159311967392E+01	.9934358092311E+00	-.5244590455615E-02	.5095549029736E+00	-.1023097358296E-02
.6464471613740E+01	.9950892076008E+00	-.4163154078384E-02	.5098639675633E+00	-.8083681500018E-03
.6784665220075E+01	.9964072593715E+00	-.3231657613388E-02	.5101073270537E+00	-.6229992423541E-03
.7120669380383E+01	.9974341277382E+00	-.2448555673770E-02	.5102940221250E+00	-.4672751770644E-03
.7473300108252E+01	.9982145127915E+00	-.1807239449655E-02	.5104332203609E+00	-.3402403055255E-03
.7843414090128E+01	.9987918725438E+00	-.1296671587171E-02	.5105338131879E+00	-.2398459598849E-03
.8231910007580E+01	.9992068317366E+00	-.9023785368179E-03	.5106040586959E+00	-.1631871562199E-03
.8639729979013E+01	.9994959059805E+00	-.6076840010118E-03	.5106513004618E+00	-.1067992138782E-03
.9067861172205E+01	.9996906333181E+00	-.3950348523588E-03	.5106817835279E+00	-.6697714042244E-04
.9517337634901E+01	.9998171556349E+00	-.2472603997310E-03	.5107005763486E+00	-.4007843419116E-04
.9989242381276E+01	.9998962363227E+00	-.1486216375910E-03	.5107115937712E+00	-.2277411390750E-04
.1048470975823E+02	.9999436483067E+00	-.8554784978129E-04	.5107177034721E+00	-.1222297378693E-04
.1100492809882E+02	.9999708279305E+00	-.4701591002845E-04	.5107208892045E+00	-.6158425010549E-05
.1155114265313E+02	.9999856723560E+00	-.2459008805879E-04	.5107224404886E+00	-.2892771390346E-05
.1212465877224E+02	.9999933630975E+00	-.1219204683263E-04	.5107231404657E+00	-.1256831212681E-05
.1272684531159E+02	.9999971223662E+00	-.5703013269284E-05	.5107234305217E+00	-.5004994108152E-06
.1335913821688E+02	.9999988438288E+00	-.2500746623225E-05	.5107235397460E+00	-.1907527539157E-06
.1402304426041E+02	.9999995753464E+00	-.1018949814627E-05	.5107235766575E+00	-.5845990964116E-07
.1472014490549E+02	.9999998600703E+00	-.3810490092354E-06	.5107235876823E+00	-.1667585143956E-07
.1545210029060E+02	.9999999597407E+00	-.1284974622462E-06	.5107235905369E+00	-.4115530051356E-08
.1622065333840E+02	.9999999903016E+00	-.3808267254561E-07	.5107235911611E+00	-.8565420575785E-09
.1702763400596E+02	.9999999981809E+00	-.9532829898647E-08	.5107235912721E+00	-.1447960946906E-09
.1787496369911E+02	.9999999997729E+00	-.18693867644486E-08	.5107235912871E+00	-.1861974678196E-10
.1876465987574E+02	.1000000000000E+01	-.28688975550965E-09	.5107235912884E+00	-.1705533900762E-11

REFERENCES

1. Michel, Roger: Investigation of Boundary Layer Transition on Airfoils. ONERA Rapp. No. 1/1578 A, July 1951.

2. Schlichting, Hermann (J. Kestin, transl.): Boundary-Layer Theory, Sixth ed. McGraw-Hill Book Co., Inc., c.1968.

3. Saric, William S.; and Nayfeh, Ali H.: Non-Parallel Stability of Boundary-Layer Flows. VPI-E-75-5, Virginia Polytech. Inst. & State Univ., Feb. 1975.

4. Mack, Leslie M.: On the Stability of the Boundary Layer on a Transonic Swept Wing. AIAA Paper 79-0264, Jan. 1979.

5. Srokowski, Andrew J.; and Orszag, Steven A.: Mass Flow Requirements for LFC Wing Design. AIAA Paper 77-1222, Aug. 1977.

6. Gregory, N.; Stuart, J. T.; and Walker, W. S.: On the Stability of Three-Dimensional Boundary Layers With Application to the Flow Due to a Rotating Disk. Philos. Trans. Roy. Soc. London, ser. A, vol. 248, no. 943, July 14, 1955, pp. 155-199.

7. Betchov, Robert; and Criminale, William O., Jr.: Stability of Parallel Flows. Academic Press, Inc., 1967.

8. Gaster, M.: A Note on a Relation Between Temporally-Increasing and Spatially-Increasing Disturbances in Hydrodynamic Stability. J. Fluid Mech., vol. 14, pt. 2, Oct. 1962, pp. 222-224.

9. Brown, W. Byron: Numerical Calculation of the Stability of Cross-Flow Profiles in Laminar Boundary Layers on a Rotating Disc and on a Swept-Back Wing and an Exact Calculation of the Stability of the Blasius Velocity Profile. Rep. No. NAI-59-5 (BLC-117) (Contract No. AF33(616)-3168), Northrop Aircraft, Inc., Jan. 1959. (Available from DTIC as AD 314 541.)

10. Blottner, F. G.: Computational Techniques for Boundary Layers. Paper for AGARD Lecture Series 73 on Computational Methods for Inviscid and Viscous Two- and Three-Dimensional Flow Fields (Von Karman Inst.), Feb. 17-22, 1975.

11. Schubauer, G. B.; and Skramstad, H. K.: Laminar-Boundary-Layer Oscillations and Transition on a Flat Plate. NACA Rep. 909, 1948.

12. Kaplan, Richard E.: The Stability of Laminar Incompressible Boundary Layers in the Presence of Compliant Boundaries. ASRL TR 116-1 (Contract Nonr-1841(89)), Massachusetts Inst. Technol., June 1964. (Available from DTIC as AD 601 779.)

13. Pfenninger, Werner: Laminar Flow Control Laminarization. Special Course on Concepts for Drag Reduction, AGARD-R-654, June 1977, pp. 3-1 - 3-75.

14. Bauer, F.; Garabedian, P.; and Korn, D.: A Theory of Supercritical Wing Sections, With Computer Programs and Examples. Volume 66 of Lecture Notes in Economics and Mathematical Systems, Springer-Verlag, 1972.

15. Kaups, Kalle; and Cebeci, Tuncer: Compressible Laminar Boundary Layers With Suction on Swept and Tapered Wings. J. Aircr., vol. 14, no. 7, July 1977, pp. 661-667.

16. Hefner, Jerry N.; and Bushnell, Dennis M.: Application of Stability Theory to Laminar Flow Control. AIAA Paper 79-1493, July 1979.

17. Pfenninger, W.; Reed, Helen L.; and Dagenhart, J. R.: Design Considerations of Advanced Supercritical Low Drag Suction Airfoils. Viscous Flow Drag Reduction, Gary R. Hough, ed., AIAA, c.1980, pp. 249-271.

18. Allison, Dennis O.; and Dagenhart, John R.: Design of a Laminar-Flow-Control Supercritical Airfoil for a Swept Wing. CTOL Transport Technology - 1978, NASA CP-2036, Pt. I, 1978, pp. 395-408.

TABLE I.- NONDIMENSIONAL SPATIAL AMPLIFICATION RATES

FOR STATIONARY CROSSFLOW DISTURBANCES

(a) $H_c = 0.3206$; $W_M/U_{e,t} = -0.06689$

Nondimensional wave number, $\alpha_r\delta_{10}$	Reynolds number, $R_{\delta_{10}}$						
	50.00	75.00	100.00	200.00	500.00	1000.00	2000.00
	Nondimensional spatial amplification rates, $\alpha_i\delta_{10}$						
0.00	0.0000000[a]	0.0000000[a]	0.0000000[a]	0.0000000[a]	0.0000000[a]	0.0000000[a]	0.0000000[a]
.05	.0125000[a]	.0110000[a]	.0095000[a]	.0085000[a]	.0070000[a]	.0060000[a]	.0006674
.10	.0240000[a]	.0205000[a]	.0180000[a]	.0160000[a]	.0135000[a]	.0110100	-.0029530
.20	.0277200	.0210000[a]	.0158300	.0057620	-.0033200	-.0081060	-.0117000
.40	.0228700	.0129100	.0067280	-.0052730	-.0163200	-.0217000	-.0250300
.60	.0166200	.0056830	-.0010560	-.0141800	-.0254700	-.0302100	-.0328100
.80	.0119800	.0003101	-.0068610	-.0204900	-.0312300	-.0352800	-.0373700
1.00	.0089350	-.0033690	-.0108500	-.0246000	-.0346600	-.0382200	-.0400500
1.20	.0073120	-.0055510	-.0132500	-.0269800	-.0364400	-.0397500	-.0415100
1.40	.0069690	-.0064060	-.0142900	-.0279400	-.0369800	-.0402400	-.0420600
1.60	.0078110	-.0060550	-.0141000	-.0276900	-.0365100	-.0398600	-.0418400
1.80	.0097820	-.0045720	-.0127800	-.0263400	-.0351000	-.0386600	-.0408800
2.00	.0128600	-.0019930	-.0103700	-.0239300	-.0327800	-.0366200	-.0391500
2.20	.0170400	.0016760	-.0068670	-.0204600	-.0295100	-.0337000	-.0366000
2.40	.0223500	.0064560	-.0022610	-.0158900	-.0252400	-.0298200	-.0331600
2.60	.0288100	.0123800	.0034940	-.0101500	-.0198700	-.0248300	-.0285300
2.80	.0364900	.0195100	.0104600	-.0031540	-.0132800	-.0184300	-.0222000
3.00	.0454200	.0278900	.0187000	.0052300	-.0053420	-.0113600	-.0158300
3.20	.0556600	.0375900	.0283000	.0151600	.0040220	-.0030480	-.0092210
3.40	.0672600	.0486700	.0393500	.0268500	.0150100	.0087160	.0003436
3.60	.0802800	.0611900	.0519100	.0405600	.0289800	.0240200	.0154100
3.80	.0947300	.0751600	.0660200	.0566000	.0453600	.0250200	.0146300
4.00	.1106000	.0905700	.0816600	.0756800	.0548100	.0269500	.0153500

[a]Extrapolated.

TABLE I.- Continued

(b) $H_C = 0.3670$; $W_M/U_{e,t} = -0.05767$

Nondimensional wave number, $\alpha_r \delta_{10}$	Reynolds number, $R_{\delta_{10}}$						
	50.00	75.00	100.00	200.00	500.00	1000.00	2000.00
	Nondimensional spatial amplification rates, $\alpha_i \delta_{10}$						
0.00	0.0000000[a]	0.0000000[a]	0.0000000[a]	0.0000000[a]	0.0000000[a]	0.0000000[a]	0.0000000[a]
.05	.0105000[a]	.0085000[a]	.0073000[a]	.0043000[a]	.0024000[a]	.0009000[a]	.0000319
.10	.0126000[a]	.0104700	.0089940	.0051300	.0012320	-.0005744	-.0017520
.20	.0143000[a]	.0111000[b]	.0080000[b]	.0020000[b]	-.0023670	-.0047090	-.0063330
.40	.0125000[a]	.0068170	.0030130	-.0040920	-.0101000	-.0127900	-.0143400
.60	.0091580	.0021120	-.0021050	-.0099460	-.0161700	-.0185800	-.0198300
.80	.0059290	-.0016830	-.0062120	-.0144300	-.0204400	-.0225600	-.0236100
1.00	.0035900	-.0045160	-.0092800	-.0176600	-.0234100	-.0253700	-.0263300
1.20	.0020980	-.0064530	-.0114000	-.0198700	-.0254600	-.0273800	-.0283400
1.40	.0013930	-.0075760	-.0126900	-.0212400	-.0268000	-.0287600	-.0298000
1.60	.0014310	-.0079470	-.0132200	-.0218900	-.0275300	-.0296100	-.0307700
1.80	.0021880	-.0076030	-.0130400	-.0218800	-.0276800	-.0299100	-.0312100
2.00	.0036560	-.0065580	-.0121700	-.0212200	-.0272500	-.0296400	-.0311000
2.20	.0058420	-.0048100	-.0106100	-.0199000	-.0261900	-.0287500	-.0303700
2.40	.0087640	-.0023410	-.0083300	-.0178900	-.0244700	-.0272000	-.0289600
2.60	.0124500	.0008771	-.0053120	-.0151500	-.0220400	-.0249200	-.0267700
2.80	.0169200	.0048780	-.0015120	-.0116500	-.0188300	-.0218600	-.0237100
3.00	.0222300	.0097080	.0031190	-.0073040	-.0147900	-.0179900	-.0200000
3.20	.0284200	.0154200	.0086420	-.0020590	-.0098500	-.0133500	-.0159400
3.40	.0355500	.0220800	.0151400	.0041810	-.0039540	-.0078950	-.0112900
3.60	.0436700	.0297800	.0227100	.0115400	.0030210	-.0009565	-.0050010
3.80	.0528800	.0386400	.0315000	.0201600	.0116000	.0104000	.0068150
4.00	.0632800	.0488100	.0417500	.0302700	.0228800	.0131500	.0065310

[a]Extrapolated.
[b]Interpolated.

TABLE I.- Continued

(c) $H_c = 0.4299$; $W_M/U_{e,t} = -0.04624$

Nondimensional wave number, $\alpha_r \delta_{10}$	Reynolds number, $R_{\delta_{10}}$							
	30.00	50.00	75.00	100.00	200.00	500.00	1000.00	2000.00
	Nondimensional spatial amplification rates, $\alpha_i \delta_{10}$							
0.00	0.0000000[a]	0.0000000[a]	0.0000000[a]	0.0000000[a]	0.0000000[a]	0.0000000[a]	0.0000000[a]	0.0000000[a]
.05	.0108000[a]	.0080000[a]	.0065000[a]	.0050000[a]	.0040380	.0016080	.0003859	-.0003052
.10	.0140000[a]	.0115000[a]	.0095000[a]	.0072790	.0036730	.0003593	-.0009859	-.0017540
.20	.0168000	.0123800	.0084800	.0059060	.0010550	-.0026270	-.0041920	-.0052140
.40	.0170500	.0092680	.0040920	.0010760	-.0042540	-.0084310	-.0101900	-.0111800
.60	.0145600	.0057780	.0002637	-.0029220	-.0086150	-.0129200	-.0145300	-.0153500
.80	.0124900	.0031480	-.0026640	-.0060310	-.0119800	-.0162000	-.0176800	-.0184100
1.00	.0111700	.0012750	-.0048650	-.0084070	-.0145200	-.0186800	-.0201200	-.0208100
1.20	.0105300	.0000211	-.0064680	-.0101700	-.0164500	-.0206300	-.0220800	-.0228000
1.40	.0104800	-.0006994	-.0075490	-.0114200	-.0178800	-.0221600	-.0236700	-.0244400
1.60	.0109900	-.0009274	-.0081510	-.0121900	-.0188700	-.0233000	-.0249000	-.0257300
1.80	.0120200	-.0006749	-.0082870	-.0125100	-.0194300	-.0240500	-.0257400	-.0266300
2.00	.0135900	.0000650	-.0079500	-.0123600	-.0195600	-.0243700	-.0261500	-.0271000
2.20	.0157000	.0013100	-.0071220	-.0117300	-.0192200	-.0242300	-.0260900	-.0271000
2.40	.0183700	.0030860	-.0057780	-.0105900	-.0183800	-.0235900	-.0255300	-.0266000
2.60	.0216300	.0054190	-.0038900	-.0089110	-.0170100	-.0224100	-.0244400	-.0255500
2.80	.0255200	.0083390	-.0014290	-.0066680	-.0150800	-.0206800	-.0227700	-.0239100
3.00	.0300600	.0118800	.0016340	-.0038280	-.0125600	-.0183600	-.0204800	-.0215600
3.20	.0352800	.0160600	.0053330	-.0003583	-.0094250	-.0154200	-.0175000	-.0183500
3.40	.0412200	.0209300	.0097020	.0037760	-.0056330	-.0118100	-.0137300	-.0140800
3.60	.0479200	.0265300	.0147800	.0086170	-.0011480	-.0074770	-.0091980	-.0081920
3.80	.0554100	.0328900	.0206300	.0142200	.0040790	-.0024260	-.0043550	-.0038950
4.00	.0637700	.0401000	.0273100	.0206400	.0101100	.0032440	.0005370	-.0002342

[a]Extrapolated.

TABLE I.- Continued

(d) $H_c = 0.2444$; $W_M/U_{e,t} = 0.01678$

Nondimensional wave number, $\alpha_r \delta_{10}$	Reynolds number, $R_{\delta_{10}}$							
	50.00	75.00	100.00	150.00	200.00	500.00	1000.00	2000.00
	Nondimensional spatial amplification rates, $\alpha_i \delta_{10}$							
0.00	0.0000000[a]	0.0000000[a]	0.0000000[a]	0.0000000[a]	0.0000000[a]	0.0000000[a]	0.0000000[a]	0.0000000[a]
.05	.0036000[a]	.0030000[a]	.0026000[a]	.0023000[a]	.0019470	.0011320	.0006611	.0003065
.10	.0050000[a]	.0039640	.0033500[a]	.0027640	.0022790	.0010120	.0003025	-.0002598
.20	.0058610	.0045920	.0037130	.0025860	.0018730	.0000142	-.0010880	-.0019790
.40	.0058090	.0039040	.0026730	.0011070	.0001023	-.0025720	-.0040330	-.0050200
.60	.0051910	.0029240	.0014540	-.0004300	-.0016330	-.0046430	-.0060790	-.0069430
.80	.0046910	.0021290	.0004676	-.0016370	-.0029470	-.0060170	-.0073300	-.0080770
1.00	.0044350	.0016170	-.0001934	-.0024440	-.0038060	-.0068230	-.0080120	-.0086890
1.20	.0044520	.0014100	-.0005199	-.0028720	-.0042600	-.0071830	-.0082800	-.0089340
1.40	.0047480	.0015010	-.0005296	-.0029600	-.0043610	-.0071840	-.0082290	-.0089000
1.60	.0053200	.0018800	-.0002440	-.0027420	-.0041510	-.0068800	-.0079150	-.0086340
1.80	.0061650	.0025320	.0003182	-.0022440	-.0036600	-.0063080	-.0073710	-.0081620
2.00	.0072780	.0034480	.0011420	-.0014870	-.0029080	-.0054900	-.0066130	-.0074970
2.20	.0086530	.0046170	.0022140	-.0004843	-.0019130	-.0044410	-.0056490	-.0066400
2.40	.0102900	.0060310	.0035240	.0007492	-.0006886	-.0031700	-.0044820	-.0057790
2.60	.0121700	.0076800	.0050590	.0022010	.0007536	-.0016830	-.0031150	-.0043330
2.80	.0143000	.0095540	.0068100	.0038590	.0024010	.0000174	-.0015660	-.0030090
3.00	.0166700	.0116400	.0087640	.0057110	.0042410	.0019240	.0001605	-.0015390
3.20	.0192600	.0139300	.0109100	.0077410	.0062600	.0040300	.0021650	.0005242
3.40	.0220700	.0164200	.0132300	.0099380	.0084430	.0063450	.0045250	.0035830
3.60	.0250800	.0190800	.0157200	.0122900	.0107800	.0089020	.0065910	.0042170
3.80	.0282900	.0219100	.0183600	.0147700	.0132500	.0116600	.0082330	.0049330
4.00	.0316700	.0248900	.0211400	.0173800	.0158300	.0144700	.0102000	.0057170

[a]Extrapolated.

TABLE I.- Continued

(e) $H_c = 0.2132;$ $W_M/U_{e,t} = 0.01753$

Nondimensional wave number, $\alpha_r \delta_{10}$	Reynolds number, $R_{\delta_{10}}$						
	100.00	150.00	200.00	250.00	500.00	1000.00	2000.00
	Nondimensional spatial amplification rates, $\alpha_i \delta_{10}$						
0.00	0.0000000[a]	0.0000000[a]	0.0000000[a]	0.0000000[a]	0.0000000[a]	0.0000000[a]	0.0000000[a]
.05	.0019000[a]	.0017000[a]	.0015050	.0013640	.0009490	.0006249	.0003892
.10	.0027770	.0022960	.0019560	.0017100	.0010580	.0005587	.0001577
.20	.0033800	.0025490	.0020160	.0016360	.0006088	-.0002551	-.0010030
.40	.0031240	.0018590	.0010360	.0004357	-.0012270	-.0025610	-.0035520
.60	.0024230	.0008169	-.0002276	-.0009803	-.0029660	-.0044030	-.0053630
.80	.0017730	-.0000888	-.0012740	-.0021080	-.0042050	-.0056010	-.0064710
1.00	.0013380	-.0007038	-.0019720	-.0028450	-.0049490	-.0062500	-.0070480
1.20	.0011720	-.0009987	-.0023160	-.0032050	-.0052600	-.0064540	-.0072230
1.40	.0012850	-.0009841	-.0023300	-.0032210	-.0051920	-.0062900	-.0070750
1.60	.0016680	-.0006798	-.0020420	-.0029240	-.0047680	-.0058100	-.0066500
1.80	.0023100	-.0001051	-.0014740	-.0023400	-.0040740	-.0050480	-.0059760
2.00	.0031980	.0007228	-.0006451	-.0014880	-.0030650	-.0040200	-.0050610
2.20	.0043190	.0017890	.0004277	-.0003833	-.0017660	-.0027350	-.0039140
2.40	.0056630	.0030780	.0017310	.0009605	-.0001707	-.0011910	-.0025540
2.60	.0072180	.0045780	.0032500	.0025310	.0017400	.0006173	-.0009434
2.80	.0089700	.0062740	.0049690	.0043140	.0040020	.0027510	.0012580
3.00	.0109100	.0081480	.0068700	.0062880	.0066790	.0052930	.0036810
3.20	.0130100	.0101800	.0089290	.0084250	.0098820	.0077790	.0047600
3.40	.0152800	.0123600	.0111200	.0106900	.0135300	.0100400	.0057640
3.60	.0176800	.0146600	.0134200	.0130200	.0170800	.0139500	.0061880
3.80	.0202100	.0170400	.0157600	.0153800	.0199800	.0187300	.0061880[a]
4.00	.0228400	.0195000	.0181400	.0177200	.0218700	.0172900	.0061880[a]

[a]Extrapolated.

TABLE I.- Continued

(f) $H_c = 0.1847$; $W_M/U_{e,t} = 0.02234$

Nondimensional wave number, $\alpha_r \delta_{10}$	Reynolds number, $R_{\delta_{10}}$						
	100.00	150.00	200.00	250.00	500.00	1000.00	2000.00
	Nondimensional spatial amplification rates, $\alpha_i \delta_{10}$						
0.00	0.0000000[a]	0.0000000[a]	0.0000000[a]	0.0000000[a]	0.0000000[a]	0.0000000[a]	0.0000000[a]
.05	.0020000[a]	.0018000[a]	.0016000[a]	.0015370	.0012000[a]	.0008000[a]	.0005977
.10	.0030000[a]	.0026710	.0023620	.0021280	.0014890	.0009684	.0005129
.20	.0041540	.0033500	.0028190	.0024310	.0013410	.0003470	-.0005927
.40	.0045190	.0031880	.0022930	.0016220	-.0003434	-.0020770	-.0034860
.60	.0041910	.0024100	.0012060	.0003104	-.0022060	-.0042220	-.0057030
.80	.0038000	.0016570	.0002317	-.0008085	-.0036070	-.0056900	-.0071070
1.00	.0035890	.0011680	-.0004101	-.0015410	-.0044770	-.0065240	-.0078370
1.20	.0036510	.0010120	-.0006763	-.0018680	-.0048620	-.0068180	-.0080310
1.40	.0040150	.0011940	-.0005813	-.0018160	-.0048200	-.0066520	-.0077930
1.60	.0046780	.0016930	-.0001558	-.0014240	-.0044100	-.0060950	-.0071990
1.80	.0056260	.0024850	.0005659	-.0007333	-.0036820	-.0052000	-.0063050
2.00	.0068390	.0035390	.0015480	.0002179	-.0026870	-.0040180	-.0051570
2.20	.0082950	.0048260	.0027560	.0013900	-.0014720	-.0025930	-.0037920
2.40	.0099710	.0063140	.0041550	.0027450	-.0000866	-.0009724	-.0022230
2.60	.0118400	.0079750	.0057110	.0042470	.0014250	.0008016	-.0005212
2.80	.0138800	.0097810	.0073950	.0058650	.0030240	.0026760	.0011510
3.00	.0160700	.0117100	.0091820	.0075720	.0046790	.0046120	.0028740
3.20	.0183800	.0137300	.0110500	.0093470	.0063680	.0066280	.0049610
3.40	.0208000	.0158400	.0129800	.0111800	.0080740	.0087390	.0072790
3.60	.0233200	.0180200	.0149700	.0130500	.0097870	.0108100	.0087760
3.80	.0259200	.0202500	.0170000	.0149500	.0115000	.0127000	.0100100
4.00	.0285800	.0225400	.0190700	.0168900	.0132200	.0146100	.0118400

[a]Extrapolated.

TABLE I.- Continued

(g) $H_c = 0.1668;$ $W_M/U_{e,t} = 0.02927$

Nondimensional wave number, $\alpha_r \delta_{10}$	Reynolds number, $R_{\delta_{10}}$							
	150.00	200.00	250.00	300.00	400.00	500.00	1000.00	2000.00
	Nondimensional spatial amplification rates, $\alpha_i \delta_{10}$							
0.00	0.0000000[a]	0.0000000[a]	0.0000000[a]	0.0000000[a]	0.0000000[a]	0.0000000[a]	0.0000000[a]	0.0000000[a]
.05	.0022000[a]	.0019460[b]	.0018370[b]	.0016000[a]	.0014000[a]	.0012500[a]	.0011000[a]	.0008929
.10	.0034000[a]	.0031000[b]	.0028000[b]	.0025000[a]	.0022860	.0020880	.0015380	.0010270[b]
.20	.0044570	.0039090	.0035030	.0031830	.0026930	.0023220	.0011690	.0000000[b]
.40	.0049520	.0039550	.0031880	.0025630	.0015800	.0008212	-.0014510	-.0034510
.60	.0045200	.0030990	.0020100	.0011320	-.0002181	-.0012260	-.0040490	-.0063050
.80	.0039770	.0022240	.0009038	-.0001416	-.0017150	-.0028610	-.0059340	-.0082230
1.00	.0036680	.0016650	.0001802	-.0009791	-.0026950	-.0039220	-.0070910	-.0093070
1.20	.0037100	.0015090	-.0001018	-.0013450	-.0031600	-.0044350	-.0076110	-.0096990
1.40	.0041250	.0017530	.0000368	-.0012750	-.0031630	-.0044670	-.0075900	-.0095270
1.60	.0048930	.0023630	.0005513	-.0008199	-.0027690	-.0040890	-.0071160	-.0088930
1.80	.0059810	.0032960	.0013920	-.0000362	-.0020380	-.0033690	-.0062660	-.0078810
2.00	.0073520	.0045080	.0025090	.0010240	-.0010310	-.0023690	-.0051070	-.0065670
2.20	.0089690	.0059570	.0038580	.0023120	.0002030	-.0011410	-.0036990	-.0050000
2.40	.0108000	.0076060	.0054000	.0037890	.0016190	.0002665	-.0020920	-.0032210
2.60	.0128100	.0094230	.0071020	.0054190	.0031810	.0018170	-.0003297	-.0012760
2.80	.0149700	.0113800	.0089360	.0071760	.0048610	.0034780	.0015520	.0007595
3.00	.0172700	.0134600	.0108800	.0090370	.0066350	.0052270	.0035180	.0028560
3.20	.0196800	.0156400	.0129200	.0109800	.0084860	.0070450	.0055410	.0051030
3.40	.0222000	.0179200	.0150400	.0130100	.0104000	.0089170	.0076160	.0075640
3.60	.0248100	.0202700	.0172400	.0151000	.0123700	.0108300	.0097340	.0100300
3.80	.0275000	.0227000	.0195000	.0172400	.0143800	.0127900	.0118500	.0122400
4.00	.0302700	.0251900	.0218100	.0194300	.0164300	.0147700	.0139300	.0143800

[a]Extrapolated.
[b]Interpolated.

TABLE I.- Continued

(h) $H_c = 0.1535$; $W_M/U_{e,t} = 0.05636$

Nondimensional wave number, $\alpha_r \delta_{10}$	Reynolds number, $R_{\delta_{10}}$							
	200.00	300.00	350.00	400.00	500.00	750.00	1000.00	2000.00
	Nondimensional spatial amplification rates, $\alpha_i \delta_{10}$							
0.00	0.0000000[a]	0.0000000[a]	0.0000000[a]	0.0000000[a]	0.0000000[a]	0.0000000[a]	0.0000000[a]	0.0000000[a]
.05	.0034000[a]	.0028000[a]	.0027000[a]	.0026000[a]	.0025000[a]	.0024000[a]	.0023500[a]	.0022230
.10	.0062000[a]	.0052000	.0049000[a]	.0047000[a]	.0045000[a]	.0042000[a]	.0039240	.0028620
.20	.0086720	.0076510	.0072460	.0068800	.0062350	.0049390	.0039240	.0012520
.40	.0104700	.0079850	.0069640	.0060480	.0044580	.0014510	-.0006952	-.0055480
.60	.0099720	.0060510	.0044940	.0031310	.0008441	-.0032230	-.0059510	-.0116800
.80	.0090230	.0039720	.0020330	.0003643	-.0023740	-.0070740	-.0101100	-.0161900
1.00	.0083850	.0024430	.0002165	-.0016760	-.0047350	-.0098510	-.0130600	-.0192100
1.20	.0082900	.0015960	-.0008646	-.0029350	-.0062410	-.0116500	-.0149500	-.0210100
1.40	.0087580	.0013930	-.0012690	-.0034900	-.0069970	-.0126100	-.0159400	-.0218300
1.60	.0097420	.0017570	-.0010870	-.0034410	-.0071180	-.0128800	-.0162100	-.0218600
1.80	.0111800	.0026050	-.0004070	-.0028810	-.0067050	-.0125800	-.0158800	-.0212700
2.00	.0130100	.0038670	.0006970	-.0018870	-.0058450	-.0118000	-.0150400	-.0201300
2.20	.0151800	.0054850	.0021640	-.0005248	-.0046030	-.0106100	-.0137900	-.0186400
2.40	.0176600	.0074140	.0039470	.0011580	-.0030320	-.0090800	-.0121700	-.0167700
2.60	.0204000	.0096180	.0060080	.0031230	-.0011740	-.0072480	-.0102500	-.0145900
2.80	.0233800	.0120700	.0083190	.0053390	.0009390	-.0051510	-.0080470	-.0121600
3.00	.0265900	.0147500	.0108600	.0077820	.0032820	-.0028170	-.0056020	-.0094910
3.20	.0300100	.0176300	.0136000	.0104300	.0058340	-.0002694	-.0029340	-.0062500
3.40	.0336300	.0207100	.0165400	.0132800	.0085790	.0024750	-.0000637	-.0035790
3.60	.0374400	.0239800	.0196600	.0163100	.0115000	.0053990	.0029920	-.0003471
3.80	.0414200	.0274200	.0229600	.0195000	.0145900	.0084910	.0062210	.0030870
4.00	.0455800	.0310200	.0264100	.0228500	.0178400	.0117400	.0096150	.0067210

[a]Extrapolated.

TABLE I.- Continued

(i) $H_c = 0.1608;$ $W_M/U_{e,t} = 0.07730$

Nondimensional wave number, $\alpha_r \delta_{10}$	Reynolds number, $R_{\delta_{10}}$							
	200.00	250.00	300.00	350.00	400.00	600.00	1000.00	2000.00
	Nondimensional spatial amplification rates, $\alpha_i \delta_{10}$							
0.00	0.0000000[a]	0.0000000[a]	0.0000000[a]	0.0000000[a]	0.0000000[a]	0.0000000[a]	0.0000000[a]	0.0000000[a]
.05	.0053000[a]	.0048000[a]	.0043000[a]	.0037500[a]	.0032000[a]	.0028000[a]	.0017000[a]	.0008000[a]
.10	.0085000[a]	.0075000[a]	.0067000[a]	.0060000[a]	.0055000[a]	.0045000[a]	.0029000[a]	.0016000[a]
.20	.0115000[a]	.0105000[a]	.0094130	.0087220	.0081140	.0062190	.0037660	.0004423
.40	.0126900	.0106300	.0083110	.0074340	.0061430	.0022110	-.0025620	-.0082290
.60	.0113000	.0082360	.0057160	.0035950	.0017780	-.0035290	-.0095110	-.0160200
.80	.0093620	.0055040	.0024020	-.0001596	-.0023190	-.0084400	-.0150200	-.0217600
1.00	.0078410	.0033750	-.0001541	-.0030280	-.0054210	-.0120600	-.0189300	-.0256100
1.20	.0070520	.0020930	-.0017730	-.0048850	-.0074520	-.0144400	-.0214200	-.0279000
1.40	.0070390	.0016560	-.0024910	-.0057980	-.0085010	-.0157400	-.0227200	-.0289200
1.60	.0077530	.0019900	-.0024060	-.0058780	-.0086940	-.0161000	-.0230100	-.0289400
1.80	.0091220	.0030030	-.0016180	-.0052380	-.0081500	-.0156900	-.0224700	-.0281300
2.00	.0110700	.0046140	-.0002195	-.0039740	-.0069720	-.0146000	-.0212300	-.0266600
2.20	.0135300	.0067480	.0017120	-.0021690	-.0052450	-.0129400	-.0193900	-.0246000
2.40	.0164500	.0093460	.0041130	.0001099	-.0030390	-.0107900	-.0170300	-.0221000
2.60	.0197800	.0123600	.0069310	.0028080	-.0004113	-.0082020	-.0142100	-.0191900
2.80	.0234900	.0157400	.0101200	.0058820	.0025930	-.0052280	-.0110000	-.0159400
3.00	.0275400	.0194700	.0136500	.0092950	.0059370	-.0019100	-.0074180	-.0123700
3.20	.0319100	.0235100	.0175000	.0130200	.0095890	.0017200	-.0035100	-.0084840
3.40	.0365800	.0278500	.0216300	.0170200	.0135200	.0056330	.0007053	-.0042780
3.60	.0415200	.0324500	.0260200	.0212900	.0177200	.0098040	.0052120	.0002259
3.80	.0467400	.0373100	.0306700	.0258000	.0221500	.0142100	.0099920	.0049260
4.00	.0522000	.0424200	.0355500	.0305400	.0268100	.0188400	.0150200	.0097250

[a]Extrapolated.

TABLE I.- Concluded

(j) $H_c = 0.1812$; $W_M/U_{e,t} = 0.06187$

Nondimensional wave number, $\alpha_r \delta_{10}$	Reynolds number, $R_{\delta_{10}}$							
	150.00	200.00	250.00	300.00	400.00	600.00	1000.00	2000.00
	Nondimensional spatial amplification rates, $\alpha_i \delta_{10}$							
0.00	0.0000000[a]	0.0000000[a]	0.0000000[a]	0.0000000[a]	0.0000000[a]	0.0000000[a]	0.0000000[a]	0.0000000[a]
.05	.0017000[a]	.0015500[a]	.0013500[a]	.0012500[a]	.0012000[a]	.0011500[a]	.0008500[a]	.0055000[a]
.10	.0034000[a]	.0031000[a]	.0027000[a]	.0025000[a]	.0024000[a]	.0021000[a]	.0017000[a]	.0114600
.20	.0060000[a]	.0052000[a]	.0048000[a]	.0046000	.0042310	.0029650	.0014940	-.0003086
.40	.0088830	.0069730	.0055300	.0043760	.0026080	.0002450	-.0024460	-.0054380
.60	.0083710	.0056610	.0036210	.0020080	-.0004162	-.0035210	-.0068260	-.0102000
.80	.0076380	.0039880	.0014920	-.0004462	-.0032900	-.0068010	-.0103700	-.0138000
1.00	.0064990	.0025930	-.0002363	-.0023980	-.0055110	-.0092500	-.0129000	-.0162600
1.20	.0060380	.0017100	-.0013740	-.0037010	-.0069880	-.0108600	-.0145100	-.0177400
1.40	.0060720	.0013890	-.0019040	-.0043590	-.0077900	-.0117200	-.0153100	-.0184100
1.60	.0066070	.0016070	-.0018650	-.0044280	-.0079620	-.0119200	-.0154200	-.0184100
1.80	.0076140	.0023200	-.0013160	-.0039730	-.0075920	-.0115500	-.0149400	-.0178600
2.00	.0090530	.0034770	-.0003140	-.0030590	-.0067510	-.0107000	-.0139700	-.0170000[b]
2.20	.0108800	.0050290	.0010860	-.0017440	-.0055040	-.0094380	-.0125900	-.0156000[b]
2.40	.0130600	.0069300	.0028350	-.0000795	-.0039060	-.0078160	-.0108400	-.0137400
2.60	.0155600	.0091430	.0048920	.0018910	-.0020050	-.0058870	-.0087890	-.0117900
2.80	.0183500	.0116300	.0072200	.0041280	.0001603	-.0036950	-.0064730	-.0096080
3.00	.0213900	.0143700	.0097880	.0066010	.0025540	-.0012760	-.0039210	-.0071750
3.20	.0246600	.0173300	.0125700	.0092790	.0051480	.0013370	-.0011540	-.0044570
3.40	.0281500	.0204800	.0155400	.0121400	.0079150	.0041160	.0017990	-.0015210
3.60	.0318300	.0238200	.0186800	.0151600	.0108300	.0070420	.0048860	.0014140
3.80	.0356900	.0273200	.0219700	.0183300	.0138800	.0101000	.0080600	.0042430
4.00	.0397100	.0309700	.0254000	.0216200	.0170300	.0132500	.0113300	.0071660

[a]Extrapolated.

[b]Interpolated.

TABLE II.- CRITICAL CROSSFLOW REYNOLDS NUMBER

VERSUS SHAPE FACTOR

Shape factor	Critical Reynolds number
0.1535	325
.1588	305
.1608	270
.1668	244
.168	206[a]
.1748	228
.1761	235
.1812	219
.1847	176
.1933	154
.211	143[a]
.2132	121
.2352	102
.2444	92
.2453	83
.292	67[a]
.3203	66.5
.3206	61
.3439	58
.3670	53
.4299	48
.4626	43.5
.4759	44

[a]Brown, ref. 9.

TABLE III.- DIMENSIONAL AMPLIFICATION RATES FOR NOMINAL AND SCALED CROSSFLOW VELOCITY

PROFILES ON 970 AIRFOIL UPPER SURFACE AT $x/c = 0.020$ FOR DESIGN CONDITION

Reynolds number	Temporal amplification rate, 1/s		Group velocity, m/s		Spatial amplification rate, 1/m	
	Nominal	Scaled (a)	Nominal	Scaled (a)	Nominal	Scaled (a)
$\alpha_r \delta_{10} = 0.0008$						
30	-8 465.93	-8 889.33	245.399	245.435	34.499	36.219
50	-2 096.70	-2 202.28	241.202	241.229	8.693	9.129
75	1 715.58	1 838.36	238.139	238.163	-7.355	-7.719
100	3 928.26	4 123.90	235.879	235.901	-16.654	-17.481
200	7 637.42	8 018.57	230.900	230.918	-33.077	-34.725
500	10 153.53	10 660.55	227.003	227.021	-44.729	-46.958
1000	10 996.03	11 545.16	225.219	225.233	-48.824	-51.259
2000	11 360.91	11 927.90	223.536	223.527	-50.824	-53.362
$\alpha_r \delta_{10} = 0.0018$						
30	-9 008.05	-9 459.61	271.295	271.305	33.204	34.867
50	493.64	517.03	264.889	264.899	-1.864	-1.952
75	5 967.89	6 264.91	260.795	260.805	-22.883	-24.021
100	8 928.96	9 373.99	258.548	258.558	-34.535	-36.255
200	13 681.25	14 363.85	254.943	254.952	-53.664	-56.339
500	16 716.20	17 550.70	251.724	251.738	-66.407	-69.718
1000	17 735.48	18 611.77	249.546	249.355	-71.071	-74.640
2000	18 238.57	19 080.50	248.035	246.476	-73.532	-77.413

[a] $k = 1.05$.
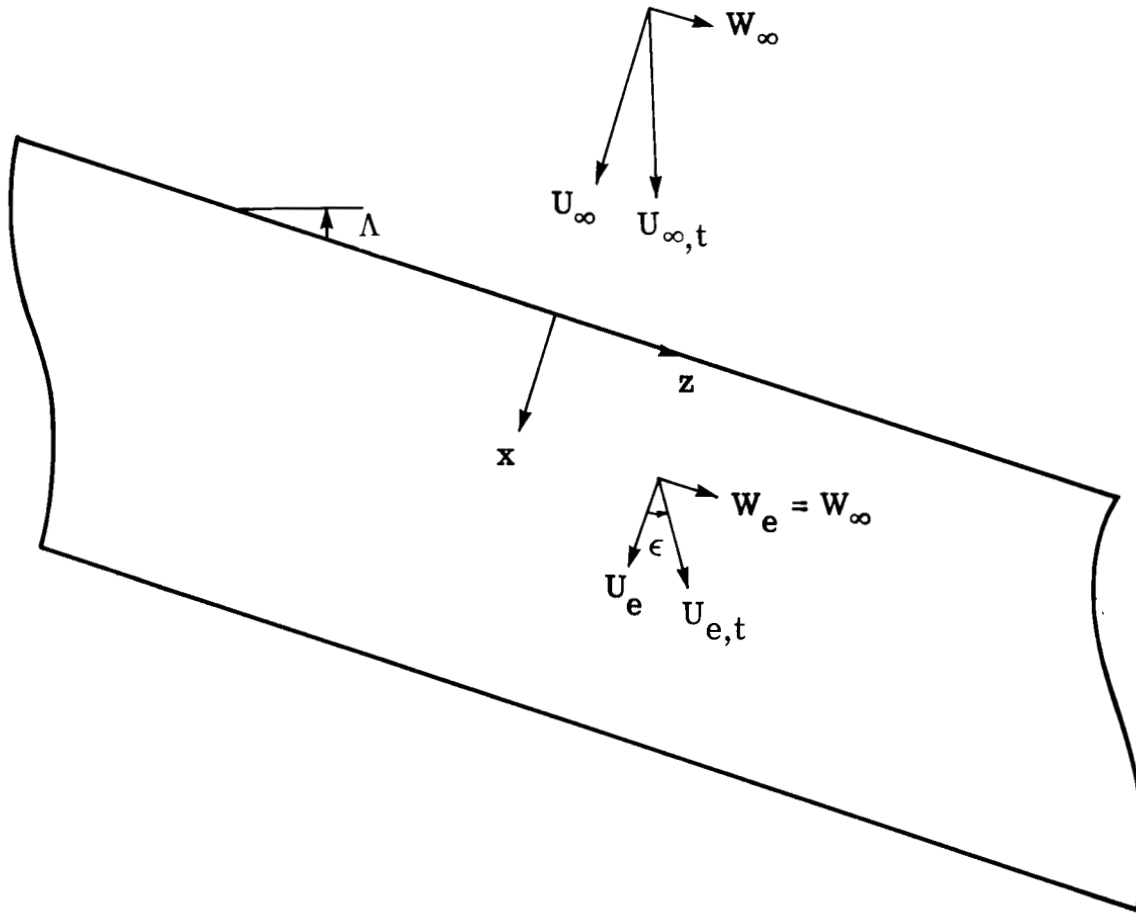
Figure 1.- Coordinate system. $\varepsilon = \text{arc tan} \dfrac{W_e}{U_e}$.
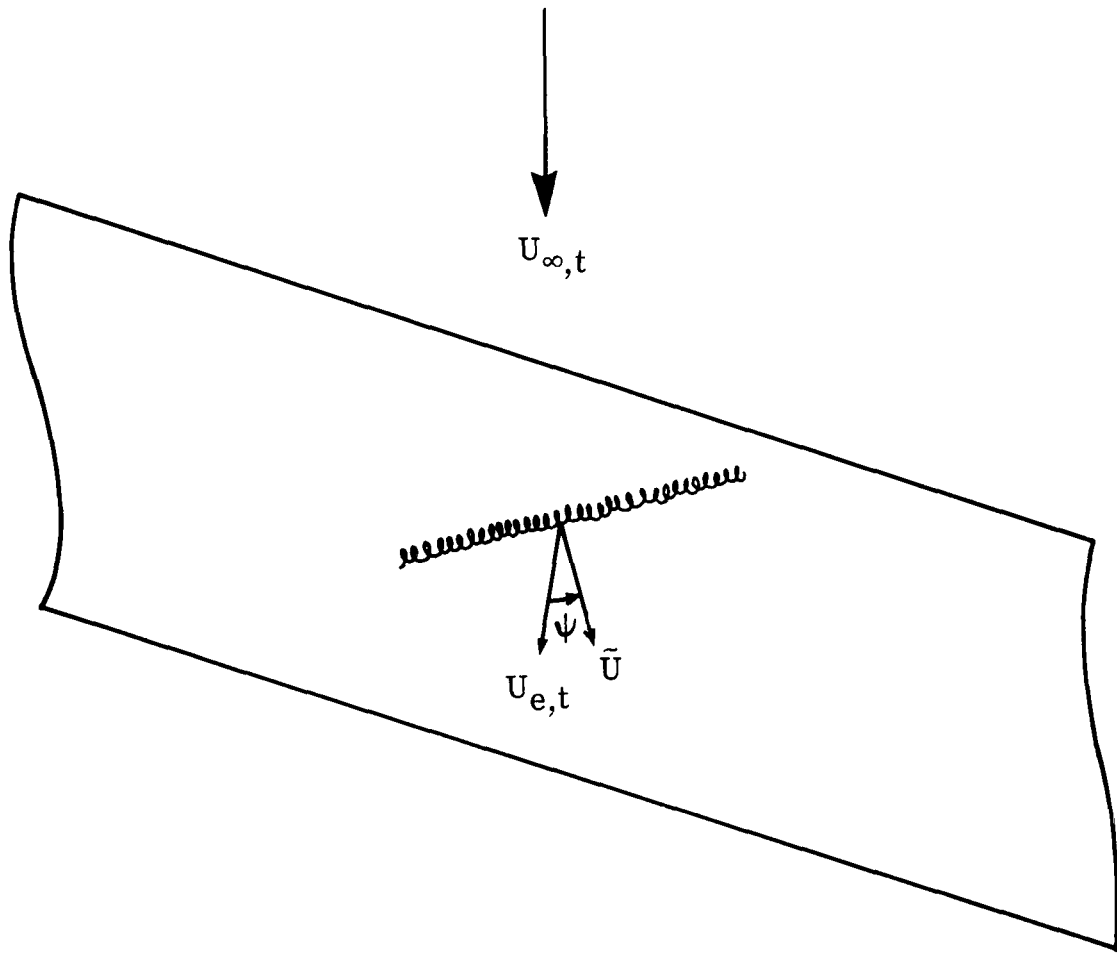
Figure 2.- Orientation of a disturbance wave. $\psi = \text{arc tan} \frac{\alpha_3}{\alpha_1} - \varepsilon.$
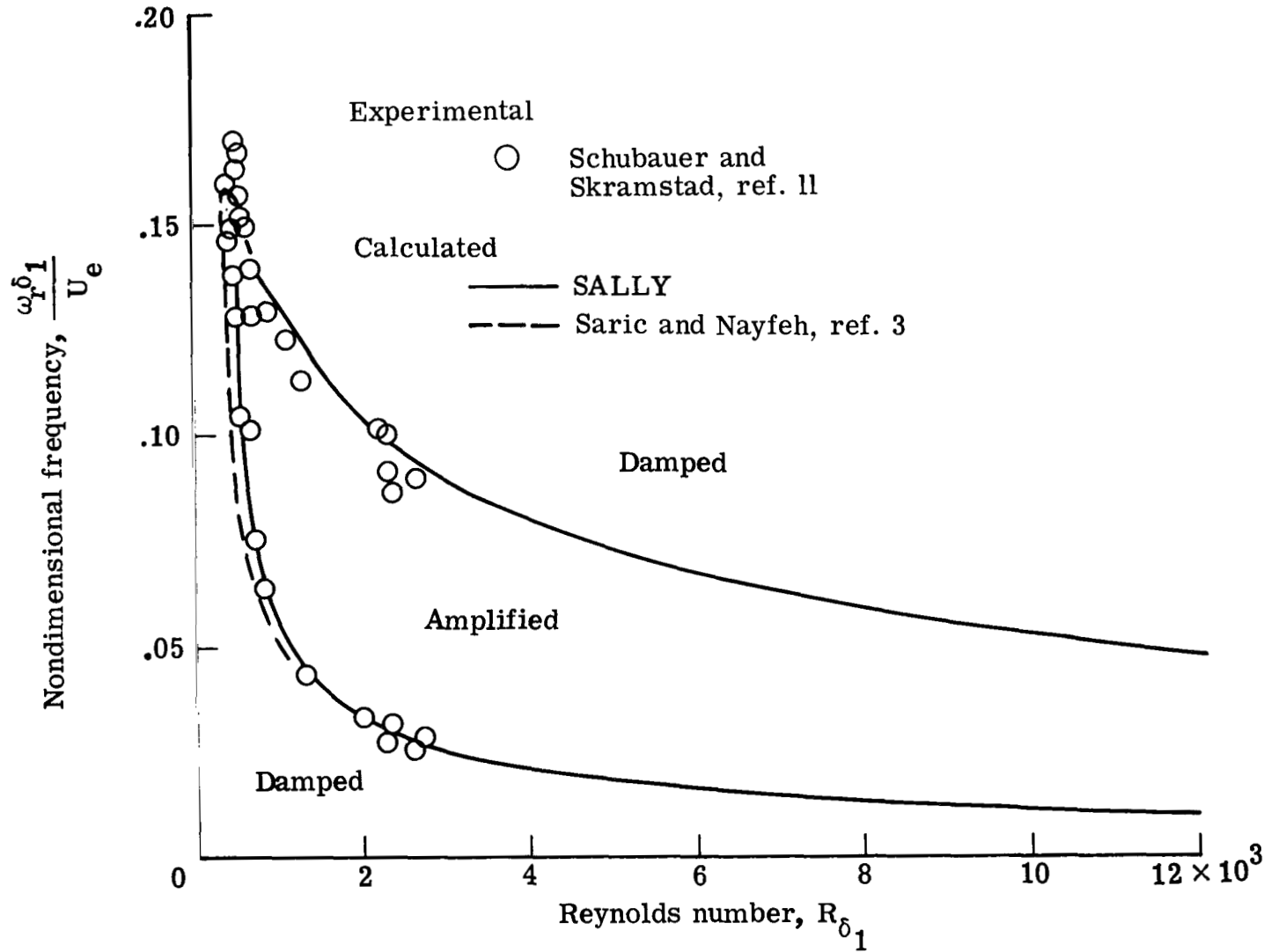
Figure 3.- Comparison of experimental and theoretical neutral stability data for Blasius boundary layer.
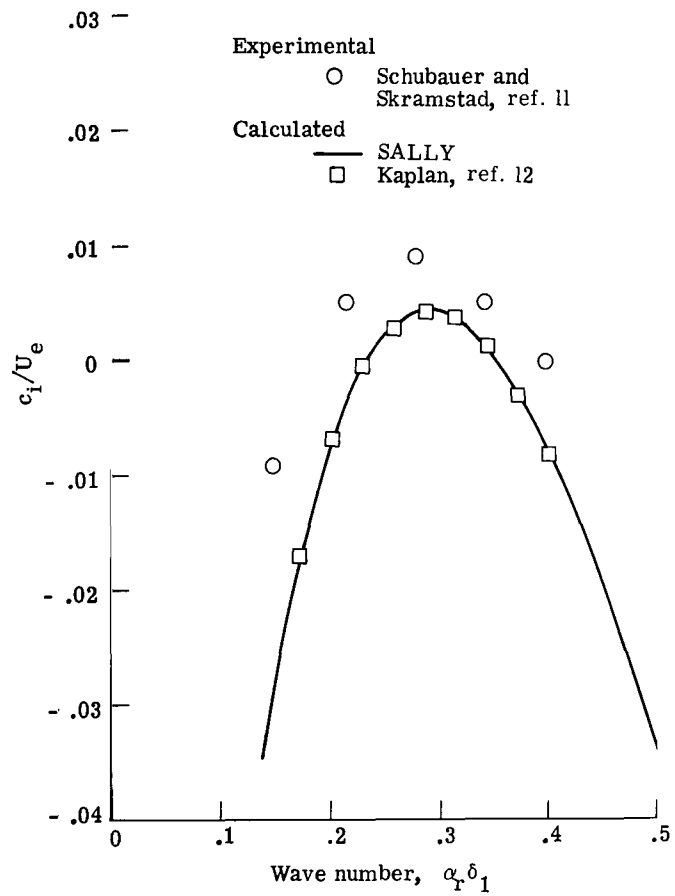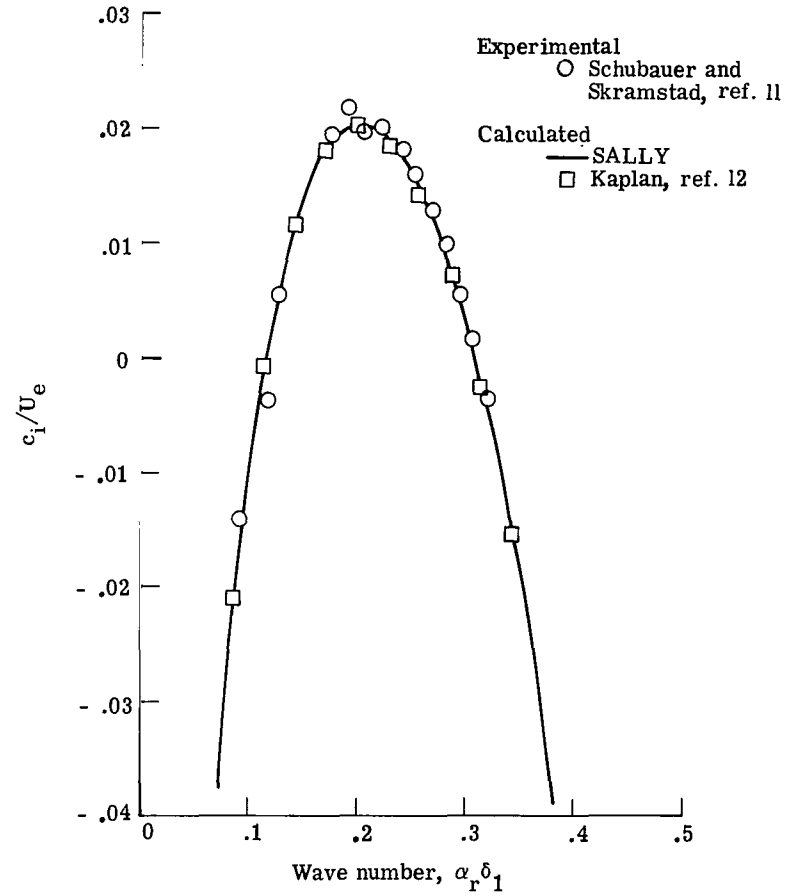
Figure 4.- Temporal stability data for Blasius boundary layer.
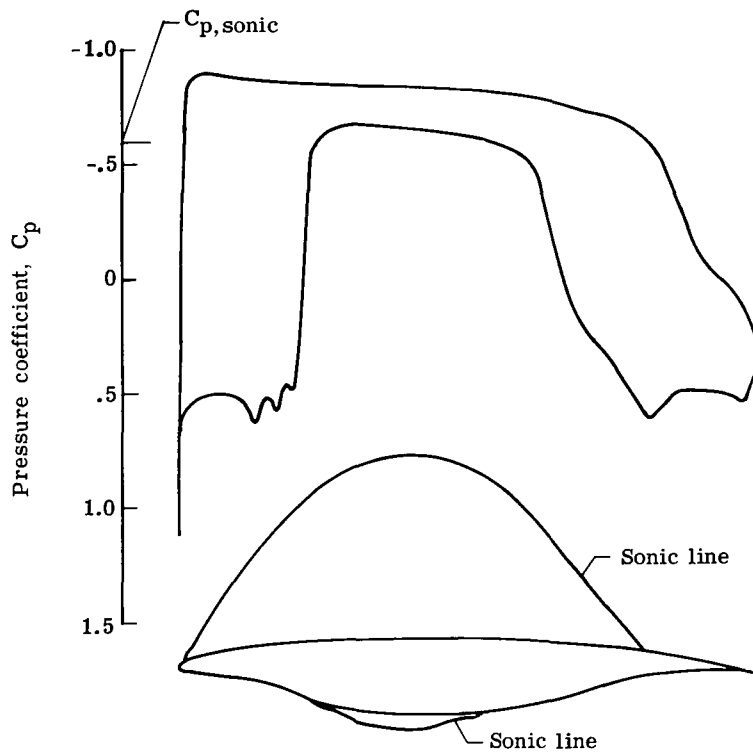
Figure 5.- Pressure distribution for 970 airfoil at
$M_{\infty,n} = 0.749$ and $c_l = 0.675$.
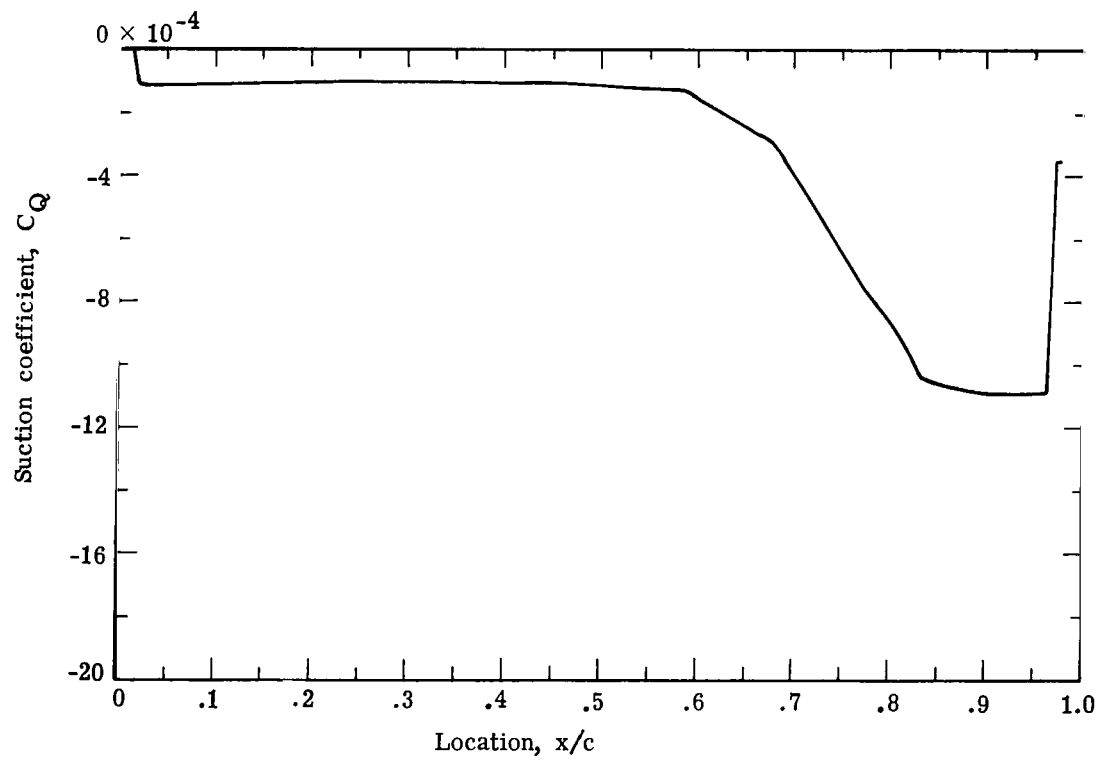
Figure 6.- Suction distribution for upper surface of 970 airfoil at $M_{\infty,n} = 0.749$, $c_l = 0.675$, $R_c = 25 \times 10^6$, and $\Lambda = 25°$.
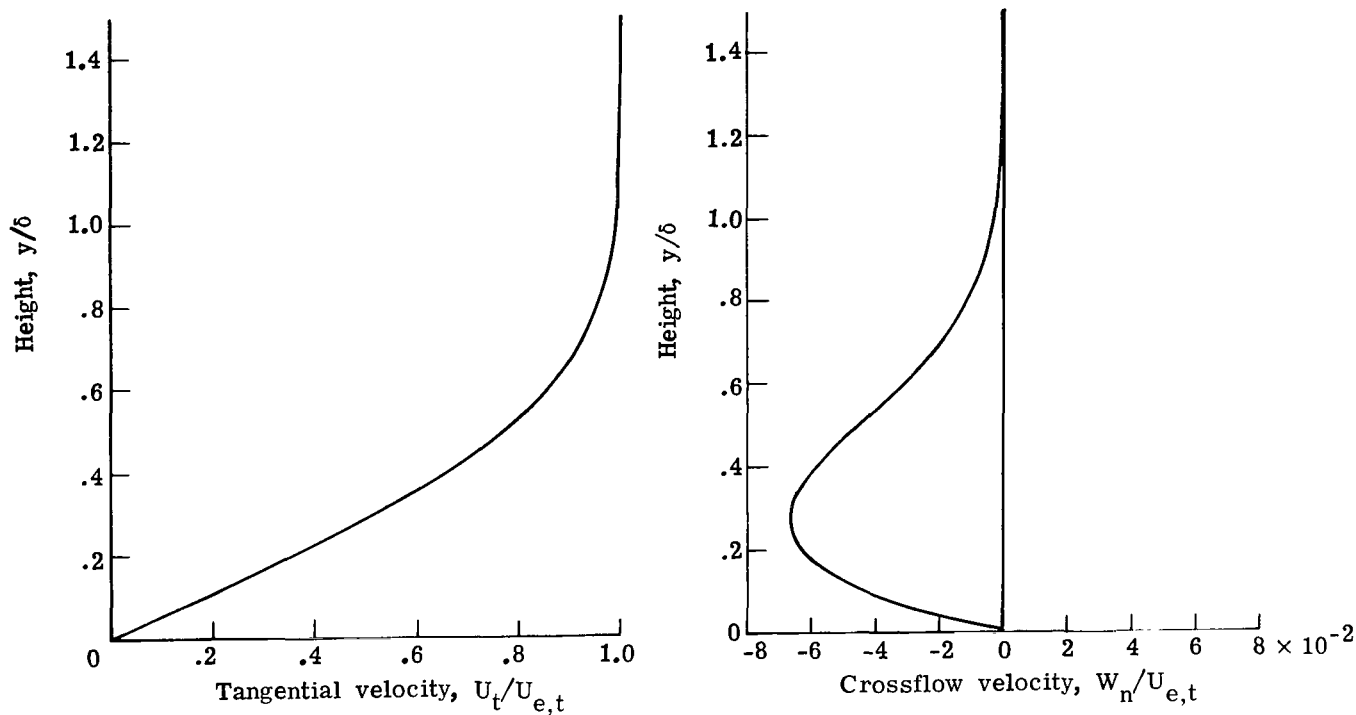
(a) $x/c = 0$.
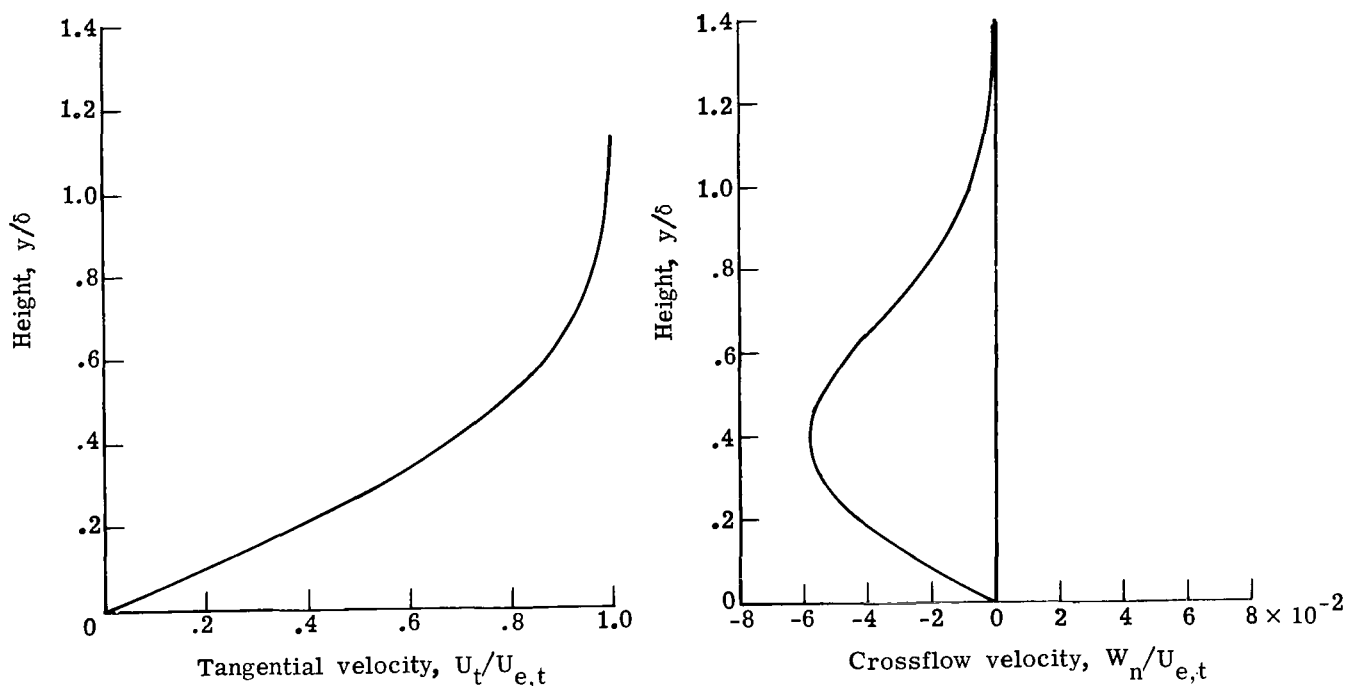
(b) $x/c = 0.015$.

Figure 7.- Nondimensional tangential and crossflow velocity profiles on 970 airfoil at desing condition. Upper surface; $M_{\infty,n} = 0.749$; $c_l = 0.675$; $R_c = 25 \times 10^6$; $\Lambda = 25°$.
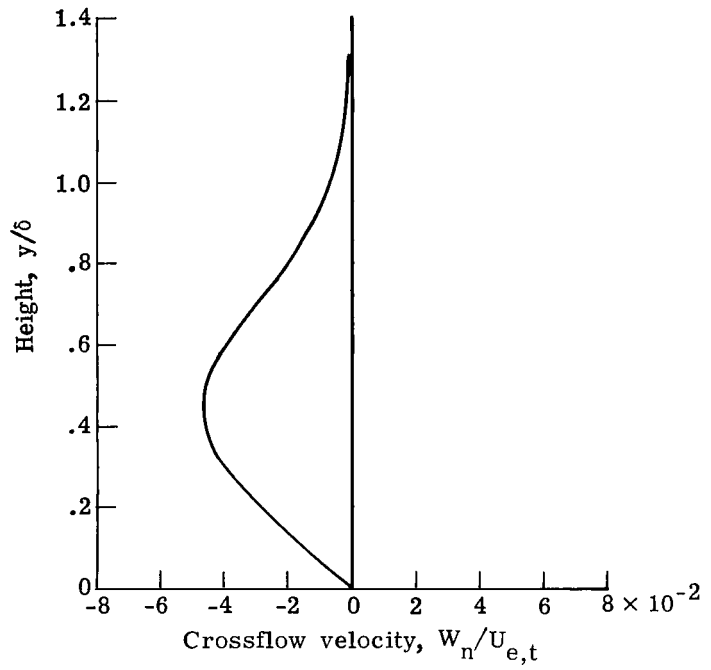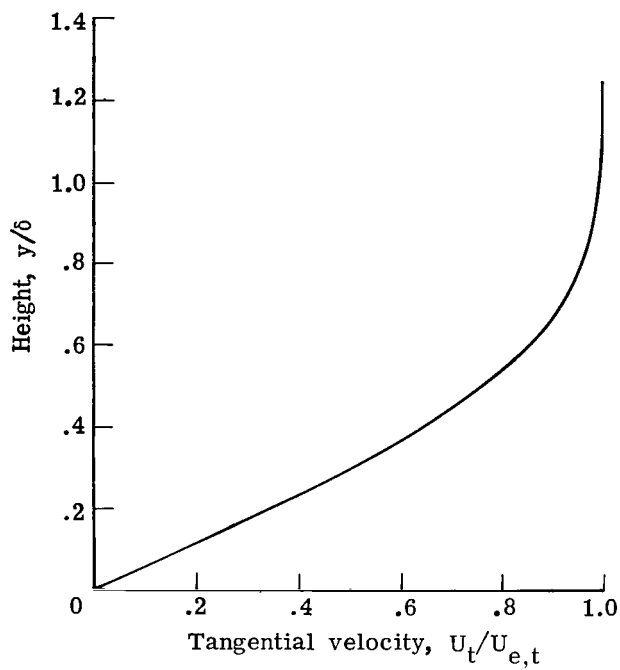
(c)   x/c = 0.020.
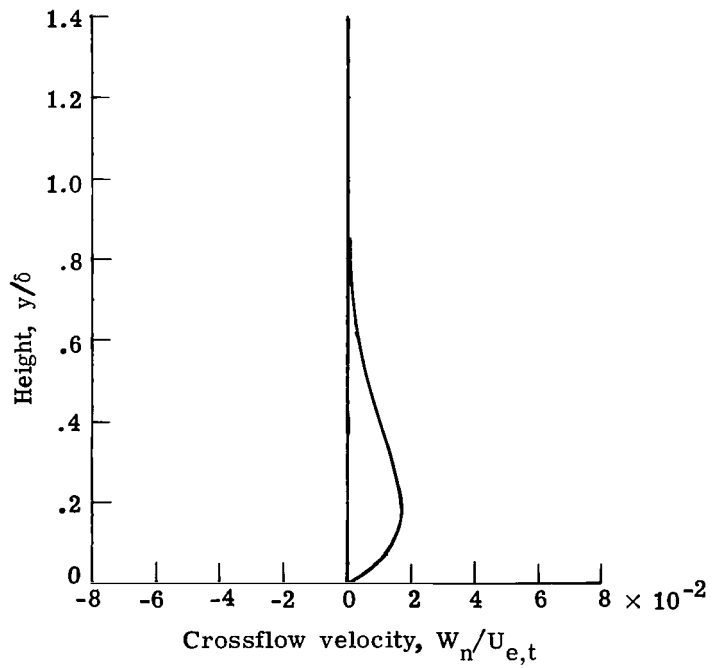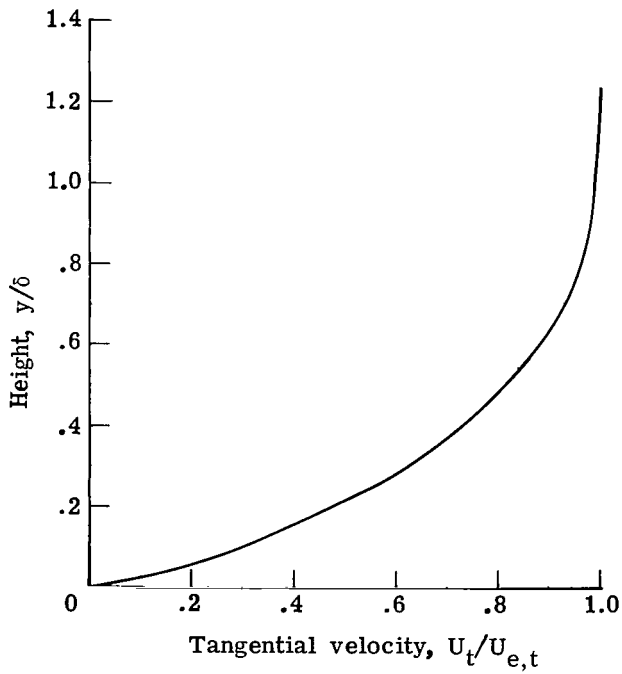
(d)   x/c = 0.711.

Figure 7.- Continued.
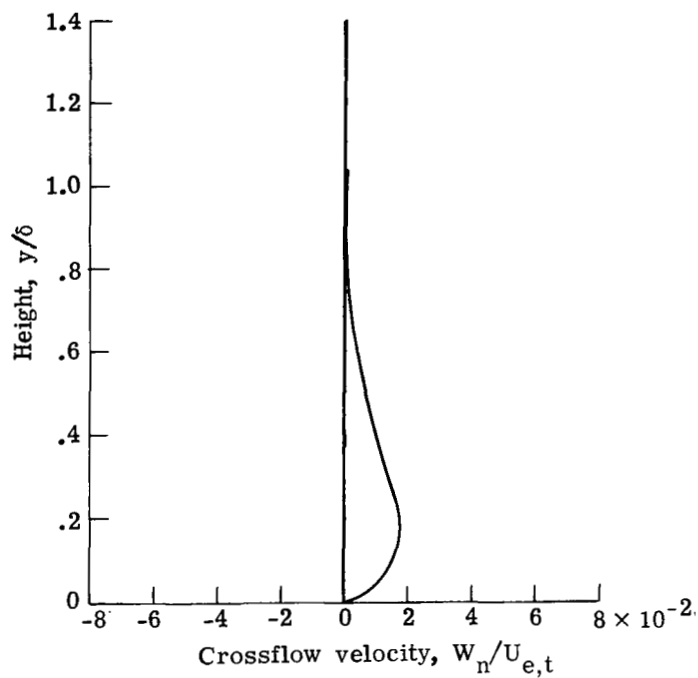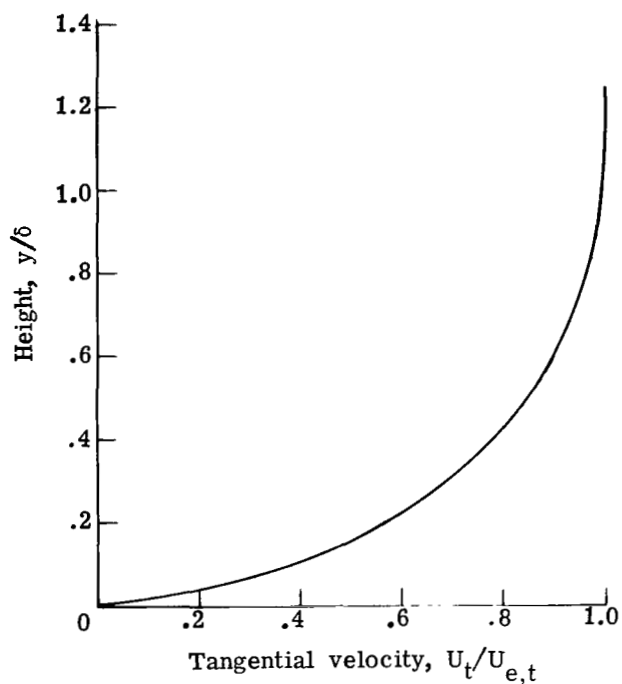
(e) x/c = 0.761.
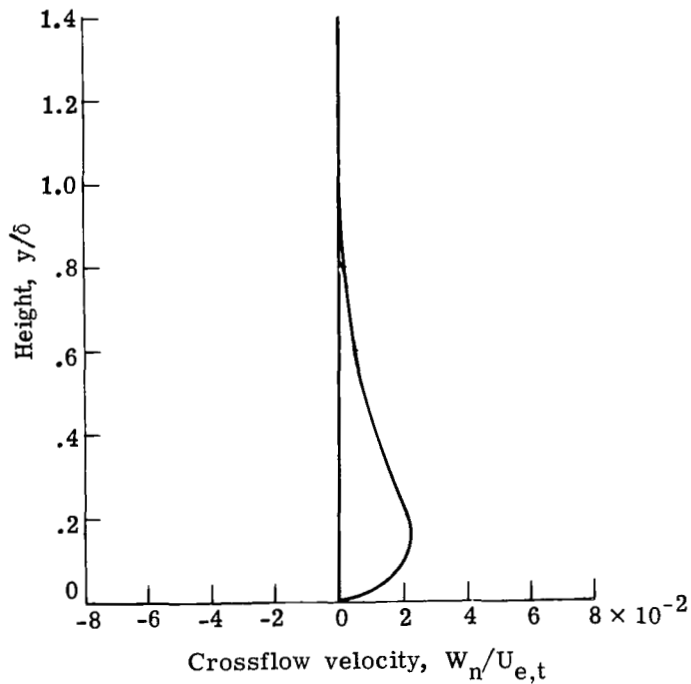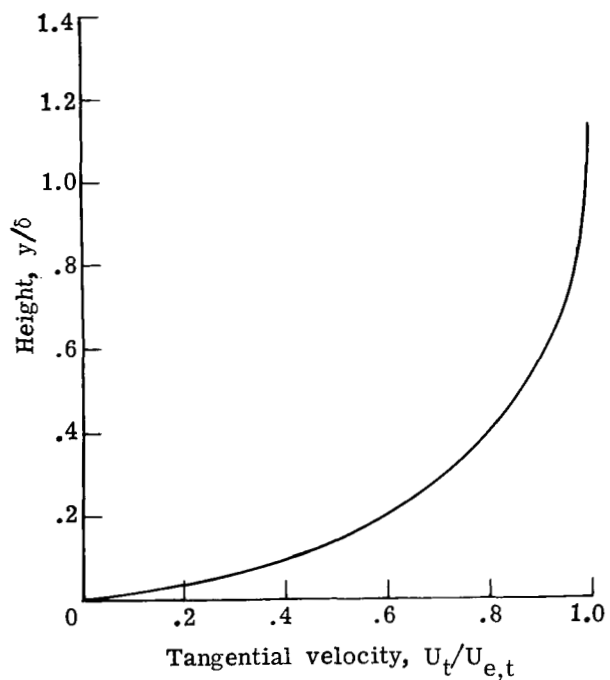
(f) x/c = 0.791.

Figure 7.- Continued.
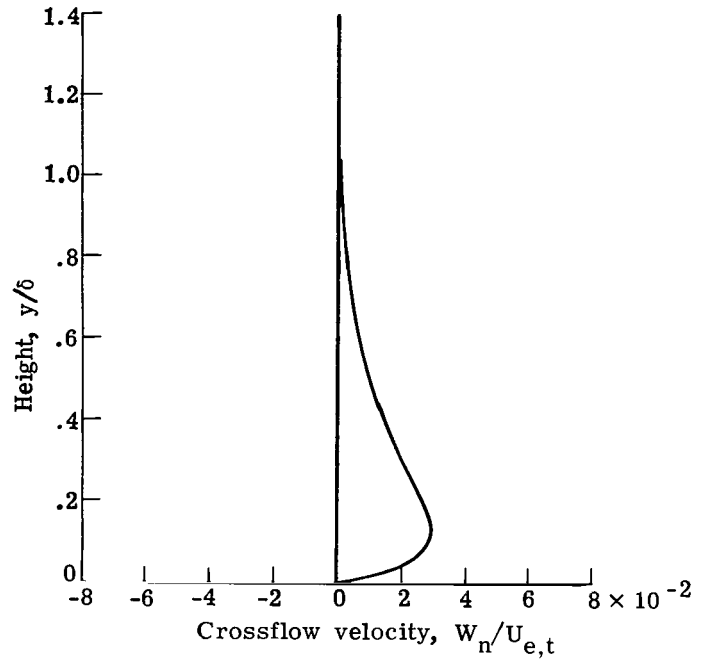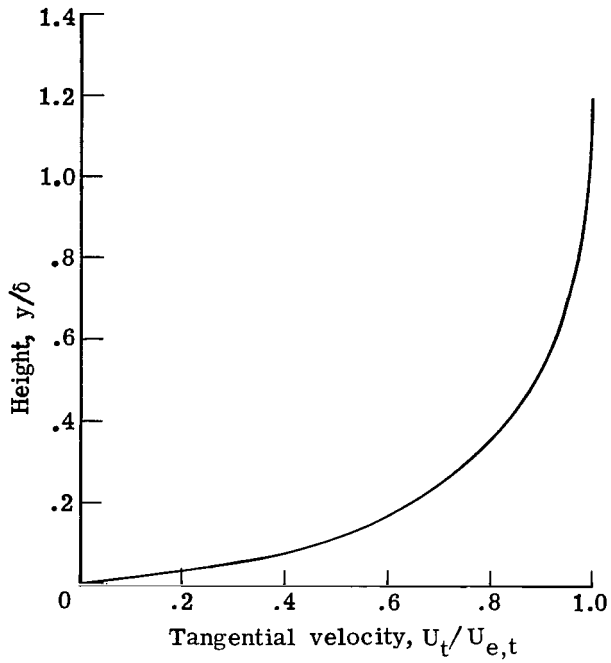
(g)   x/c = 0.820.
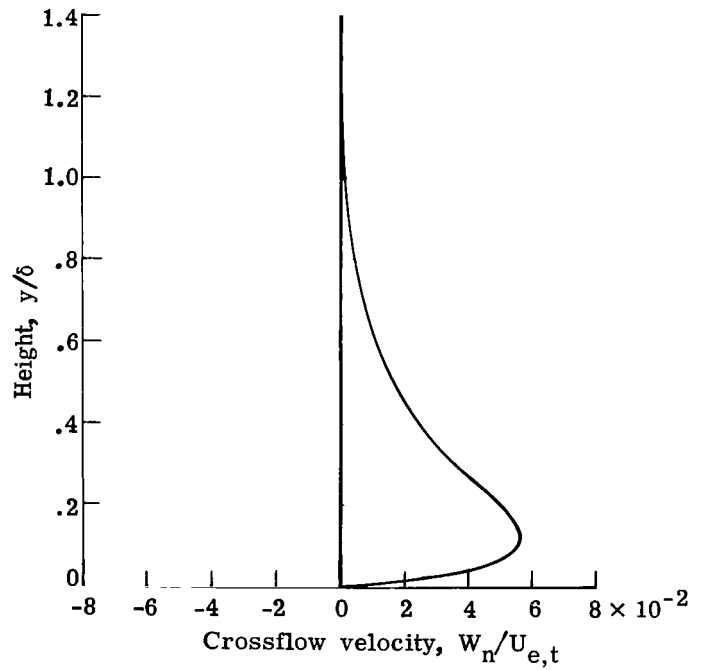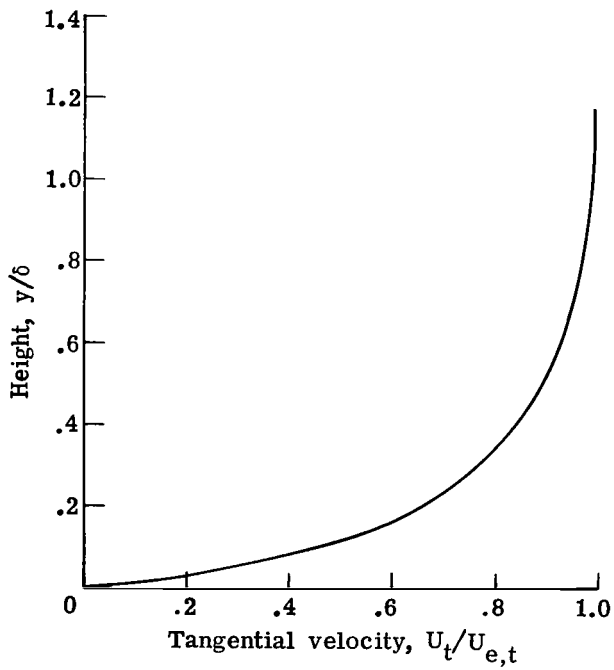
(h)   x/c = 0.860.

Figure 7.- Continued.
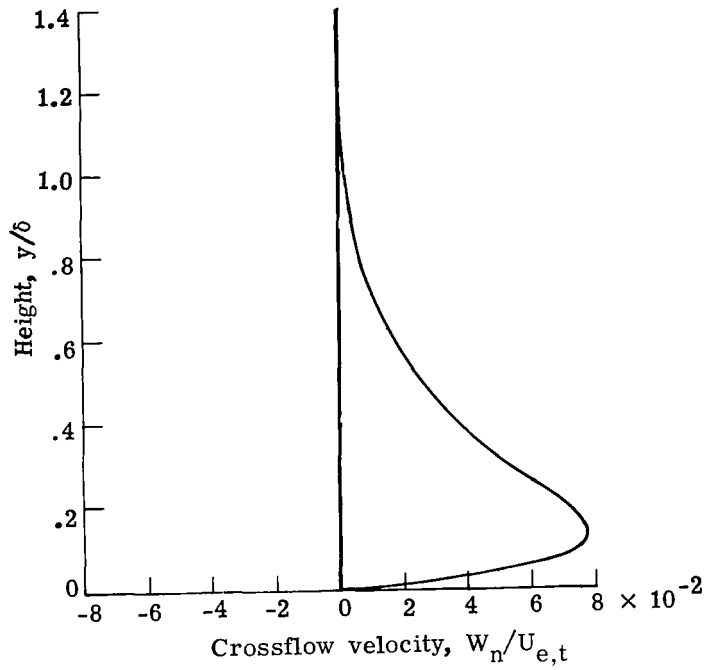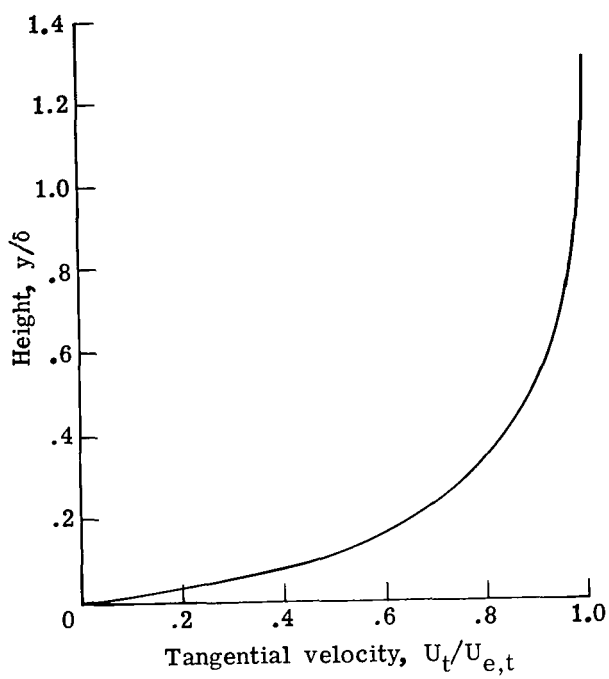
(i) x/c = 0.897.
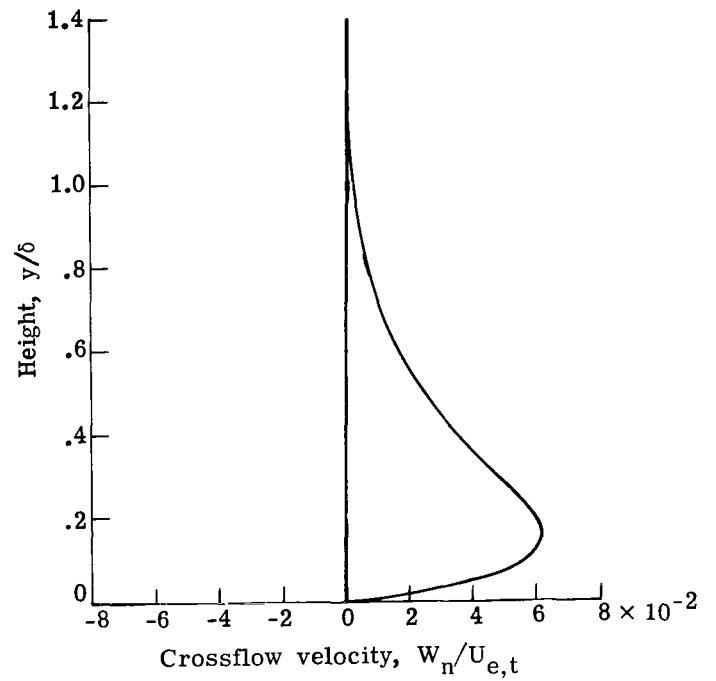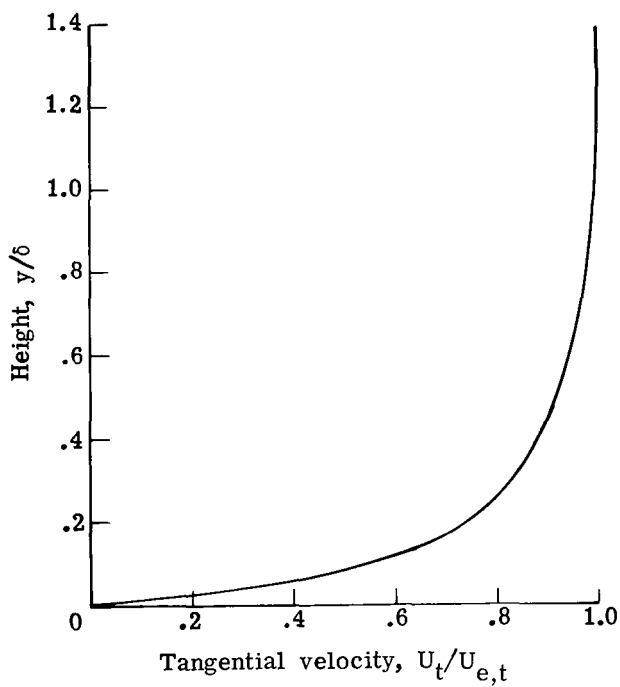
(j) x/c = 0.965.

Figure 7.- Concluded.
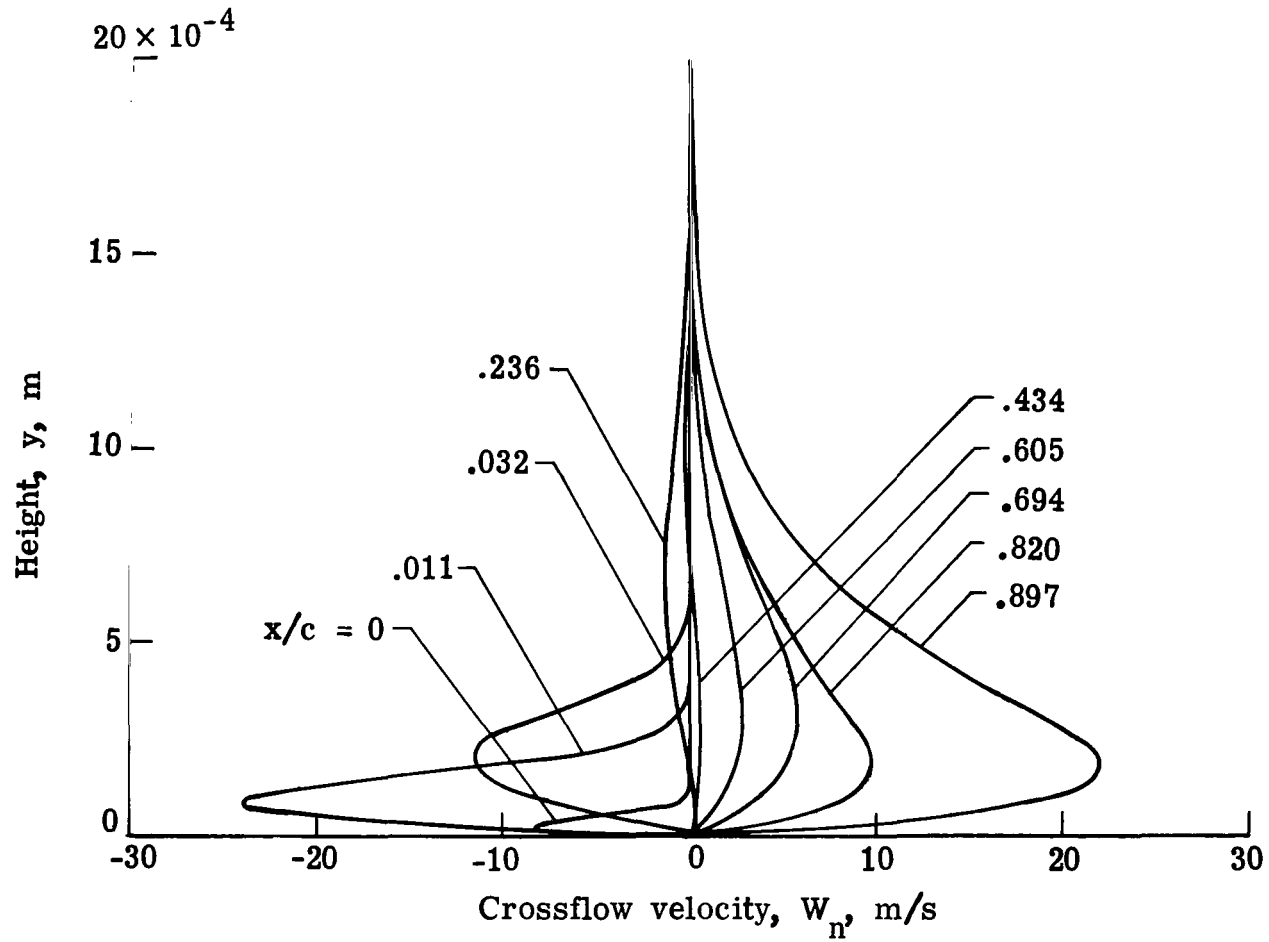
Figure 8.- Dimensional crossflow velocity profiles on upper surface of 970 airfoil at design condition. $M_{\infty,n} = 0.749$; $c_l = 0.675$; $R_c = 25 \times 10^6$; $\Lambda = 25°$.
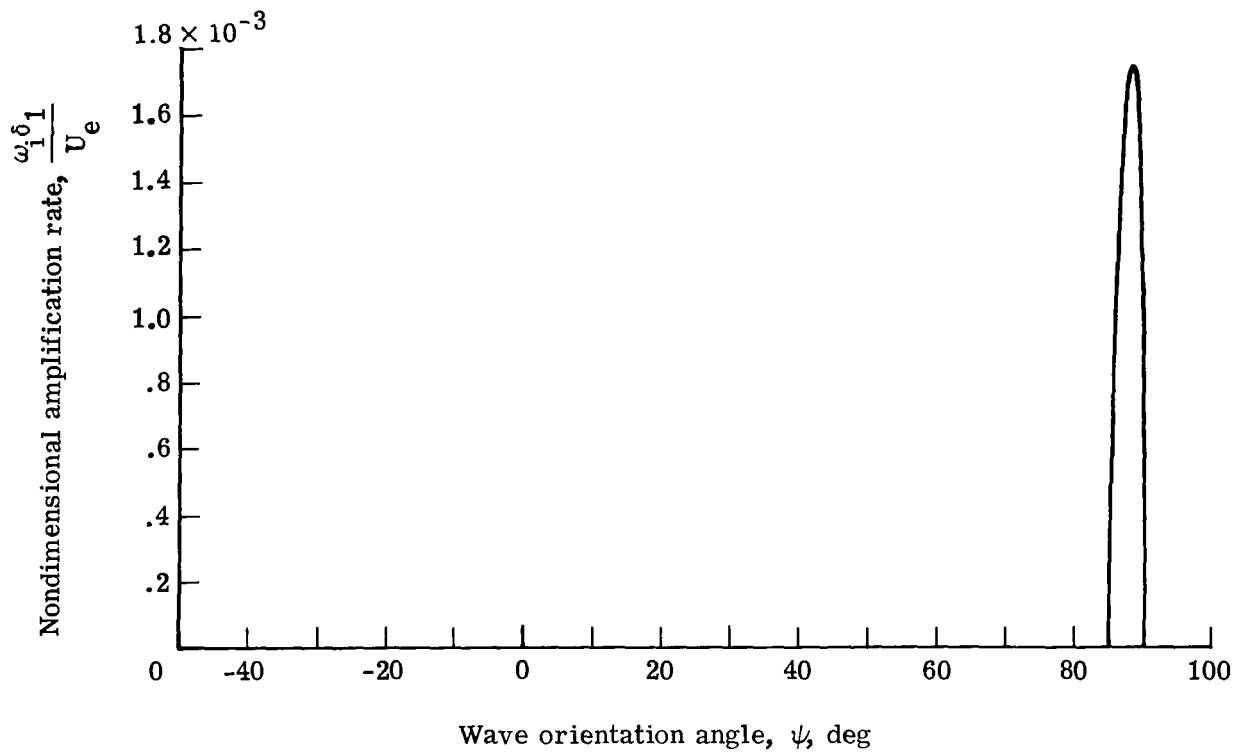
(a) $\lambda/c = 0.0012$.
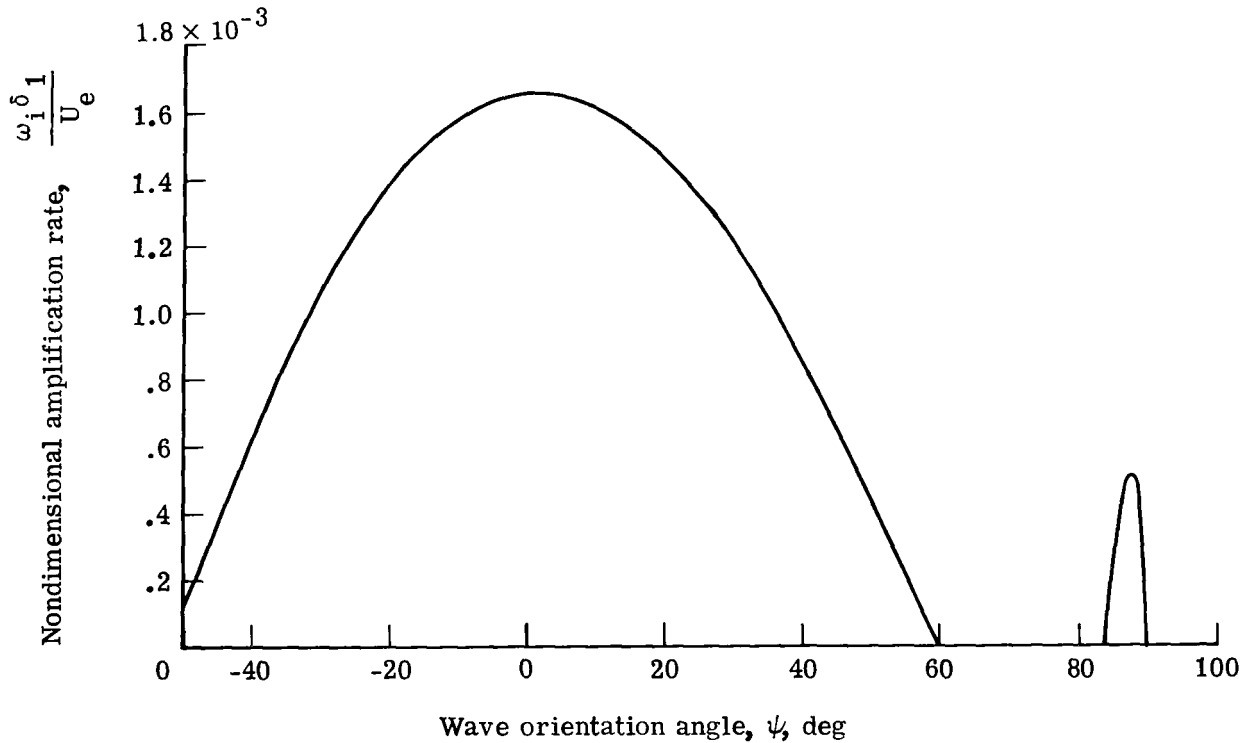
(b) $\lambda/c = 0.0030$.

Figure 9.- Temporal amplification rate versus orientation angle.
970 airfoil upper surface; $R_c = 25 \times 10^6$; $M_{\infty,n} = 0.749$;
$c_l = 0.675$; $\Lambda = 25°$; $x/c = 0.0644$.
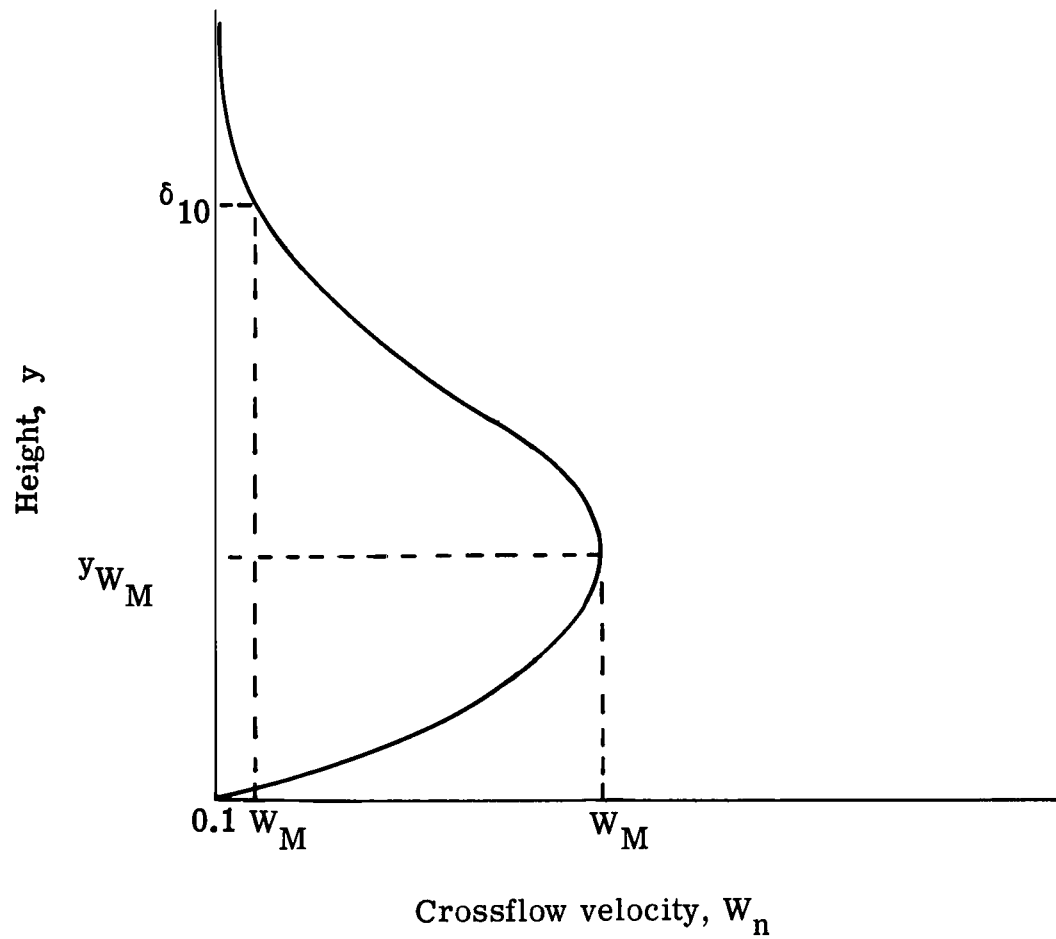
Figure 10.- Definitions of crossflow shape factor and Reynolds number.

$$H_c = y_{W_M}/\delta_{10}; \quad R_{\delta_{10}} = \frac{\rho_e |W_M| \delta_{10}}{\mu_e}.$$
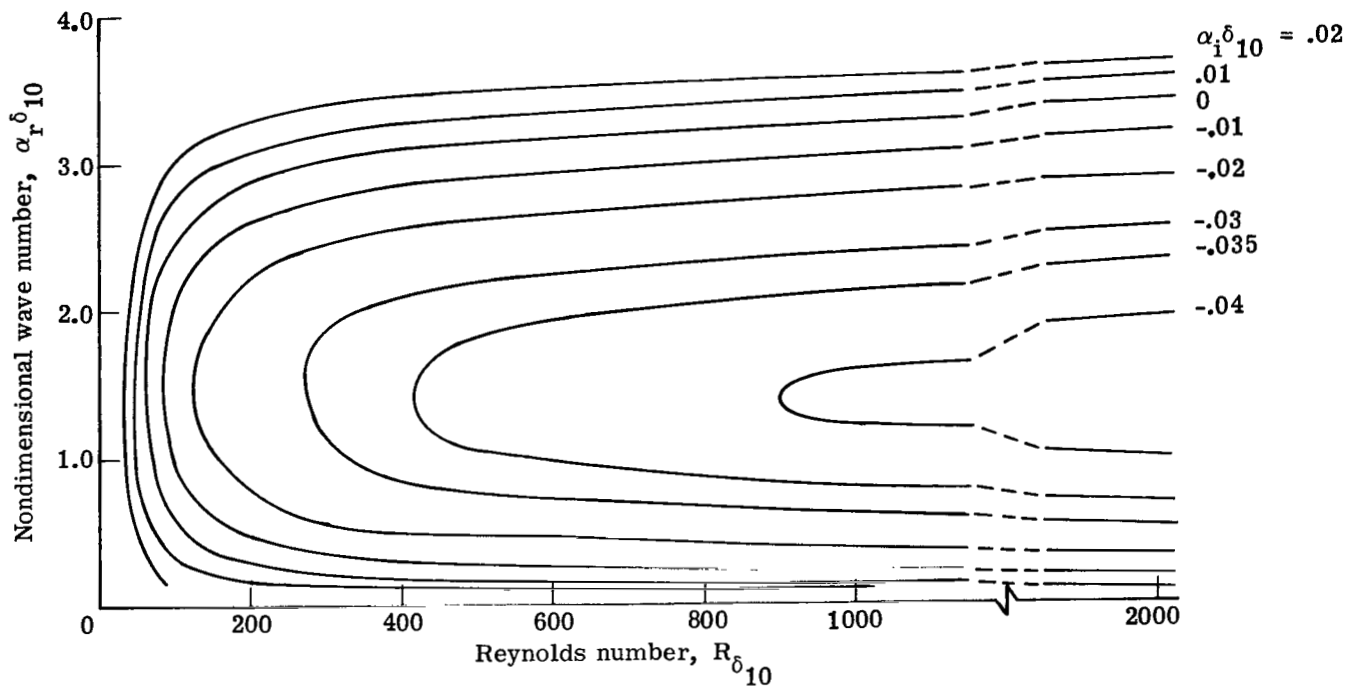
(a) $H_c = 0.3206$ and $W_M/U_{e,t} = -0.06689$.
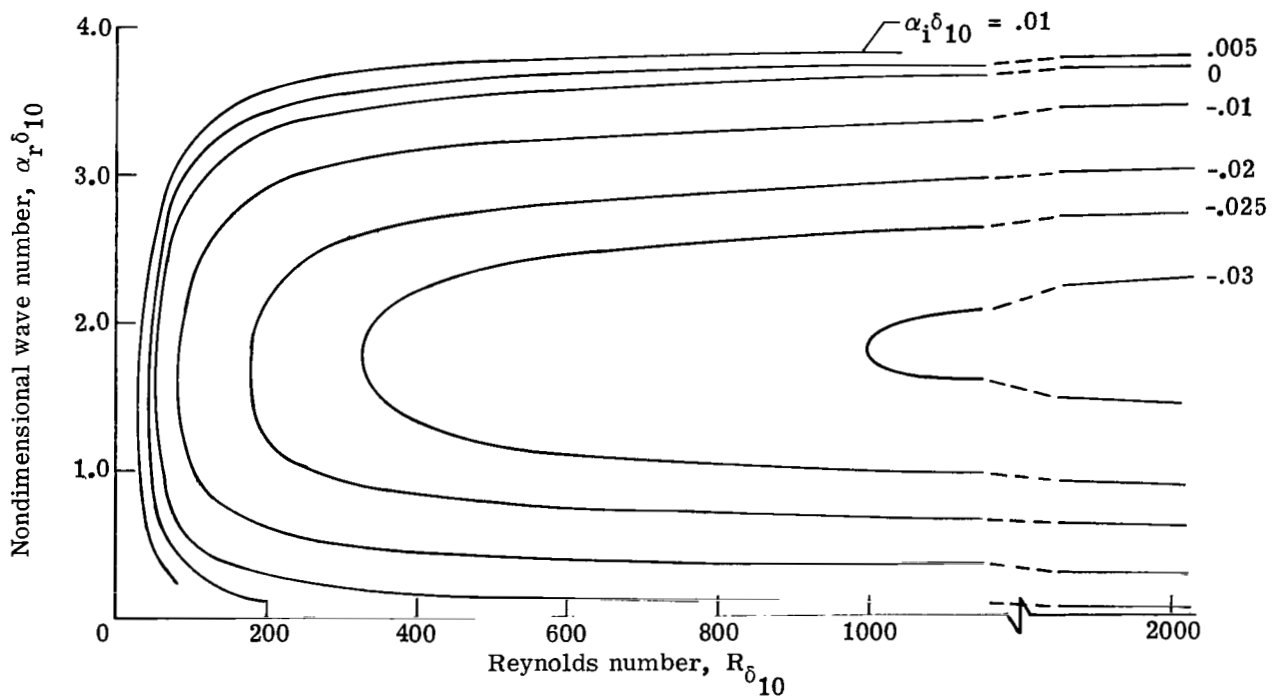
(b) $H_c = 0.3670$ and $W_M/U_{e,t} = -0.05767$.

Figure 11.- Nondimensional spatial amplification rate curves for stationary crossflow disturbances.
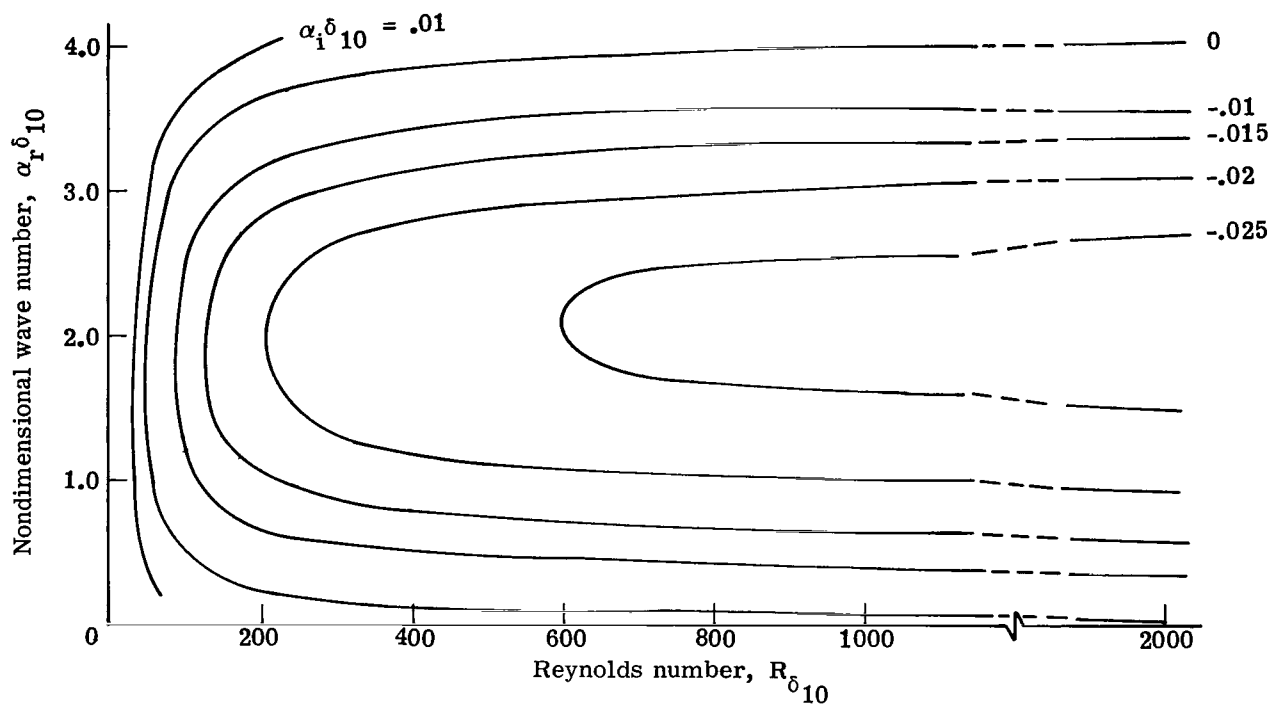
(c) $H_c = 0.4299$ and $W_M/U_{e,t} = -0.04624$.
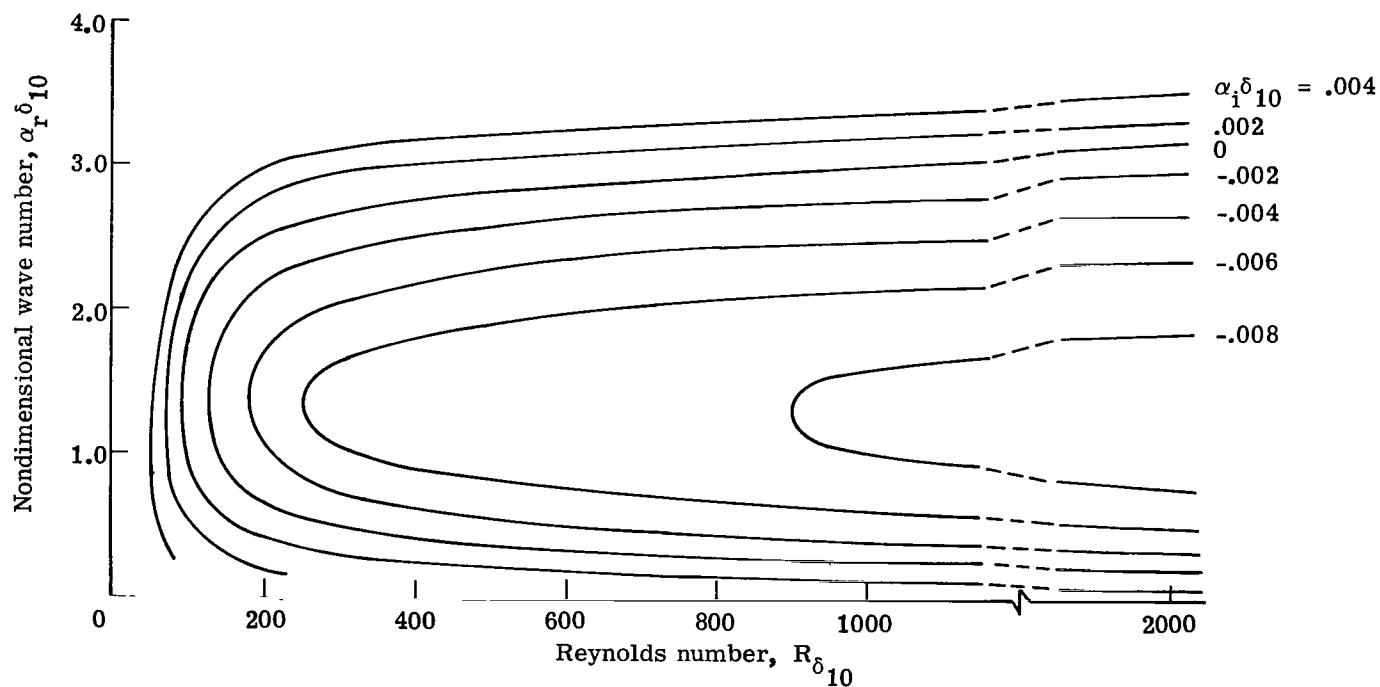
(d) $H_c = 0.2444$ and $W_M/U_{e,t} = 0.01678$.

Figure 11.- Continued.
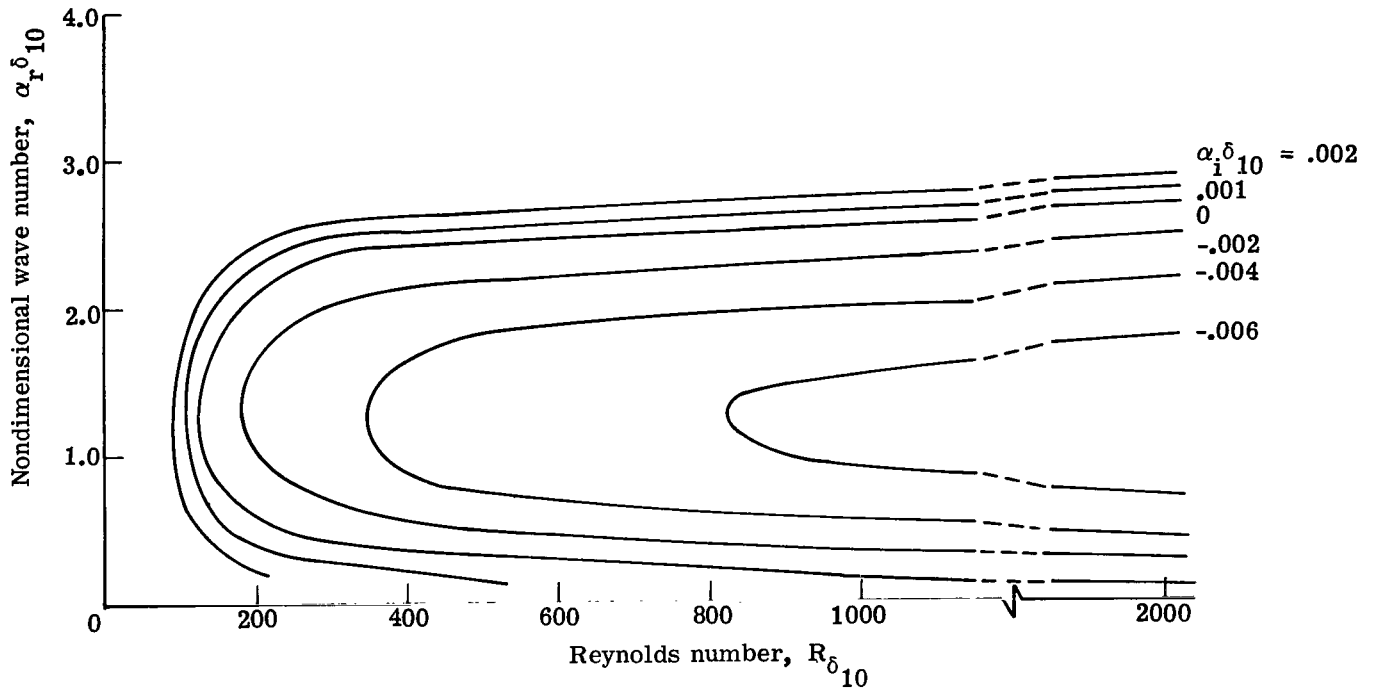
(e) H_c = 0.2132 and $W_M/U_{e,t}$ = 0.01753.
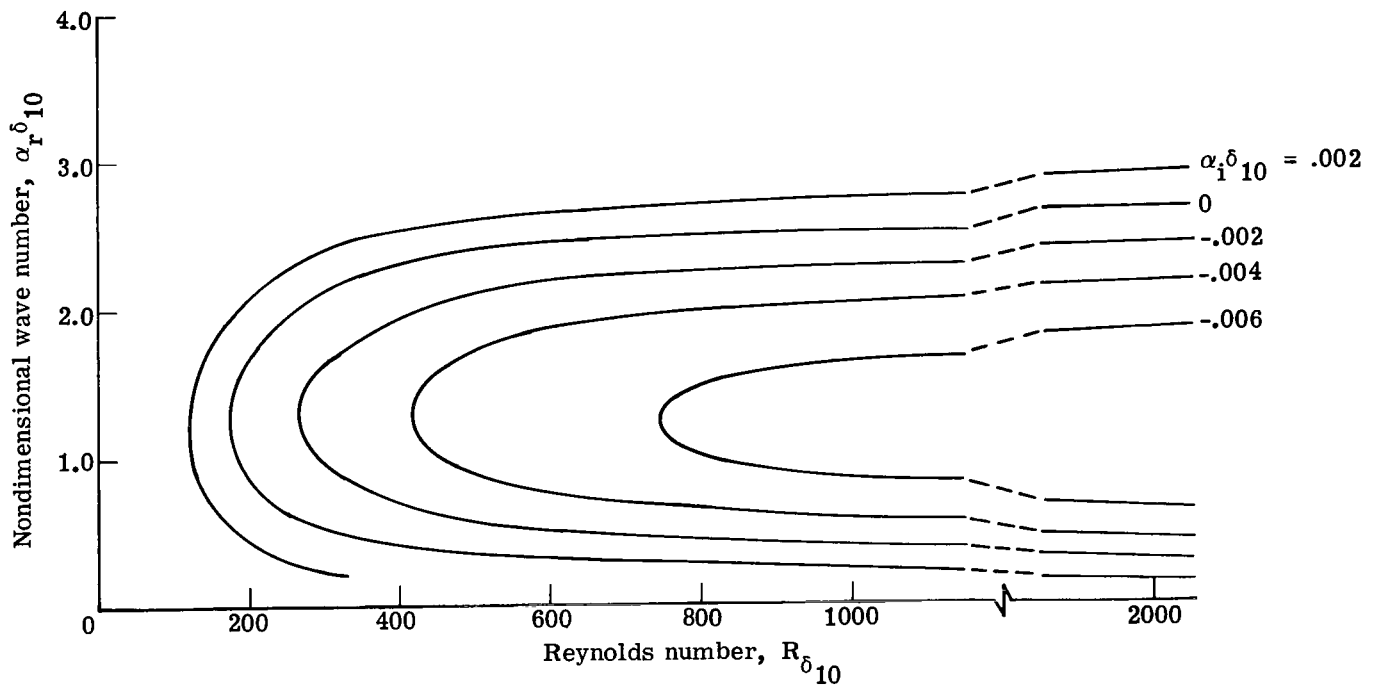
(f) H_c = 0.1847 and $W_M/U_{e,t}$ = 0.02234.

Figure 11.- Continued.
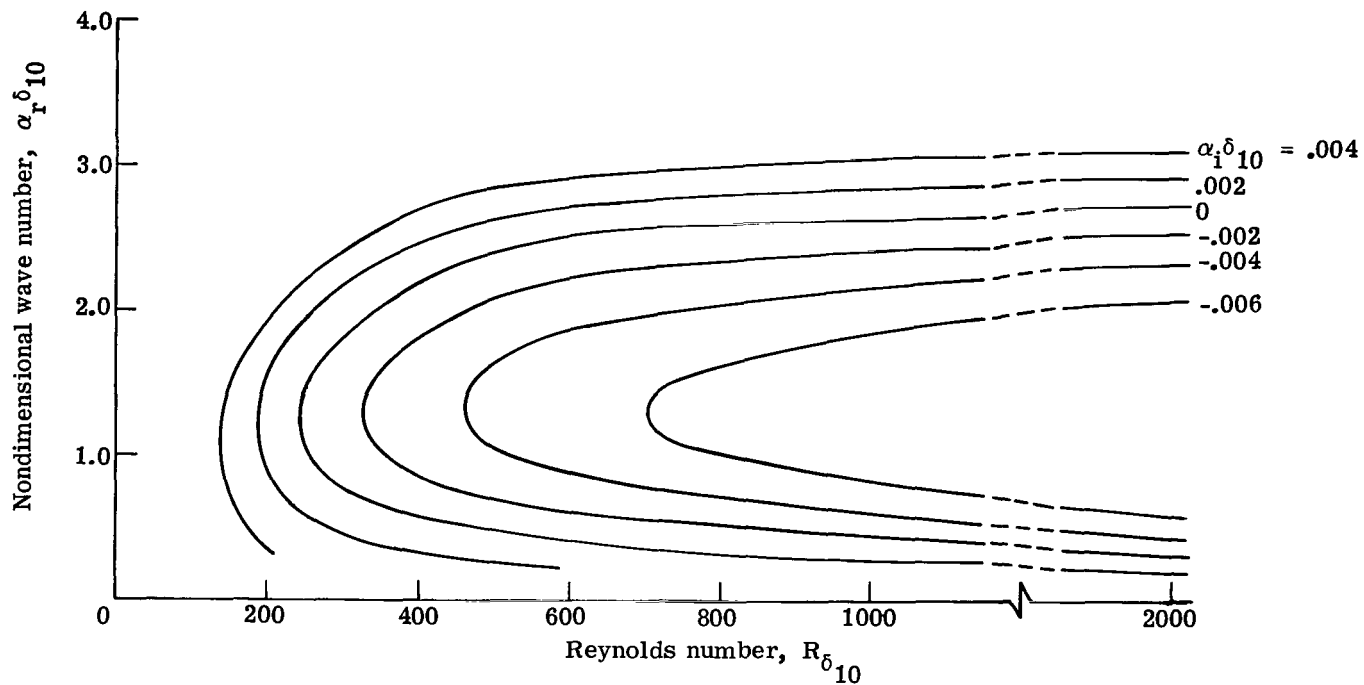
(g) $H_c = 0.1668$ and $W_M/U_{e,t} = 0.02927$.
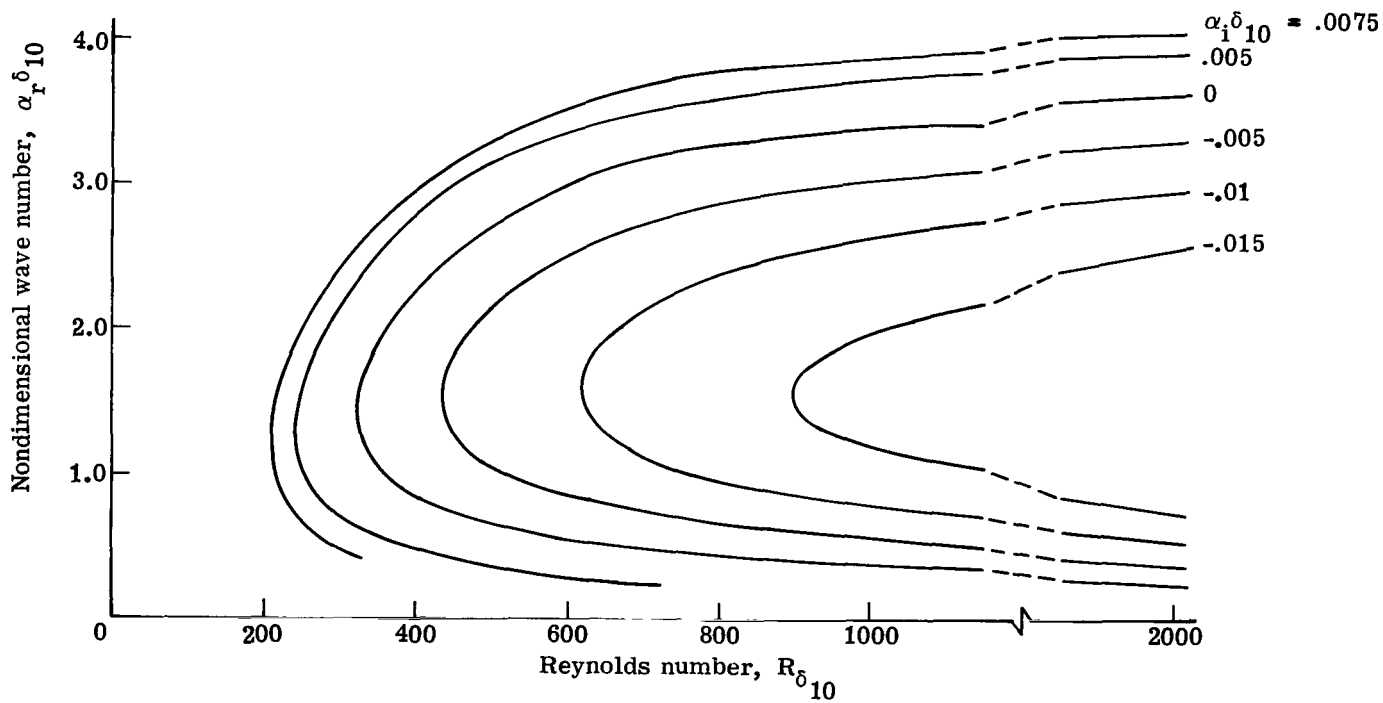
(h) $H_c = 0.1535$ and $W_M/U_{e,t} = 0.05636$.

Figure 11.- Continued.
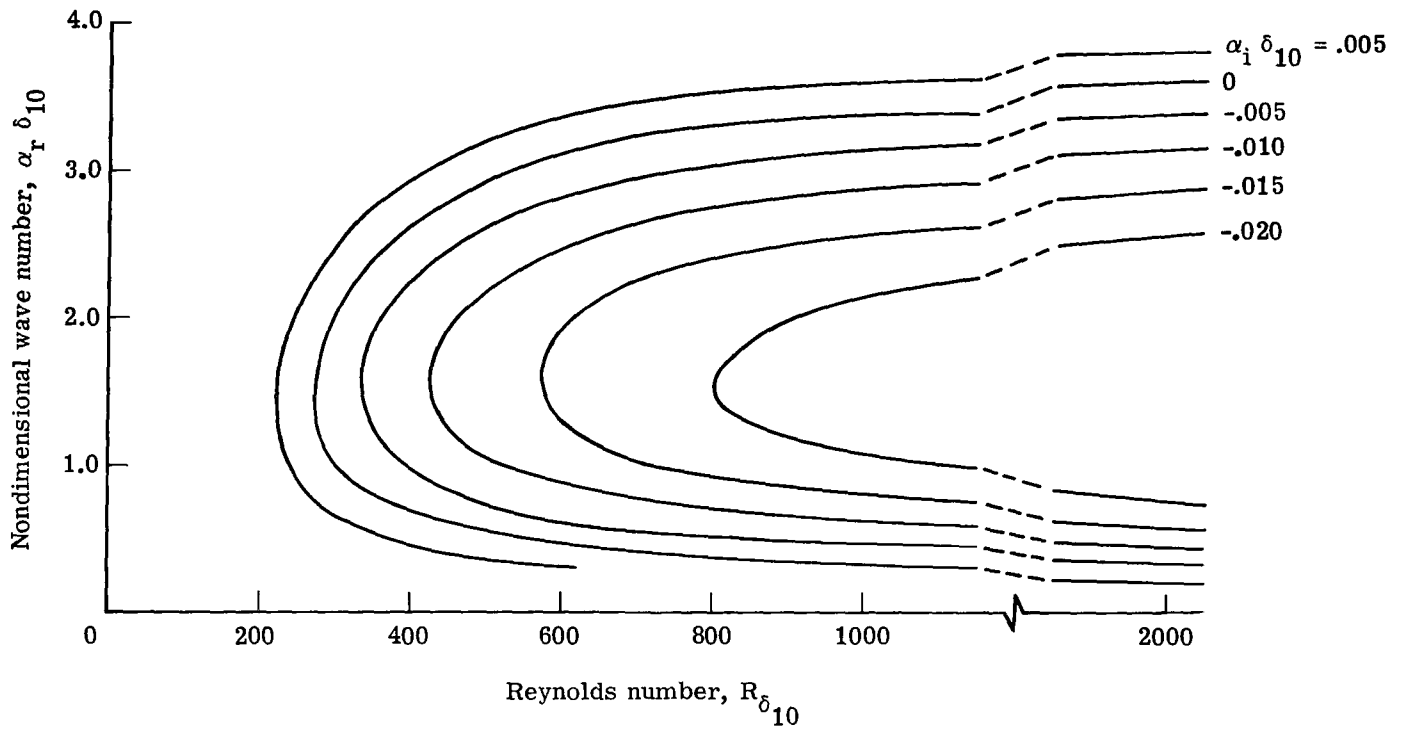
(i) $H_c = 0.1608$ and $W_M/U_{e,t} = 0.07730$.
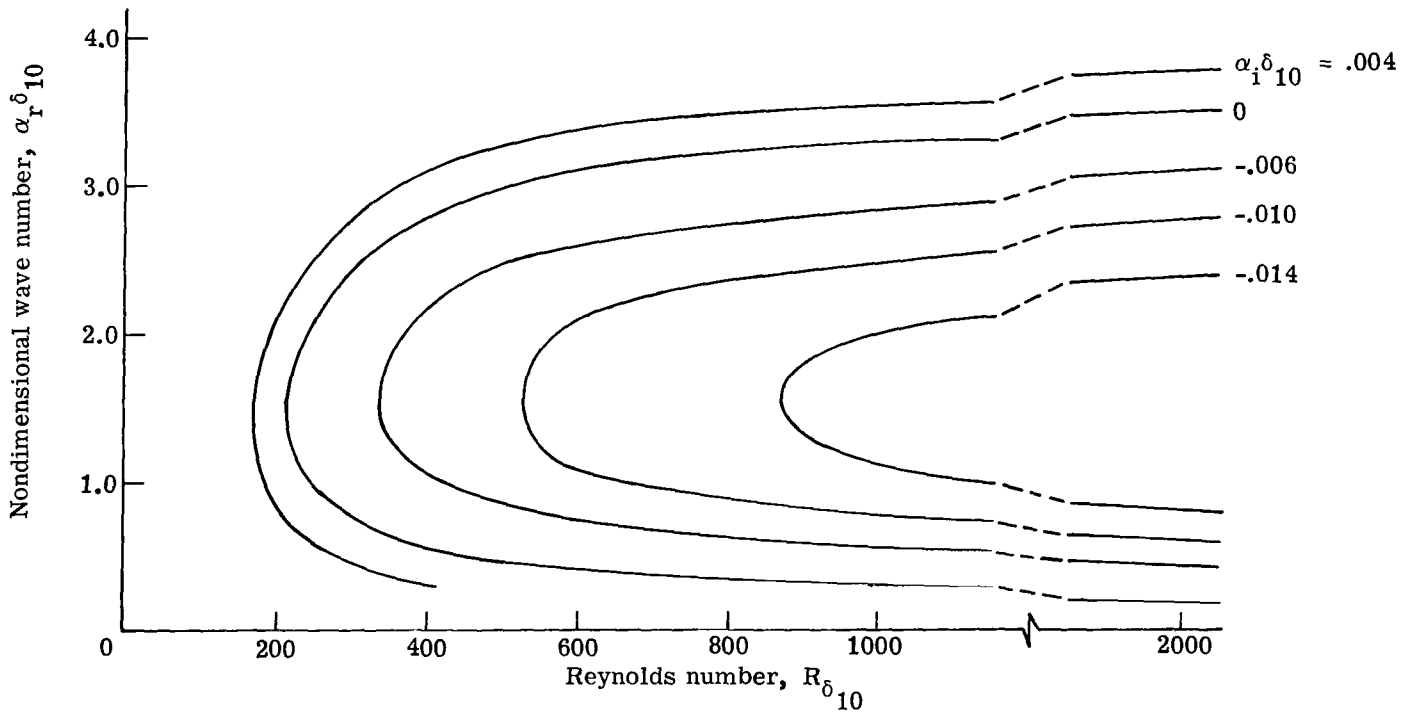
(j) $H_c = 0.1812$ and $W_M/U_{e,t} = 0.06187$.

Figure 11.- Concluded.
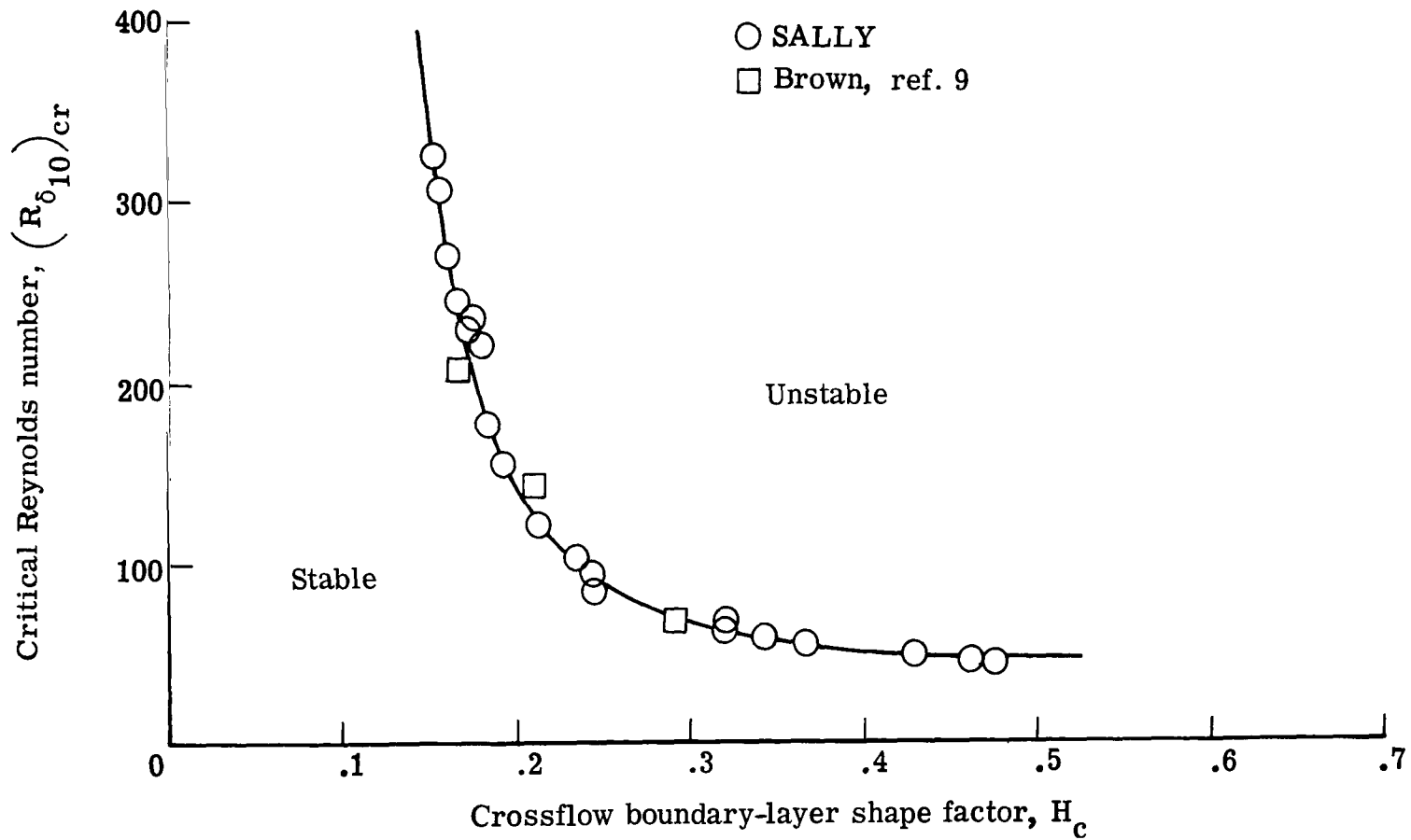
Figure 12.- Critical crossflow Reynolds number versus shape factor.
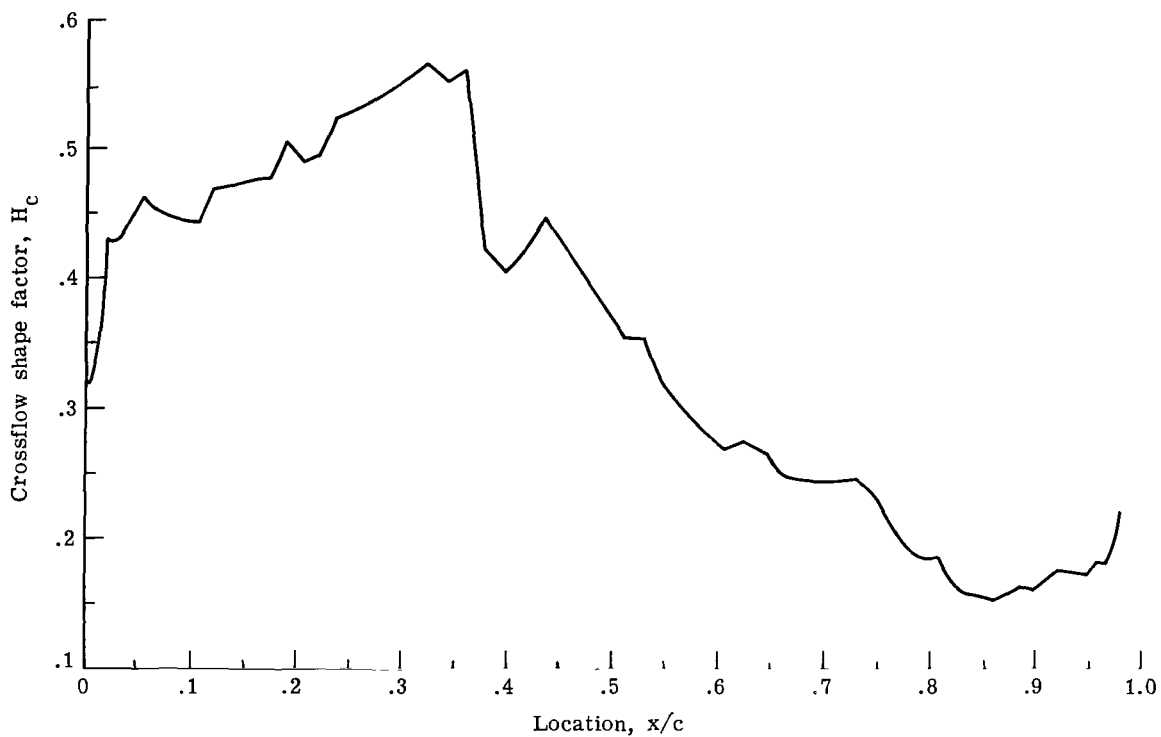
Figure 13.- Crossflow shape factor versus x/c for 970 airfoil. Upper surface; $M_{\infty,n} = 0.749$; $c_l = 0.675$; $R_c = 25 \times 10^6$; $\Lambda = 25°$.
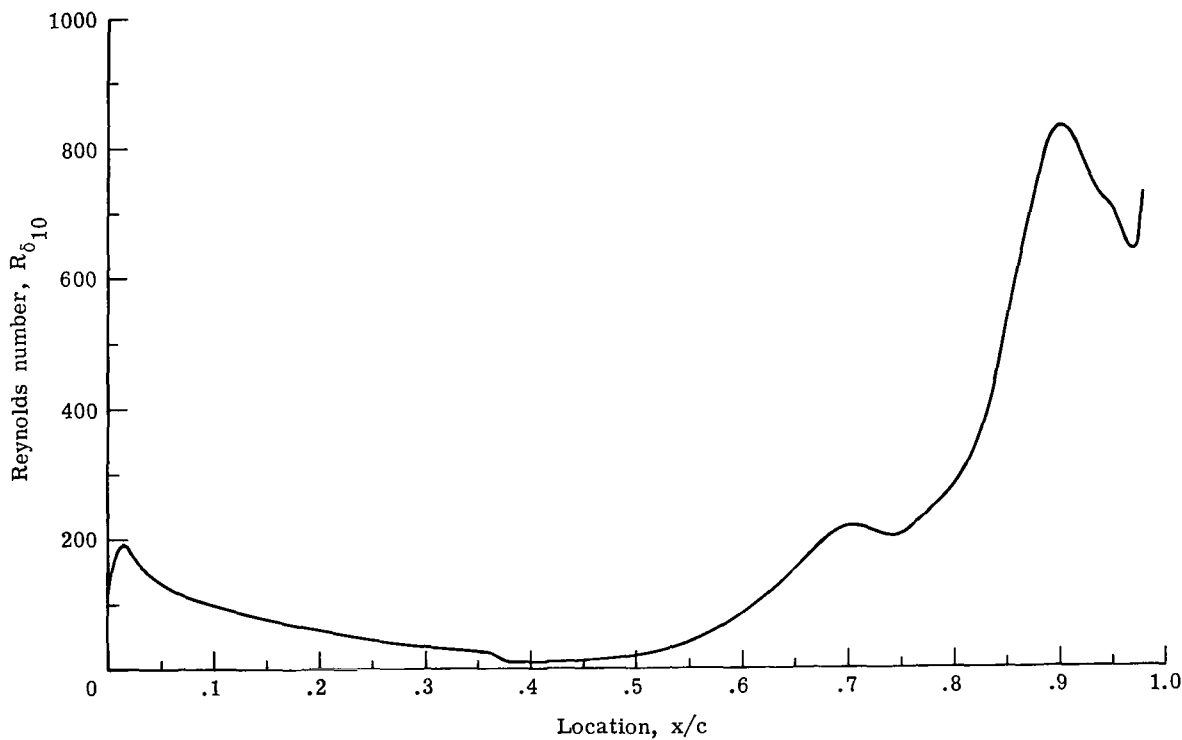
Figure 14.- Crossflow Reynolds number versus x/c for 970 airfoil. Upper surface; $M_{\infty,n} = 0.749$; $c_l = 0.675$; $R_c = 25 \times 10^6$; $\Lambda = 25°$.

76
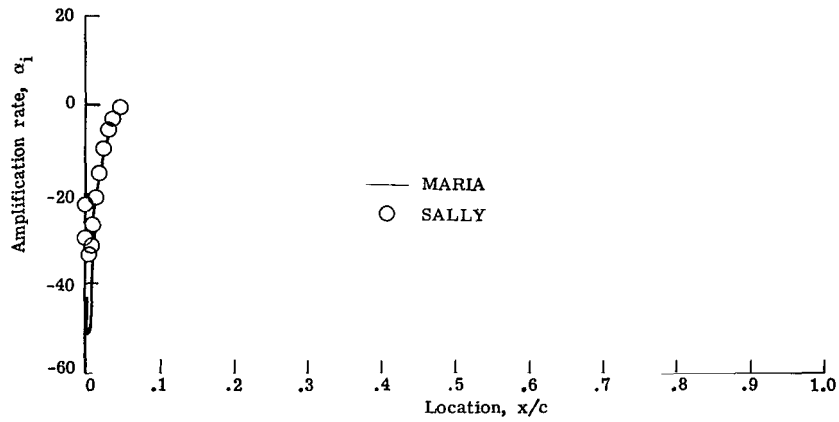
(a) $\lambda/c = 0.0004$.
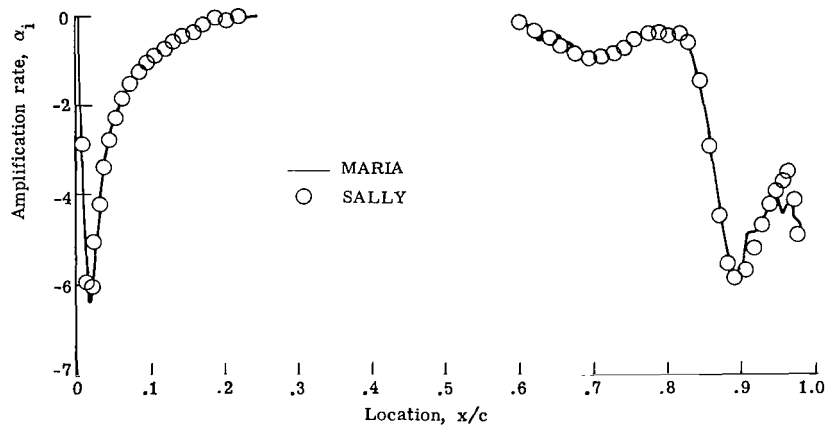
(b) $\lambda/c = 0.0016$.
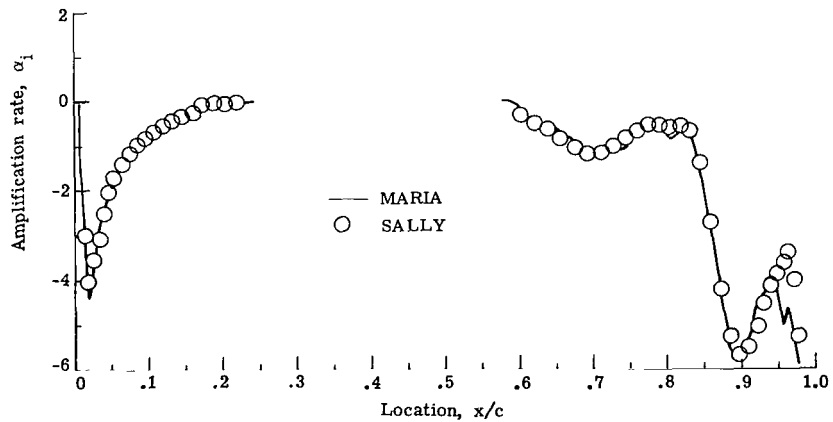
(c) $\lambda/c = 0.0020$.

Figure 15.- Amplification rate versus location for three wavelengths on 970 airfoil at design condition. Upper surface; $M_{\infty,n} = 0.749$; $c_l = 0.675$; $R_c = 25 \times 10^6$; $\Lambda = 25°$; $f = 0$.
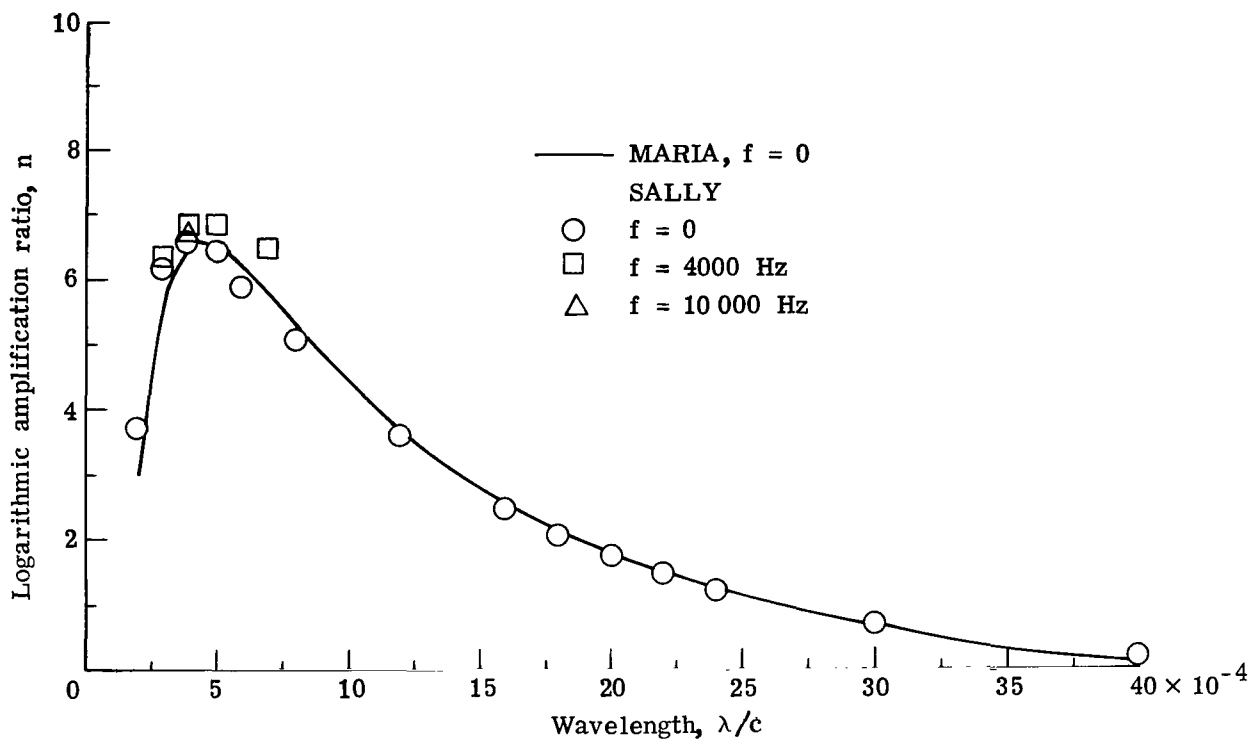
(a) Region 1 from x/c = 0 to 0.38.
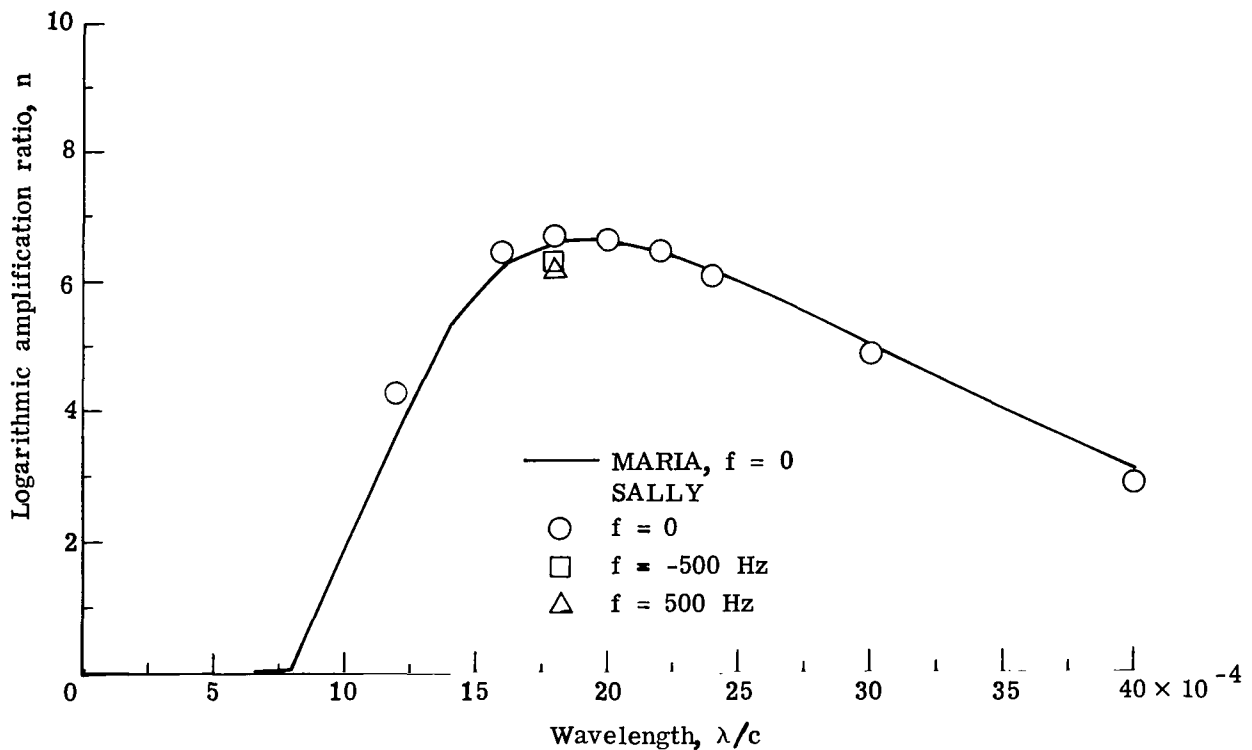
(b) Region 2 from x/c = 0.38 to 1.0.

Figure 16.- Logarithmic amplification ratio versus wavelength for upper surface of 970 airfoil at design condition for regions 1 and 2. $M_{\infty,n} = 0.749$; $c_l = 0.675$; $R_c = 25 \times 10^6$; $\Lambda = 25°$.
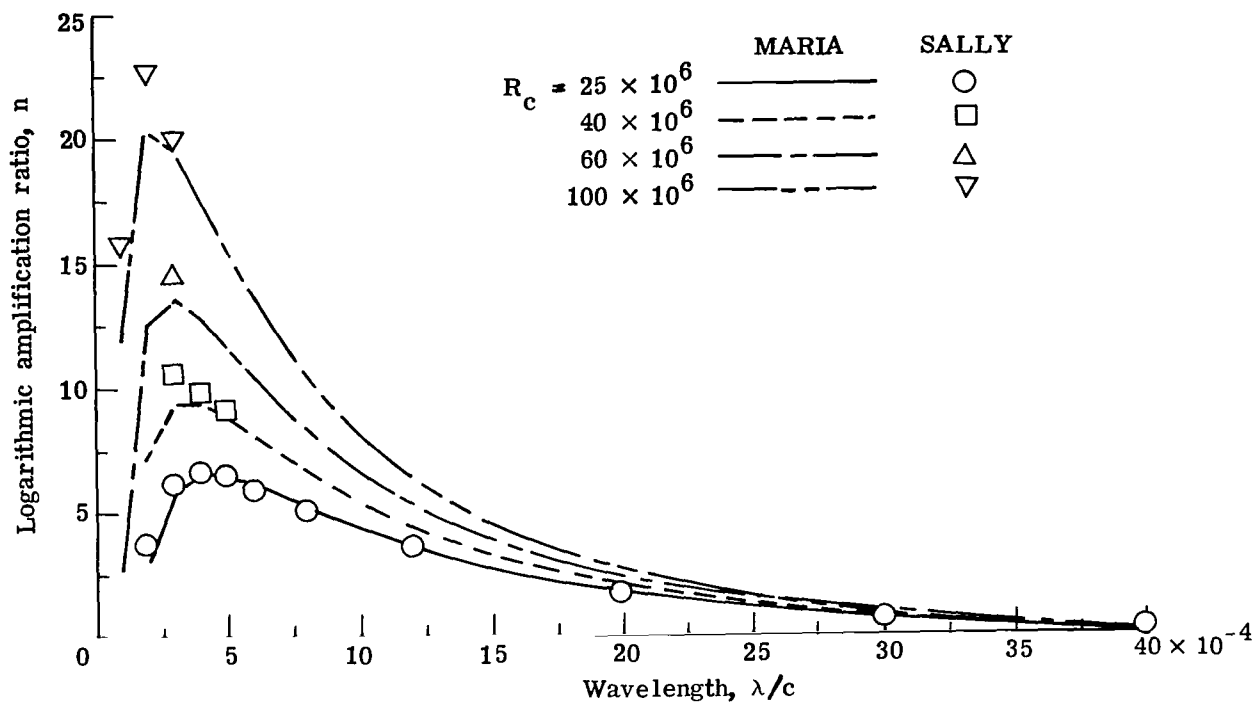
(a) Region 1.
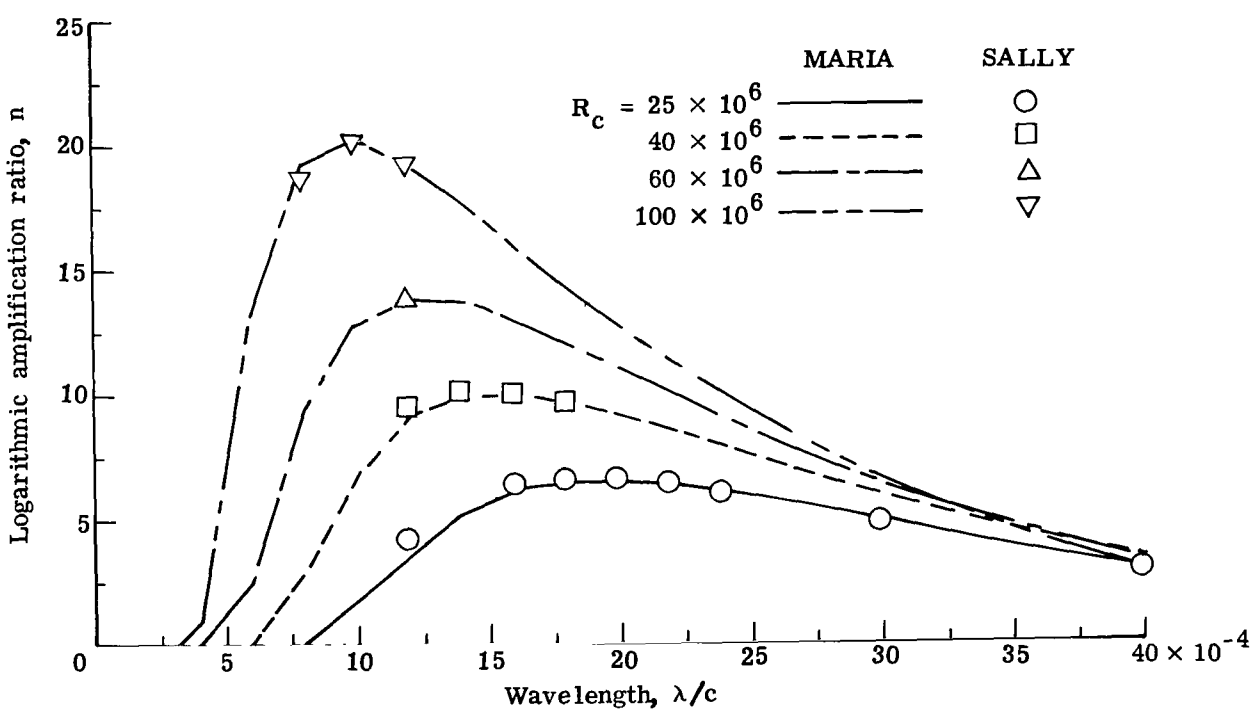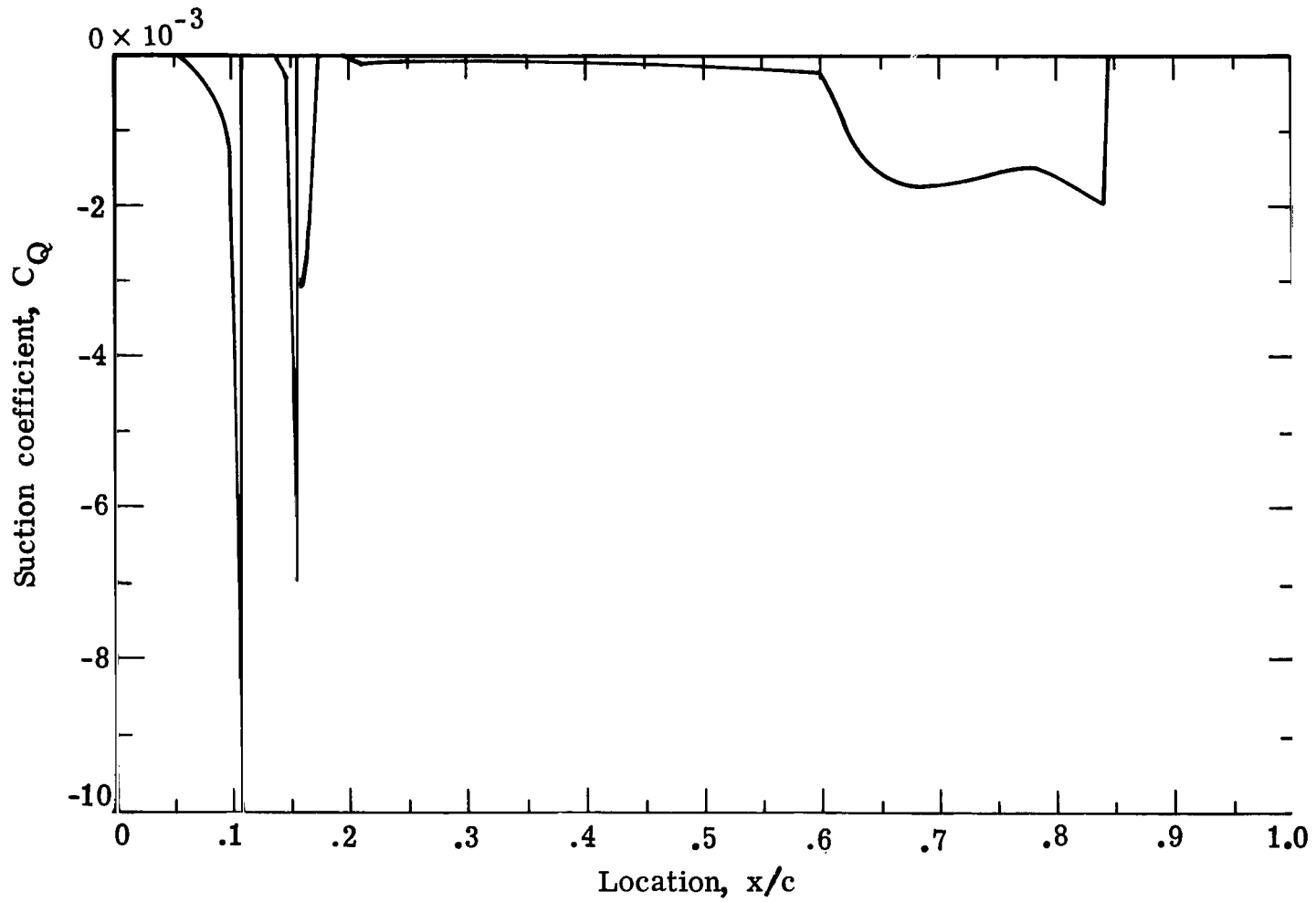

(b) Region 2.

Figure 17.- Logarithmic amplification ratio versus wavelength for upper surface of 970 airfoil at several Reynolds numbers for regions 1 and 2. $M_{\infty,n} = 0.749$; $c_l = 0.675$; $\Lambda = 25°$; $f = 0$.
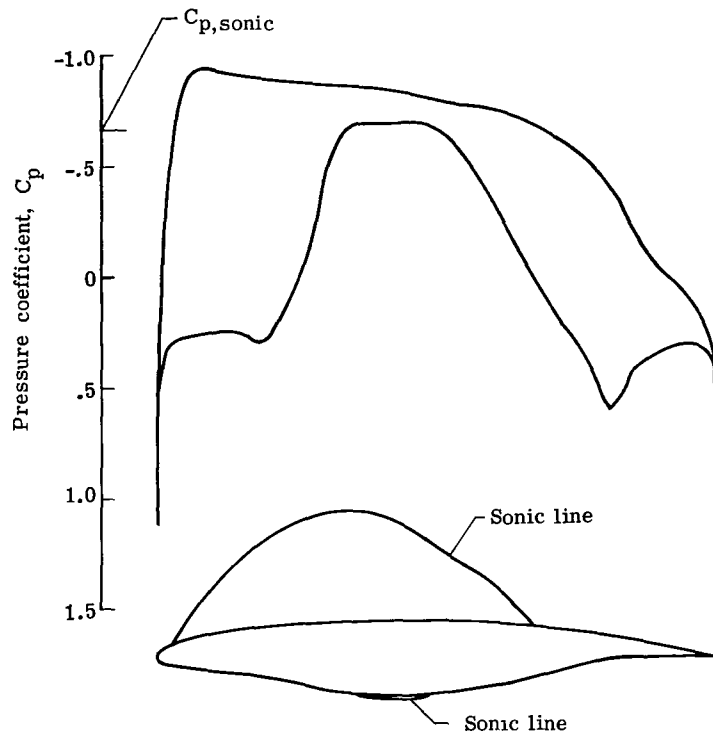
Figure 18.- Pressure distribution for LFC-73-06-135 airfoil at $M_{\infty,n} = 0.73$ and $c_l = 0.60$.
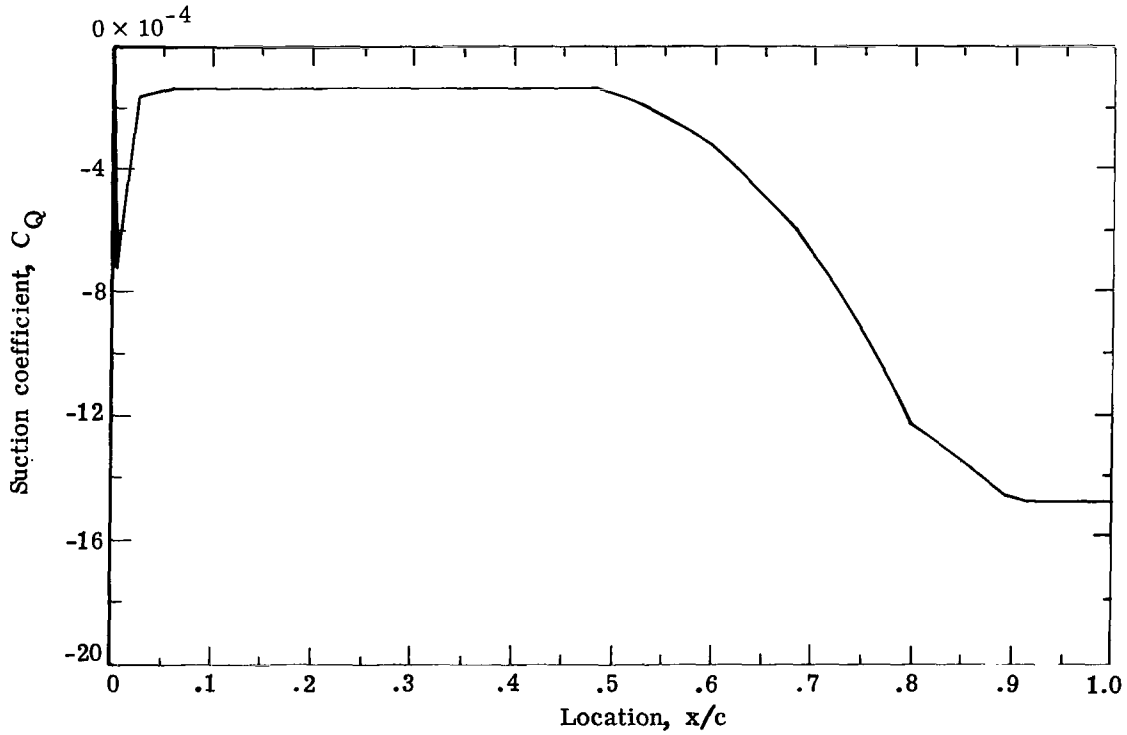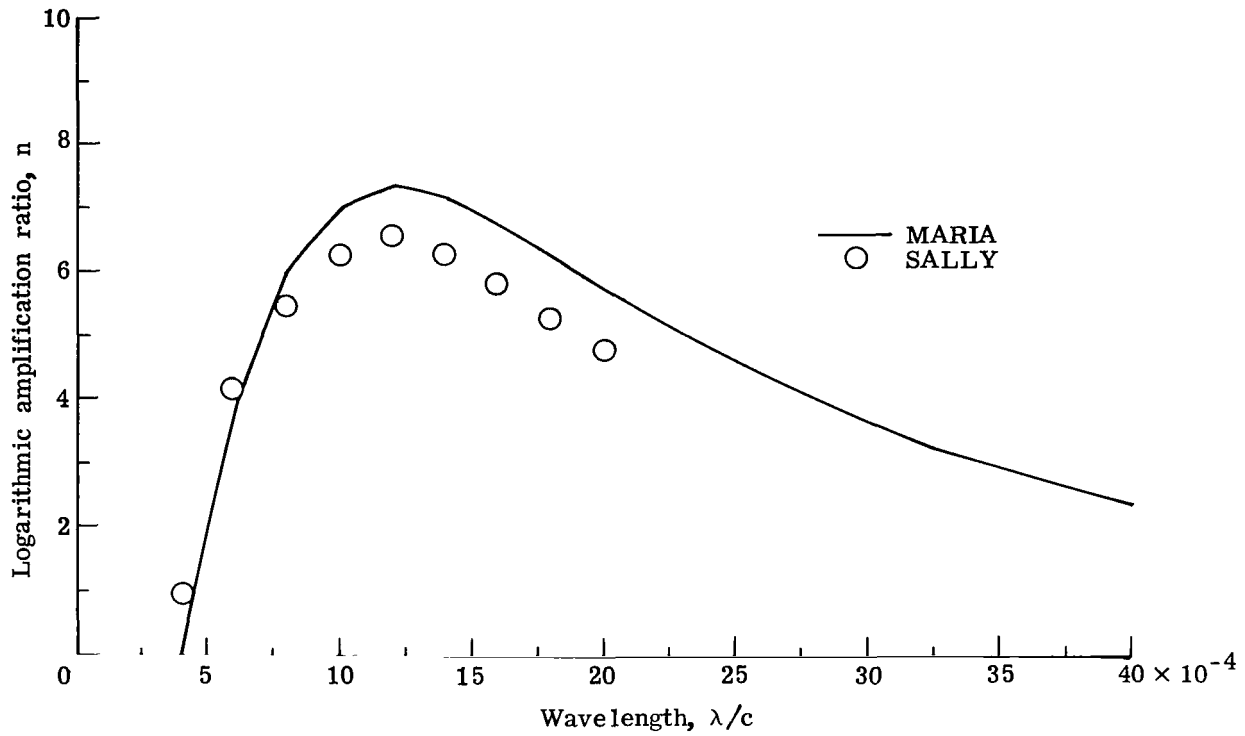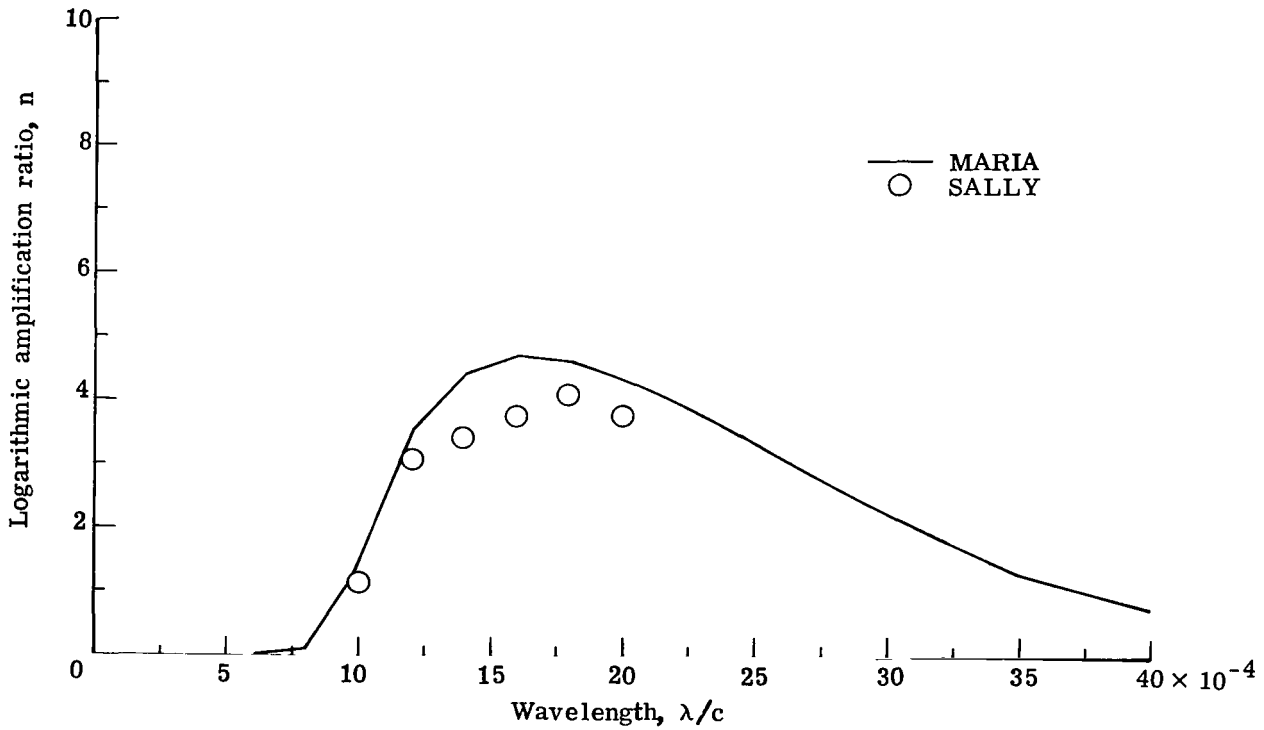

Figure 19.- Suction distribution for upper surface of LFC-73-06-135 airfoil at design condition. $M_{\infty,n} = 0.73$; $c_l = 0.60$; $R_c = 15 \times 10^6$; $\Lambda = 35°$.
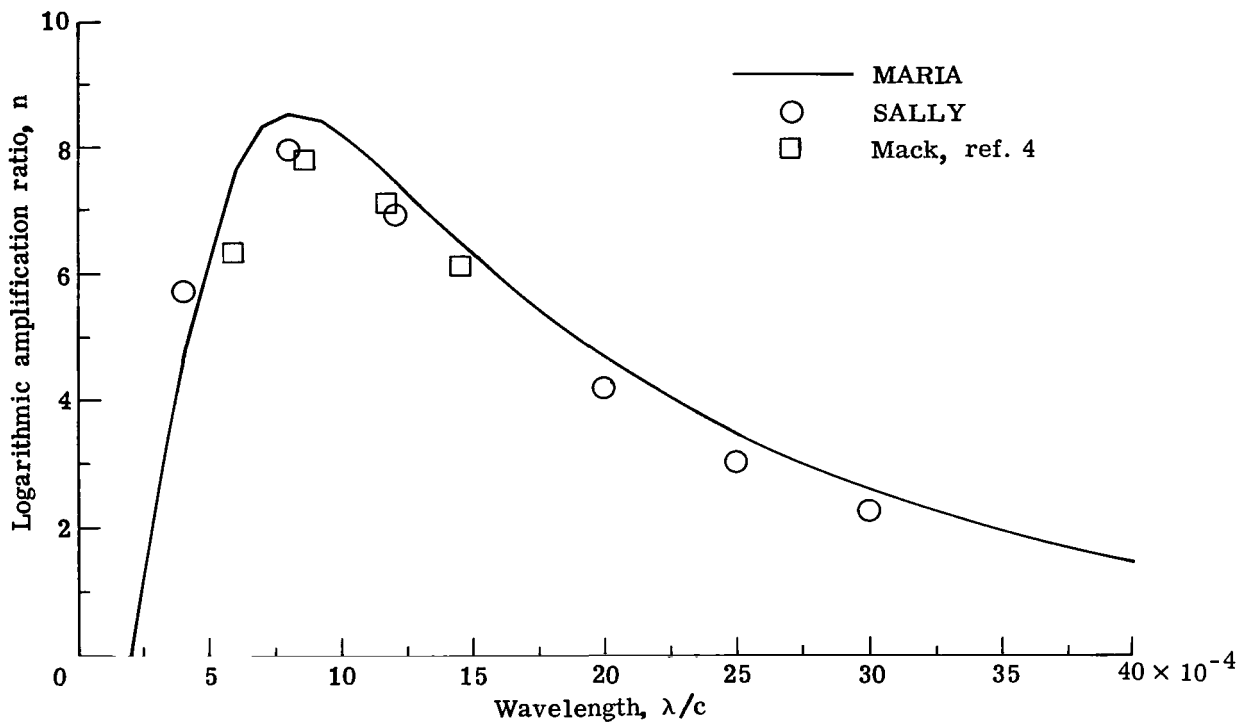
(a) Region 1 from x/c = 0 to 0.37.
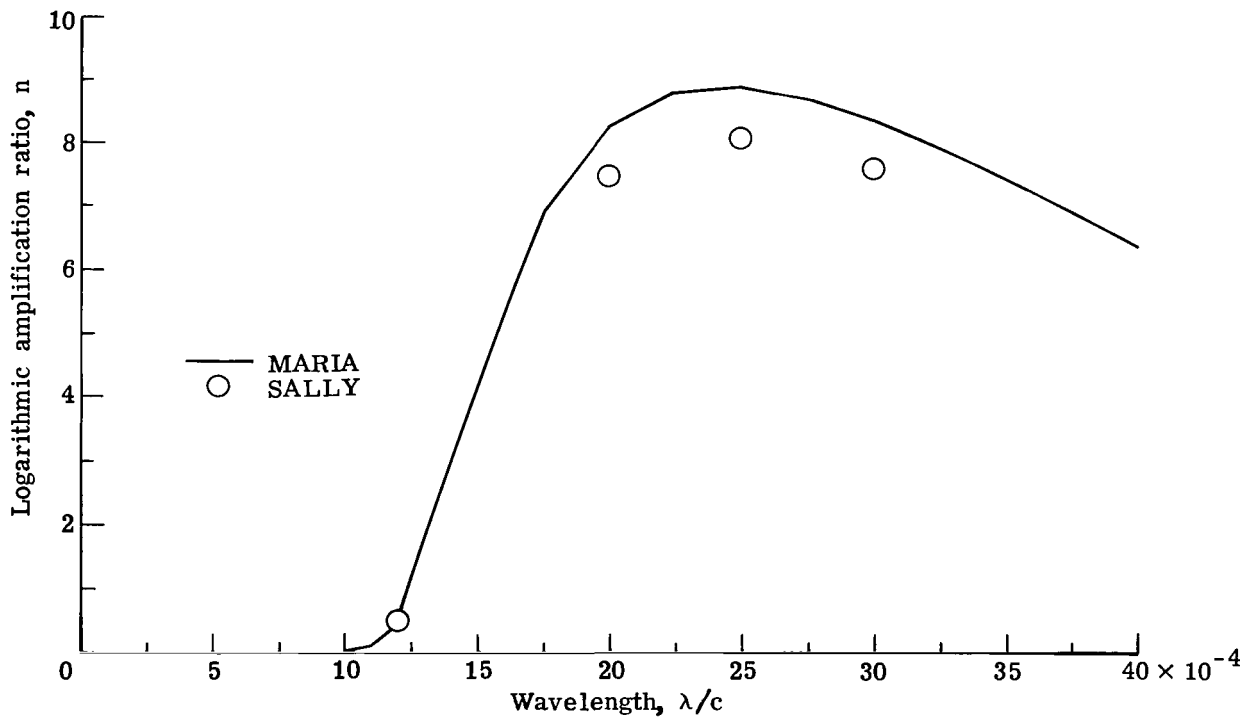
(b) Region 2 from x/c = 0.37 to 1.0.

Figure 20.- Logarithmic amplification ratio versus wavelength for upper surface of LFC-73-06-135 airfoil at design condition for regions 1 and 2. $M_{\infty,n}$ = 0.73; c_l = 0.60; R_c = 15 × 10^6; Λ = 35°; f = 0.
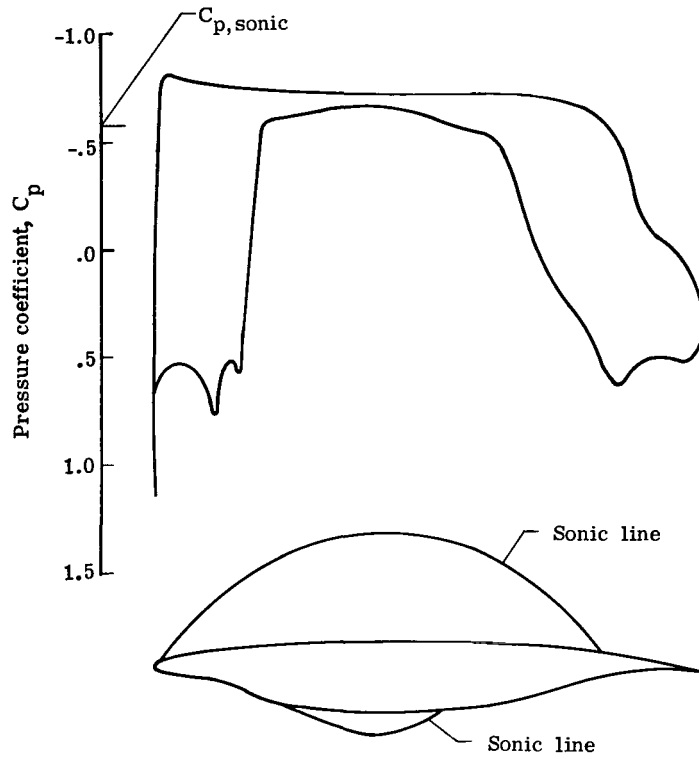
Figure 21.- Pressure distribution for 989C airfoil at $M_{\infty,n} = 0.755$ and $c_l = 0.55$.
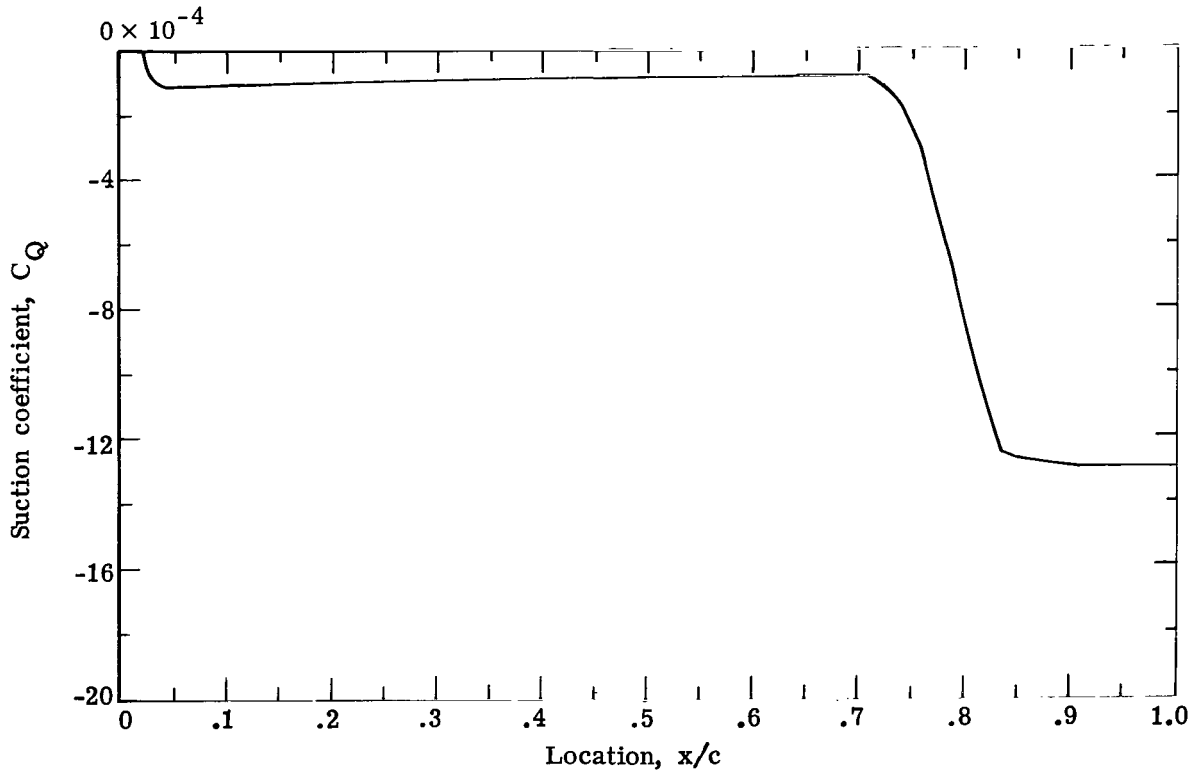
Figure 22.- Suction distribution for upper surface of 989C airfoil at design condition. $M_{\infty,n} = 0.755$; $c_l = 0.55$; $R_c = 20 \times 10^6$; $\Lambda = 23°$.
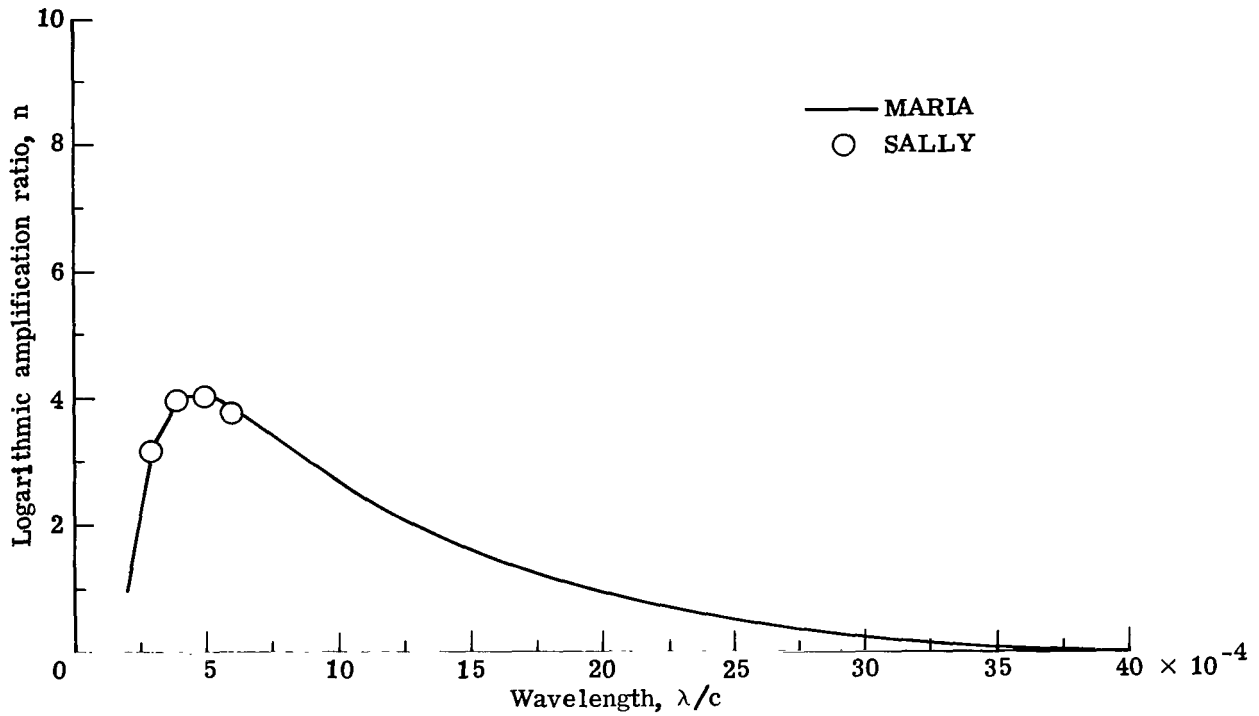
(a) Region 1 from x/c = 0 to 0.32.
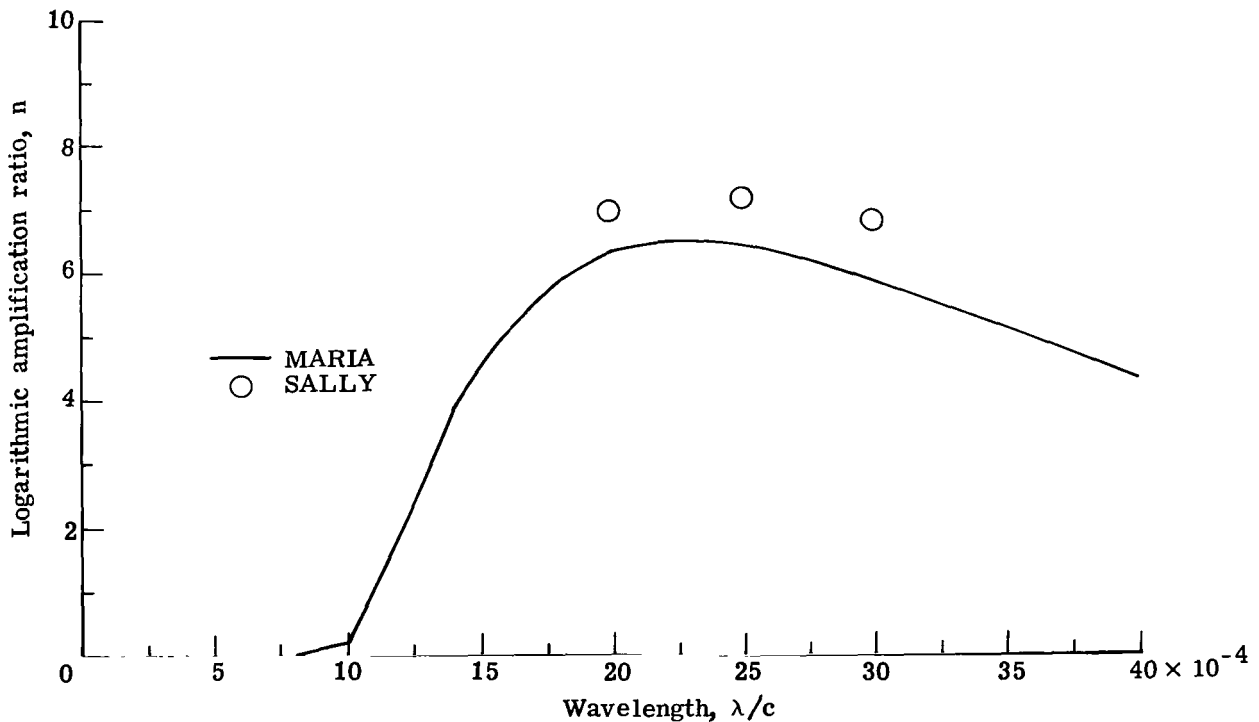
(b) Region 4 from x/c = 0.62 to 1.0.

Figure 23.- Logarithmic amplification ratio versus wavelength for upper
surface of 989C airfoil at design condition for regions 1 and 4.
$M_{\infty,n}$ = 0.755; c_l = 0.55; R_c = 20 × 10^6; Λ = 23°; f = 0.

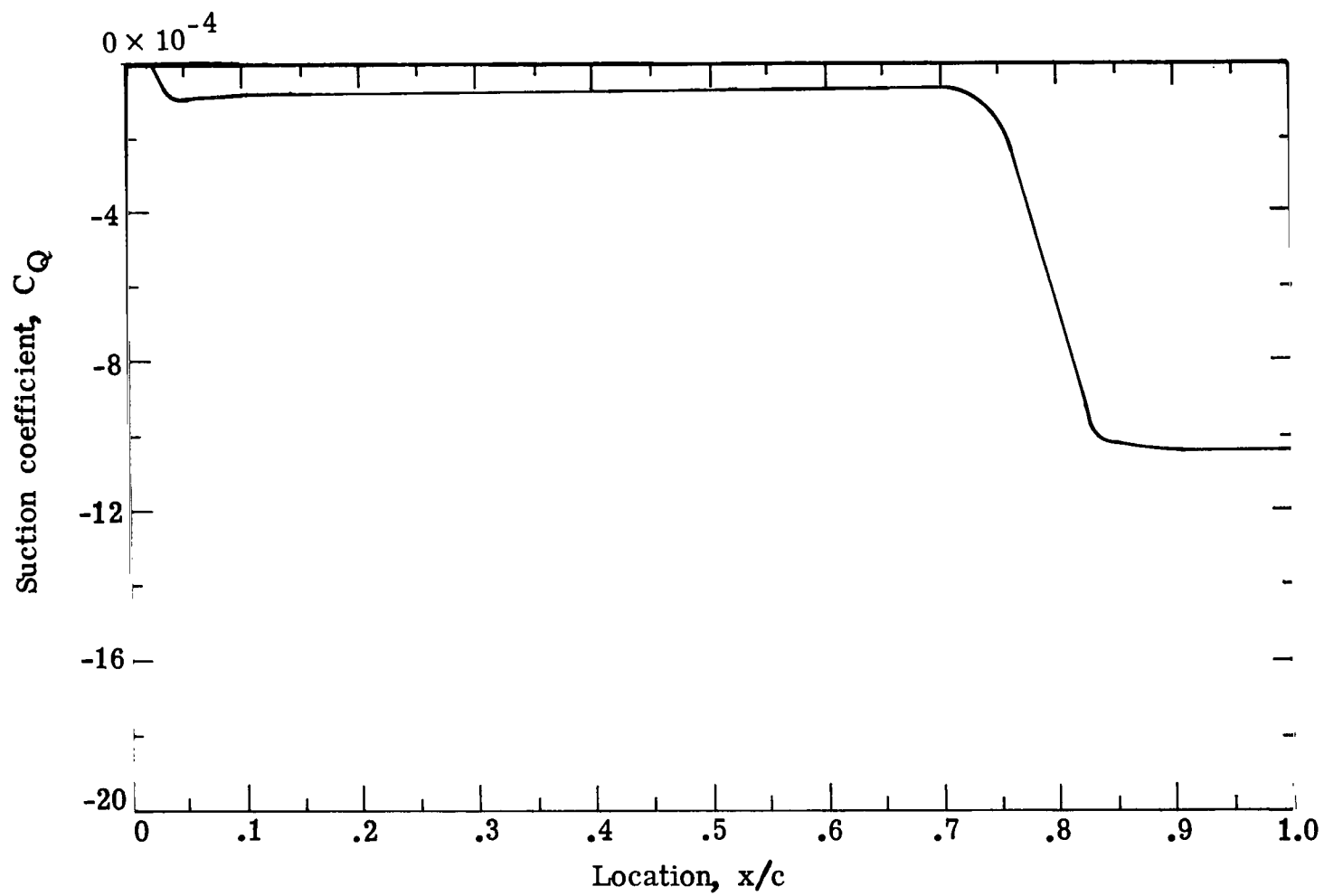Figure 24.- Suction distribution for lower surface of 989C airfoil at design condition. $M_{\infty,n} = 0.755$; $c_l = 0.55$; $R_c = 20 \times 10^6$; $\Lambda = 23°$.

(a) Region 5 from x/c = 0.16 to 0.51.

(b) Region 6 from x/c = 0.51 to 0.87.

Figure 25.- Logarithmic amplification ratio versus wavelength for lower surface of 989C airfoil at design condition for regions 5 and 6. $M_{\infty,n}$ = 0.755; c_l = 0.55; R_c = 20 × 10^6; Λ = 23°;   f = 0.
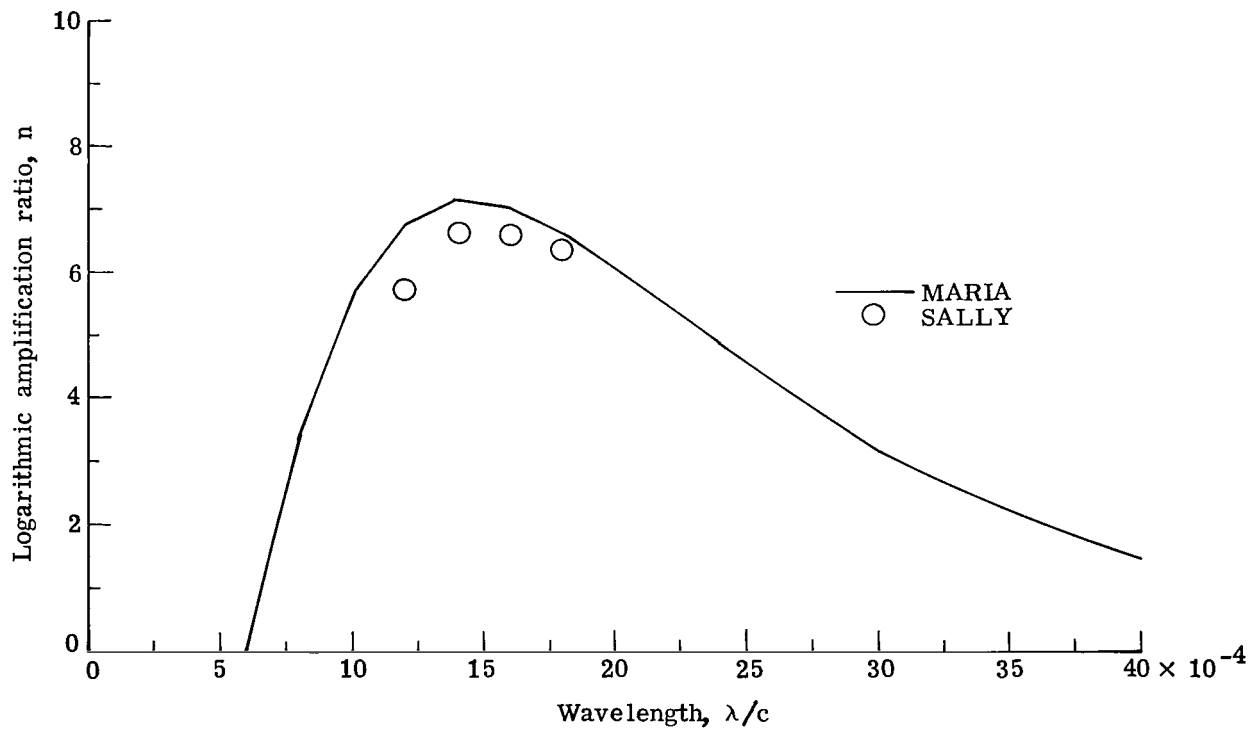
Figure 26.- Suction distribution for upper surface of 989C airfoil at $M_{\infty,n} = 0.755$, $c_l = 0.55$, $R_c = 40 \times 10^6$, and $\Lambda = 23°$.
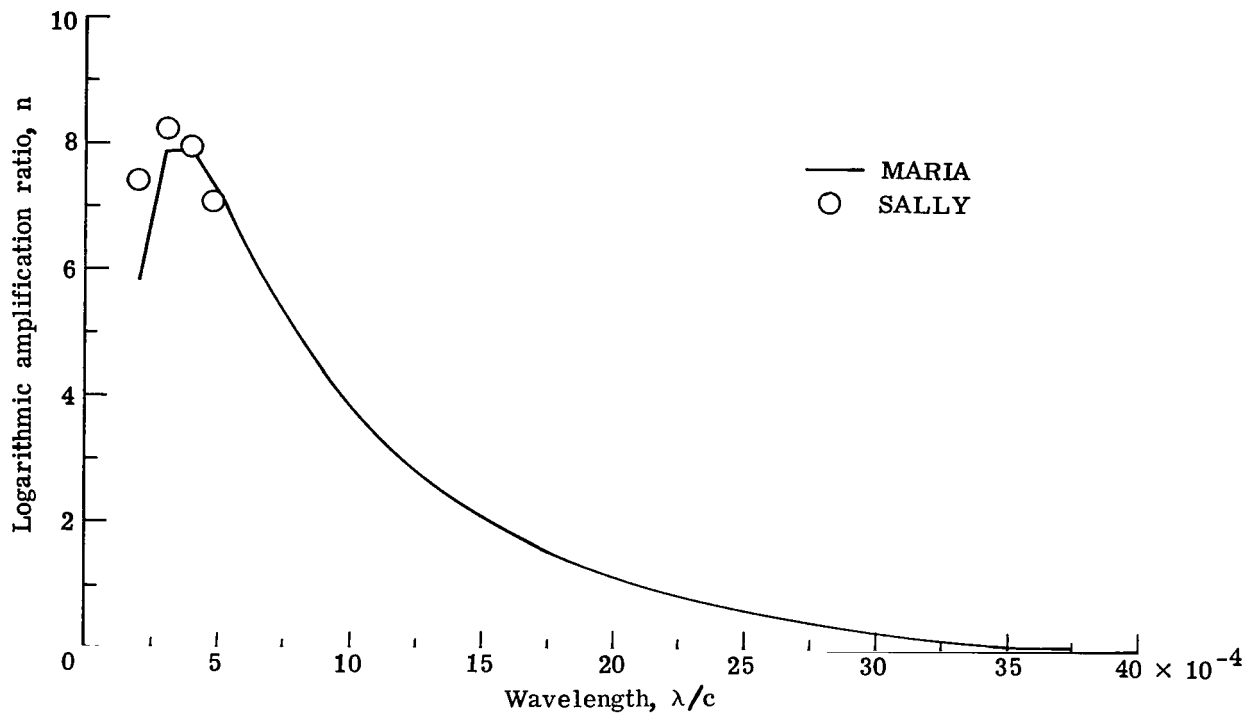
(a) Region 1 from x/c = 0 to 0.27.

(b) Region 2 at x/c = 0.27 to 1.0.

Figure 27.- Logarithmic amplification ratio versus wavelength for upper surface of 989C airfoil at $R_c = 40 \times 10^6$ for regions 1 and 2. $M_{\infty,n} = 0.755$; $c_l = 0.55$; $\Lambda = 23°$; f = 0.

1. Report No.	2. Government Accession No.	3. Recipient's Catalog No.
NASA TP-1902		

4. Title and Subtitle	5. Report Date
AMPLIFIED CROSSFLOW DISTURBANCES IN THE LAMINAR BOUNDARY LAYER ON SWEPT WINGS WITH SUCTION	November 1981
	6. Performing Organization Code
	534-01-13-14

7. Author(s)	8. Performing Organization Report No.
J. Ray Dagenhart	L-14423
	10. Work Unit No.

9. Performing Organization Name and Address	11. Contract or Grant No.
NASA Langley Research Center Hampton, VA 23665	
	13. Type of Report and Period Covered

12. Sponsoring Agency Name and Address	Technical Paper
National Aeronautics and Space Administration Washington, DC 20546	14. Sponsoring Agency Code

15. Supplementary Notes

16. Abstract

Solution charts of the Orr-Sommerfeld equation for stationary crossflow disturbances are presented for 10 typical velocity profiles on a swept laminar-flow-control (LFC) wing. The critical crossflow Reynolds number is shown to be a function of a boundary-layer shape factor. Amplification rates for crossflow disturbances are shown to be proportional to the maximum crossflow velocity. A computer stability program called MARIA, employing the amplification rate data for the 10 crossflow velocity profiles, is constructed. This code is shown to adequately approximate more involved computer stability codes using less than 2 percent as much computer time while retaining the essential physical disturbance growth model.

17. Key Words (Suggested by Author(s))	18. Distribution Statement
Laminar flow control Boundary layer Stability, crossflow Suction	Unclassified - Unlimited
	Subject Category 34

19. Security Classif. (of this report)	20. Security Classif. (of this page)	21. No. of Pages	22. Price
Unclassified	Unclassified	88	A05

National Aeronautics and
Space Administration

Washington, D.C.
20546

Official Business
Penalty for Private Use $300

THIRD-CLASS BULK RATE

NASA

POSTMASTER: If Undeliverable (Section 158
                Postal Manual) Do Not Return